CFD-DEM simulation for Advanced Chemical Recycling of Mixed Plastic Waste

LUNDS UNIVERSITET
Lunds Tekniska Högskola

by Ellen Che Belcher

Supervisors: Senior Lecturer Hesameddin Fatehi & Dr. Aurélia Vallier

Thesis for the Degree of Master of Science in Engineering
Department of Energy Sciences
Division of Fluid Mechanics
Lund University
2026

This degree project for the degree of Master of Science in Engineering has been conducted at the Division of Fluid Mechanics, Department of Energy Sciences, Faculty of Engineering, Lund University in collaboration with the Virtual Modelling team at Tetra Pak Packaging Solutions AB in Lund.

Supervisor at Tetra Pak Packaging Solutions AB was Dr. Aurélia Vallier. Supervisor at the Division of Fluid Mechanics was Senior Lecturer Hesameddin Fatehi.

Examiner at Lund University was Senior Lecturer Rixin Yu.

Department of Energy Sciences
Division of Fluid Mechanics
Lund University

ISRN LUTMDN/TMHP-26/5685-SE
ISSN 0282-1990

Typeset in LaTeX
Lund 2026

Abstract

Global plastic waste production has more than doubled in the past two decades, with plastic packaging accounting for 40% in 2019. Due to low recycling rates, pollution and limited fossil resources, increasing circularity in the plastic industry has become increasingly important. Chemical recycling through pyrolysis, unlike mechanical recycling, can treat contaminated, mixed plastic waste and increase circularity by producing hydrocarbons appropriate for re-polymerization.

A coupled CFD-DEM model was employed to investigate heat transfer in a rotary kiln reactor, simulating pyrolysis of three plastics. Polyethylene (PE) and polypropylene (PP), two common plastics found in post-consumer waste, were studied combined with polyAl, the residual material from recycling of Tetra Pak's paper-based food packaging. The study focused on evaluating heating patterns of plastic mixes and assessing the potential of polyAl, due to its aluminium content, to act as a heat carrier.

PE was found to have the lowest volumetric heat capacity and highest thermal diffusivity, making this a better heat carrier material than polyAl. PolyAl required the most energy to heat, resulting in lower average particle temperatures at all times compared to PP and PE. Five cases with different particle mixes were run to observe how particle interactions affect particle heating patterns. PE and polyAl experienced decreased heating rates when mixed with other particle types. PP experienced very small changes in heating rates that may fall within numerical uncertainties of the simulations.

Additionally, CFD-DEM showed good potential for R&D work of chemical recycling. Further work to achieve an accurate multi-scale process model, resolving chemical reactions and internal particle heat transfer, was identified.

Acknowledgements

I would like to thank my supervisors Hesameddin Fatehi and Aurélia Vallier, for their guidance and support throughout this project. Thank you for all the insightful discussions and constructive feedback. This work has been a highly educational experience, and I am especially grateful to Hesam for his guidance on navigating the unfamiliar and extensive field of chemical recycling.

Thank you to the Virtual Modelling team at Tetra Pak for welcoming me so kindly, and a special thank you to Malin Lind for her support with CFD.

I am very grateful for the financial support I received from Bengt Ingeströms Stipendiefond, which enabled me to carry out this master's thesis project.

I also wish to thank my friends and family for their support and encouragement. Thank you for listening to me talk through my thoughts on CFD-DEM, plastic waste and chemical recycling. Finally, thank you to everyone who made my study years at LTH so very enjoyable.

Ellen Che Belcher
Lund, May 2026

Contents

Nomenclature

Roman Letters

A	Surface area	$[m^2]$
A_p	Projected particle area	$[m^2]$
A_s	Particle surface area	$[m^2]$
Bi	Biot number	
C_{rest}	Coefficient of restitution	
C_d	Drag coefficient	
C_{fs}	Static friction coefficient	
c_p	Specific heat	$[J\,kg^{-1}\,K^{-1}]$
C_{vol}	Volumetric heat capacity	$[J\,m^{-3}\,K^{-1}]$
D	Diameter	[m]
d	Particle overlap at contact point	[m]
E	Total energy	$[J\,kg^{-1}]$
E	Young's modulus	[Pa]
e	Internal energy	$[J\,kg^{-1}]$
F	Force	[N]
G	Shear modulus	[Pa]
H	Total enthalpy	$[J\,kg^{-1}]$
h	Heat transfer coefficient	$[W\,m^{-2}\,K^{-1}]$
K	Spring stiffness	$[N\,m^{-1}]$
k	Thermal conductivity	$[Wm^{-1}K^{-1}]$
L_c	Characteristic length	[m]
m	Mass	[kg]
M_{eq}	Equivalent particle mass	[kg]
N	Damping	$[N\,s\,m^{-1}]$
N_{damp}	Damping coefficient	
n_π	Number of particles within parcel π	
Nu	Nusselt number	
p	Pressure	[Pa]
Pr	Prandtl number	

Q_s	Heat source term particle energy equation	[W]
Q_t	Convective heat transfer from fluid to particle	[W]
R	Radius	[m]
r_c	Contact area radius	[m]
Re	Reynolds number	
s_{int}	Internal source term	
T	Temperature	[K]
t	Time	[s]
t_p	Particle residence time	[s]
V	Volume	[m^3]
w	Wen-Yu exponent	
$\mathbf{a}$	Area vector	[m^2]
$\mathbf{F}_b$	Resulting body force vector	[N]
$\mathbf{f}_b$	Body force vector	[N]
$\mathbf{F}_{cm}$	Contact model force vector	[N]
$\mathbf{F}_c$	Contact force vector	[N]
$\mathbf{F}_d$	Drag force vector	[N]
$\mathbf{F}_g$	Gravity force vector	[N]
$\mathbf{F}_s$	Resulting surface force vector	[N]
$\mathbf{I}_p$	Particle moment of inertia	[kg m^2]
$\mathbf{M}_b$	Drag torque	[N m]
$\mathbf{M}_c$	Contact torque	[N m]
$\mathbf{n}$	Normal direction vector	
$\mathbf{q}$	Heat flux vector	[W m^{-2}]
$\mathbf{S}_E$	Energy source term field	[W m^{-3}]
$\mathbf{S}_V$	Momentum source term field	[N m^{-3}]
$\mathbf{T}$	Viscous stress tensor	[Pa]
$\mathbf{t}$	Tangential direction vector	
$\mathbf{v}$	Velocity vector	[m s^{-1}]
$\mathbf{v}_p$	Instantaneous particle velocity vector	[m s^{-1}]
$\mathbf{v}_s$	Particle slip velocity vector	[m s^{-1}]
t_{scale}	User-defined time-scale	
$V_{Rayleigh}$	Rayleigh wave speed	[m s^{-1}]

Greek Letters

α	Thermal diffusivity	[m^2 s^{-1}]

δ	Dirac delta function	
ϵ	Void fraction	
ϵ_{min}	Cutoff void fraction	
η	Volume fraction Eulerian phase	
μ	Dynamic viscosity	$[\mathrm{N\,s\,m^{-2}}]$
ν	Kinematic viscosity	$[\mathrm{m^2\,s^{-1}}]$
ν	Poisson's ratio	
ν_n	Normal velocity component of the relative sphere surface velocity at the contact point	$[\mathrm{m\,s^{-1}}]$
ν_t	Tangential velocity component of the relative sphere surface velocity at the contact point	$[\mathrm{m\,s^{-1}}]$
ν_{impact}	Normal impact velocity	$[\mathrm{m\,s^{-1}}]$
$\nu_{particle}$	Particle speed	$[\mathrm{m\,s^{-1}}]$
ϕ_c	Volume fraction Lagrangian phase	
π	Parcel	
π	Pi	
ρ	Density	$[\mathrm{kg\,m^{-3}}]$
τ_1	Rayleigh wave propagation time	[s]
τ_2	Impact duration time	[s]
τ_3	Particle transit time	[s]
ω	Angular velocity	$[\mathrm{rad\,s^{-1}}]$
σ	Stress tensor	[Pa]

Abbreviations

AP	Acidification Potential
CFD	Computational Fluid Dynamics
CRM	Chemical Recycling to Monomer
CTL	Coal to Liquid Production
DEM	Discrete Element Method
EP	Eutrophication Potential
EU	European Union
GHG	Greenhouse Gas
GWP	Global Warming Potential
HDPE	High Density Polyethylene
HTL	Hydrothermal Liquefaction
LDPE	Low Density Polyethylene

LLDPE	Linear Low Density Polyethylene
MRF	Materials Recovery Facility
MSP	Minimum Selling Price
MSW	Municipal Solid Waste
MTG	Methanol-to-Gasoline
MTO	Methanol-to-Olefins
P2F	Plastic-to-Fuel
P2P	Plastic-to-Plastic
PCW	Post-Consumer Waste
PE	Polyethylene
PET	Polyethylene Terephthalate
PO	Polyolefins
POCP	Photochemical Ozone Creating Potential
PP	Polypropylene
PS	Polystyrene
PSW	Plastic Solid Waste
PUR	Polyurethane
PVC	Polyvinyl Chloride
RDF	Refuse-Derived Fuel
SCW	Supercritical Water
TCT	Thermo-Chemical Treatments
TEA	Techno-Economic Analysis
WTE	Waste to Energy

Subscripts

eq	Equivalent
i	Particle i
j	Particle j
n	Normal
p	Particle
t	Tangential
w	Wall

1 Introduction

Plastics are versatile materials used globally in various industries for a wide range of applications [1]. They consist of organic polymers, which in turn are chains of monomers. Plastics can also contain different additives, such as pigments, to achieve specific material features or properties. Monomers are single molecular units that can primarily form chains through covalent bonds. There is considerable variation in monomer composition, which leads to many different types of plastics [2].

Plastic production and waste are increasing. Global production doubled from 234 million tonnes (Mt) in 2000 to 460 Mt in 2019. Plastic annual waste production followed the same trend, increasing from 156 Mt in 2000 to 353 Mt in 2019. The majority of plastic waste is made up of plastics with short lifetimes, and 40% of the waste comes from plastic packaging. According to the Organisation for Economic Co-operation and Development (OECD), only 9% of the global plastic waste in 2019 was recycled. The remaining percentages are allocated to nearly 50% being stored in landfills, 19% being incinerated and 22% was either burned in open pits, left in uncontrolled dumpsites, or leaked to the environment. All three routes contribute to the environmental issue of plastic pollution. Plastic is today primarily produced from fossil-based feedstock. The refining process is energy intensive, and approximately 90% of life-cycle emissions account for the production and refining process. The OECD reported an estimate of the greenhouse gas emissions from fossil-based plastics to be 1.8 gigatonnes of CO_2 equivalent in 2019. This corresponds to 3.4% of global emissions in 2019 [1]. There is clearly a global need to improve plastic waste management and recycling of plastics in order to reduce emissions and environmental impact from this sector.

Efforts are being made to both decrease plastic usage, such as the European Union's (EU) ban on certain single-use plastics in 2019, and increase recycling of plastics. In 2024, the EU approved new rules requiring member states to reduce their total packaging waste per capita compared to 2018 by 15% by 2040 [3]. In 2025, the Packaging and Packaging Waste Regulation (PPWR) entered into force, replacing the previous directive in the EU. This regulation includes new rules to reduce plastic waste and increase circularity by, for example, introducing 10% and 25% targets for minimum percentages of recycled content in plastic packages by 2030 and 2040 respectively [4]. Plastic packaging is used in many industries for different reasons. Reduction of plastic by replacement with other materials may be more difficult in some industries than others, such as in food packaging and medical applications. In medical applications, it is argued that the single-use plastics are safer than sanitizing reusable equipment [5]. In the food packaging industry, plastics are common for several reasons. It is a lightweight, affordable, moisture-resistant

material and appropriate for both dry and wet foods. These characteristics facilitate food transportation and shelf-life, important factors in reducing food waste [6].

The main recycling pathway for plastics today is through mechanical recycling, accounting for over 90% of the recycled plastic waste. The other recycling process possible for plastics is chemical recycling [7]. Mechanical recycling has significant limitations in recycling contaminated plastics and unsorted mixed plastic waste. In addition to these limitations, mechanically recycled plastics showcase a deterioration in desired mechanical properties with successive recycling [8]. Consequently, a recycling method where the mechanical properties of the material do not deteriorate is especially interesting, as this would decrease plastic waste and increase circularity. Chemical recycling is therefore gaining more attention and involves breaking down the plastic waste into its molecular building blocks to be reused in plastic production (re-polymerization) or for the production of other value-added products (e.g. materials and fuels). For the plastic-to-plastic chemical recycling, the material properties of the plastic are retained [7]. Chemical recycling of plastics can be further divided into two main categories: thermolysis and solvolysis, each encompassing multiple process methods [1]. Both categories involve complex interactions between heat transfer, chemical reactions, and multiphase flow behaviour. These process technologies are emerging, with some practical implementations already up and running, however, significant challenges still remain [7].

In collaboration with Tetra Pak, this work will investigate chemical recycling of plastic waste relevant to the food industry. Tetra Pak is a world-leading food packaging and processing company that works continuously to improve the circularity of their packaging products by increasing recycling capacity and strengthening the recycling infrastructure for their famous paper-based carton packages. Tetra Pak's carton packages not only consist of paperboard but also include layers of plastic and aluminium, combined often termed polyAl, to protect against moisture and leakage. In 2024, Tetra Pak sold 178 billion packages, making plastic recycling an important issue for Tetra Pak [9].

1.1 Aim and Objectives of Thesis

This thesis aims to investigate the potential of using the combination of the discrete element method (DEM) and computational fluid dynamics (CFD) modelling as a tool for developing chemical plastic recycling of mixed plastic waste. This will be investigated by aiming to build a multi-scale modelling setup of the complex interactions occurring in a chemical plastic recycling process, aiming to cover and include interactions between heat transfer, multiphase flow behaviour, and potentially chemical reactions. Creating a realistic numerical simulation setup for a chemical recycling process will allow further understanding of the process and be a key tool in gaining insight on the challenges of chemical plastic recycling. Achieving a full-bodied process model as such could be a key component for future process design and scaling up endeavours, as it will hopefully

give a solid grasp of both the overall process behaviour and the detailed mechanisms at play. Further, this thesis will aim to investigate the inclusion of polyAl in chemical recycling of mixed plastic waste.

To achieve the aim of this thesis, firstly, existing and potential chemical recycling methods and pathways must be investigated through a literature survey. Based on findings in the literature survey, a chemical recycling process and plastic waste composition are selected for further model development. The aim of the model development is to create a full-bodied process model, resolving flow field dynamics and creating a setup that either includes multi-physics integration or in the future can be extended to include multi-physics integration for exploring areas such as internal heat conduction of individual polymer particles and reaction kinetics. This thesis is intended as a first step toward developing an accurate multi-scale numerical model for chemical recycling of plastics, aiming to build an extendable modelling framework and identifying future research directions.

1.2 Outline of Report

Chapter 1 *Introduction* gives a short background on the topic, contextualising the thesis project and states the aim of the thesis. Chapter 2 *Literature Survey* accommodates the findings from the literature survey and relevant background information for both this thesis and potential future work. The chapter is concluded with the selection of a chemical recycling process and plastic waste composition for further model development. The selected validation paper used for model development and limitations are also described. Chapter 3 *CFD-DEM Theory* covers the fluid dynamics and particle theory applied in the simulation setup. Chapter 4 *Method* describes the simulation setup, method used for the mesh sensitivity study and validation, and the method used for the investigative CFD-DEM simulations on chemical recycling of MPW. Chapter 5 *Results* includes simulation results and noteworthy gained insights on CFD-DEM. Chapter 6 *Discussion* includes a discussion of the results found for the investigative CFD-DEM simulations on chemical recycling of MPW, a discussion on CFD-DEM as part of a multi-scale process model, a broader discussion on challenges of the selected chemical recycling method and a section on suggested future work. Lastly, chapter 7 *Conclusions* summarizes the key findings.

2 Literature Survey

Chapter 2 consists of three main parts. The first part gives an overview of plastics. This part covers terminology related to plastics, the basic chemistry of plastics which is followed by a description of plastic waste and its composition. Further, is a description of Tetra Pak's paper based packaging, explaining the material anatomy and what type of plastics the packaging contains. The plastics section is concluded with a description of plastic feedstock production. This is useful in order to understand the desired product outflow from any chemical recycling process aiming to carry out plastic-to-plastic recycling.

The second part of this chapter covers the various chemical recycling processes available and limits which process types are reviewed further.

The third part covers a literature survey on life cycle assessments (LCAs) for the limited selection of chemical recycling processes in an attempt to assess a preferred process option for plastic-to-plastic chemical recycling. Reactor options for the preferred process are described briefly, followed by an explicit statement of thesis scope regarding the selected chemical recycling process, the selected reactor type, and selected plastic waste composition used for CFD-DEM.

The extensive literature survey included in chapter 2 is intentional and thought to serve as an accessible foundation of background information on chemical recycling of MPW for future student endeavours.

2.1 Plastics

Plastics consist of organic polymers usually mixed with additives. The additives are often plasticizers, stabilizers, and/or colourants [10]. Plasticizers are additives that increase the softness and flexibility of the plastic, i.e., increasing the plasticity. Stabilizers are additives that inhibit or retard the degradation of plastics. Degradation of plastics during production or when still in use is undesired and occurs through oxidation, heat exposure, and UV light. Colourants are additives that colour the plastic. Other common additives are flame retardants [11]. Additives not only serve post-processing functions but are also necessary in enabling the processing of plastics in plastic production.

The polymers that make up plastics are man-made hydrocarbon chains. Depending on the sourcing of the hydrocarbon feedstock for the plastic production, plastic can be categorized as synthetic or bio-based. Synthetic plastics are made from fossil-based

hydrocarbon sources (crude oil, natural gas, or coal), whereas bio-based plastics are derived from renewable biomass (for example, starch, vegetable fats, and vegetable oils) [12]. Bio-based plastics provide a renewable source for plastic production and generates less greenhouse gas (GHG) emissions during production than synthetic plastics. However, the use of bio-based plastics has the potential to drive land-use changes, potentially resulting in increased GHG emissions and negative environmental impact through deforestation. Important to note is that a biomass feedstock for plastic production is not synonymous with the produced plastic being biodegradable. Waste treatment issues for bio-based plastics remain similar to those of synthetic plastics, except for bio-based biodegradable plastics. Biodegradable plastics are only biodegradable in specific environments, with poor biodegradation in natural environments [1]. Synthetic plastics dominate the market, with bio-based plastics only making up 0.5% of global plastics in 2023. Bio-based plastics are primarily used in packaging, with 45% of the total bio-based plastic market being allocated to this sector [13].

Depending on the behaviour of plastics when exposed to elevated temperature, they can be divided into thermosets or thermoplastics. Thermoplastics are plastics that show plasticity when exposed to heat, i.e., they can melt and allow reshaping. Thermosets do not show plasticity when exposed to heat and remain fixed, retaining their form and solidity. When thermosets are exposed to enough heat, they degrade and decompose [14]. The plastics typically found in municipal solid waste (MSW) are thermoplastics [15].

2.1.1 Chemistry & Terminology

The world of plastics is vast with extensive terminology which is often complicated by interchangeable wording, using nomenclature mixed with trivial names, and the absence of clear distinctions. This section aims to cover the chemistry basics of polymers, monomers, polymerization, and depolymerization needed when reviewing plastic chemical recycling processes.

Plastics can be divided into two groups: homogeneous plastics and heterogeneous plastics. Homogeneous plastics are plastics made up of one type of polymer, whereas heterogeneous plastics consist of different polymers. This should not be confused with the phrasing homogeneous and heterogeneous plastic waste. Homogeneous plastic waste contains only one type of plastic and heterogeneous plastic waste contains different types of plastics. The Greek terms homo and hetero also appear in polymer categorization. Polymers can be categorized as either heterochain polymers or homochain polymers. Homochain polymers have a C-C backbone, whereas heterochain polymers have a C-X backbone, i.e., containing a heteroatom [16]. Polyethylene (PE), polypropylene (PP), and polyvinyl chloride (PVC) are examples of homochain polymers, whereas polyethylene terephthalate (PET) is a heterochain polymer containing the heteroatom oxygen. Polymers are macromolecules with a repeating structure of monomers. The term hydrocarbon is often used to describe both monomers, oligomers and polymers.

Monomers are the single molecular building blocks that make up the polymer chains. Oligomers are molecules consisting of monomers but smaller than polymers.

Plastic production involves both micro-level processes, such as polymerization, and macro-level processes, such as feedstock production. Today's feedstock production is part of the petrochemical industry. A plastic-to-plastic chemical recycling process aims to replace feedstock production from virgin sources. As both petrochemical production processes and chemical plastic recycling treat hydrocarbon feedstock, the same terms frequently occur in both contexts. Terms such as gas, oil, liquid, wax, and solid describe the physical state of the hydrocarbons. Oil is used to describe a liquid that can contain suspended solids and dissolved gases. It is also used to describe condensable gases, whereas gas describes non-condensable gases. Waxes are solid or semi-solid hydrocarbons. In addition to state descriptors, hydrocarbons are often classified as light or heavy. Light hydrocarbons, for example, light oil, indicate a lower molecular weight and generally a shorter hydrocarbon chain. Heavy hydrocarbons, e.g., heavy oil, have higher molecular weights and generally longer hydrocarbon chains. Light hydrocarbons are found in gases and liquids, whereas heavier hydrocarbons are found in waxes and solids.

Hydrocarbons can be saturated or unsaturated, where the former indicates only single carbon bonds and the latter indicates the presence of at least one double or triple carbon bond. Further, hydrocarbons can be categorized as aliphatic or aromatic. Aliphatic hydrocarbons are the familiar carbon chains of either alkanes (containing only single covalent bonds), alkenes (double covalent bonds), or alkynes (triple covalent bonds). Aromatics are hydrocarbons containing the six-carbon benzene ring, possessing very particular resonance hybrid bonds, giving them unique characteristics. Hydrocarbon rings that do not possess this specific hybrid bonding found in benzene rings are called cycloalkanes. These are aliphatic hydrocarbon rings, distinctly different from aromatics [17]. The petrochemical industry often uses other terms for the mentioned hydrocarbon classifications. Alkanes are called paraffins. Alkenes are called olefins, and a polymer built by combining alkene/olefin monomers is a polyolefin (PO). Cycloalkanes are called naphthenes, and aromatics maintain their name aromatics.

2.1.1.1 Polymerization and Depolymerization

Polymerization is the reaction mechanism of linking monomers together to form polymers, whereas depolymerization is the mechanism of breaking polymers into their smaller building blocks (e.g., monomers and oligomers). There are two categories of polymerization: addition polymerization and condensation polymerization. Addition polymerization is the addition of monomers to build a polymer without creating any by-products. Condensation polymerization produces by-products when bonding two monomers, with H_2O being the most common by-product [12].

Condensation polymerization is often also referred to as step-growth polymerization, due to the polymerization occurring in steps. Initially, two monomers join to form a dimer with the condensation of a by-product. As mentioned, this is often water, but methanol (CH_3OH) is also a typical by-product. Two dimers are then joined to form an oligomer, with again condensation of a by-product. This carries on in steps, building oligomers of increasing weight, finally resulting in polymers. Condensation polymers typically have either ester, ether, or amide bonds, see figure 2.1, which can be depolymerized through solvolysis [18].

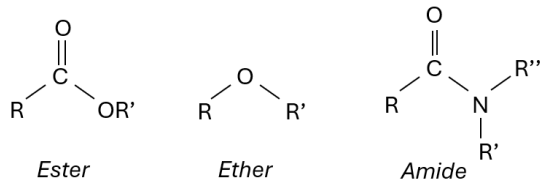

Figure 2.1: Ester, ether and amide bond often found in condensation polymers.

Polyethylene terephthalate (PET) is an example of a plastic produced by condensation polymerization [18]. By-products from condensation polymerization are often valuable raw materials in themselves and can be recycled back into the feed stream or used for other purposes. Methanol, for example, can itself be used in plastic production, as is described in section 2.1.4 *Plastic Feedstock Production*.

Addition polymerization is often referred to as chain growth polymerization. This polymerization mechanism adds monomers sequentially to a growing polymer chain [18]. Unsaturated hydrocarbons are normally used in addition polymerization, as breaking open the double or triple bonds attaches the monomers without condensation. Polymerization of, for example, PP, PE, and PVC occurs through this mechanism [18].

Propagation of the polymer chain, in addition polymerization, can occur through four reaction mechanisms: free radical reaction, anionic reaction, cationic reaction, or coordination polymerization [18]. All these mechanisms use some sort of initiator (radical species, base, acid, or transition metal complex) that reacts with the unsaturated carbon bond, forming a reactive propagation site (carbon radical, carbanion, carbocation, or terminal catalytic complex) [19]. Figure 2.2 illustrates the addition polymerization mechanism.

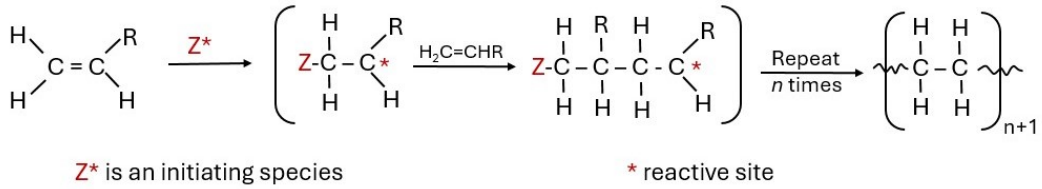

Figure 2.2: Addition polymerization.

Depolymerization occurs through chain scission, breaking the polymer chain and splitting it into smaller parts. This is usually carried out by adding heat until the vibration energy exceeds the bonding energy, proceeding to crack the chemical bonds (i.e., thermal degradation) [20]. Depolymerization entails four possible degradation mechanisms: random-chain scission, end-chain scission, chain-stripping, and cross-linking. Random-chain scission is when the polymer backbone breaks at random points, producing oligomers. End-chain scission is also known as unzipping and, as it sounds, unzips the polymer by breaking the bonds at the end of the macromolecule, producing parent monomers [21]. Chain stripping is when side chains, also called branches, attached to the polymer backbone are broken off, stripping the polymer backbone [22]. Cross-linking is when new bonds are formed during the thermal degradation process between different polymer chains or between two parts of the same chain. This gives rise to a more tangled 3D molecular structure, which often causes char formation. It is often not a single degradation mechanism occurring exclusively, but rather a mix [21]. The chain scission mechanisms often result in radical formations, and thermal degradation is therefore, in most cases, observed to have an initiation, propagation and termination step. This is due to the initial homolytic bond scission, caused by added heat, producing free radicals. Depending on the polymer the molecular structure will be different, affecting the thermal decomposition. This consequently has an effect on product formation from the thermal decomposition [20]. The temperature of the thermal decomposition also affects chain scission, with higher temperatures causing a greater extent of chain scission and consequently lighter product formation [23].

The term depolymerization is primarily used to describe the process of unzipping polymers into monomers, ready for conversion into new plastics. The term thermal decomposition is more commonly used when referring to the cracking of polymers that produces a mixture of hydrocarbons.

2.1.1.2 Polymer Heat Conductivity

Heat transfer in polymers occurs through phonon heat transfer (vibrations in the crystal lattice) as most polymer molecules do not have any free electrons. The crystallinity of a polymer affects the phonon heat transfer and thereby its thermal conductivity.

Crystalline regions have higher thermal conductivity than amorphous regions at the same temperature due to the phonon mean free path being greater in ordered crystalline regions. Amorphous regions experience faster phonon collisions and scattering due to their inherently disordered structure, both factors decreasing the phonon mean free path and thereby causing slower heat transfer and decreased thermal conductivity.

The crystallinity is affected by temperature as increasing temperature causes melting of the crystalline regions, disrupting their ordered lattice structure. Consequently, the thermal conductivity of crystalline polymers decreases with increasing temperature (to melting point). Amorphous polymers and regions also experience a decrease in thermal conductivity with increasing temperature. Phonon vibration increases with increased temperature which in amorphous regions lead to increased phonon interaction and collisions, in turn causing more scattering which decreases the phonon mean free path [24].

2.1.2 Municipal Solid Waste

Plastic packaging makes up 40% of the plastic waste generated globally, due to its short life time [1]. A lot of the plastic waste from households is made up of plastic packaging and consumer products, both with short life times. Municipal solid waste (MSW) describes the everyday waste from households, institutions (hospitals, schools, etc.) and businesses. In 2010, plastic made up 12.4%, approximately 30 million tons (Mton) of the total 250 Mton of MSW in the USA [25]. In 2017, the plastic packaging waste in Sweden was approximately 325 kton. Based on waste analyses (in Swedish *plockanalyser*) carried out by *Förpacknings- och tidningsinsamlingen*, the plastic packaging waste was primarily made up of four types of plastic; 36% low-density polyethylene (LDPE), 16% high-density polyethylene (HDPE), 22% PP and 17% PET. The remaining 9% of the plastic waste was made up of other plastics [26]. The plastic fraction of MSW is often termed plastic solid waste (PSW) or mixed plastic waste (MPW). PSW seems to in some cases include plastic waste from industries rather than solely describing the plastic fraction of MSW. In this work, the term MPW will be primarily used to describe the plastic waste fraction of MSW. According to the OECD, plastic packaging and consumer products made up 40% and 12% of the global plastics use. The most commonly used polymers and their fractions in 2019 were 5% PET, 12% HDPE, 12% LDPE, 16% PP, 11% PVC, 5% polystyrene (PS), 13% fibres, 4% polyurethane (PUR) and 22% others [1]. The data from the OECD and *Förpacknings- och tidningsinsamlingen* show that PE, PP, PET and PVC are some of the most commonly used plastics and are major components of MSW [27].

Polyethylene, PE

PE is one of the most common plastics used in Europe, together with PP [26]. It is a saturated polymer produced by addition polymerization of the monomer ethylene

C_2H_4 [28]. Ethylene is an olefin, making PE a polyolefin. Depending on the degree of polymerization, PE polymers with different molecular weights can be produced [29]. Thermal degradation of PE, like other polyolefins, occurs through all four chain scission mechanisms, resulting in a mix of hydrocarbon fractions [21]. Figure 2.3 illustrates the repeating monomer units that make up PE.

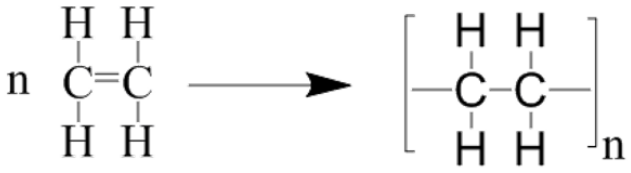

Figure 2.3: Chemical structure of PE. [30]

Branching is used to create different PE polymers. LDPE is a PE with a high branching degree (both long and short branches), giving rise to a low density as it has relatively low crystallinity. HDPE has a low branching degree, giving it a higher crystallinity and higher density. Linear-low-density polyethylene (LLDPE) is a third common PE that, similar to LDPE, has a higher degree of branching but retains a more linear structure due to it's shorter branches [31]. Figure 2.4 shows a schematic of the three PE polymers' structures.

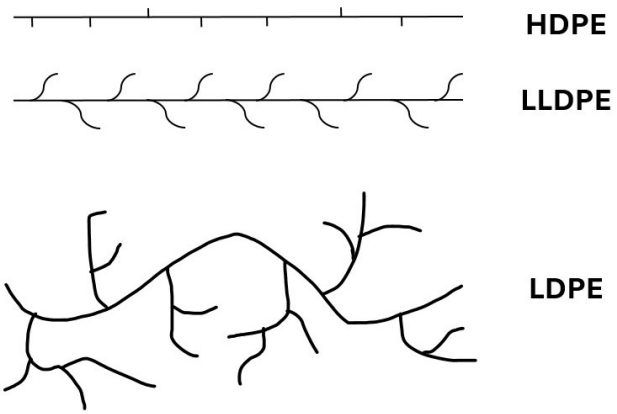

Figure 2.4: Illustration of branching for HDPE, LLDPE and LDPE.

LDPE is typically used for reusable bags, milk carton coatings, and food packaging film (a softer, more flexible plastic). LLDPE is often used for plastic film and bags. HDPE is typically used for crates and boxes, bottles (for food products, detergents, cosmetics), food containers, toys, petrol tanks, industrial wrapping and film, pipes, and houseware (i.e., a harder and more rigid plastic). PEs are thermoplastics [32].

Polypropylene, PP

PP is a linear saturated polymer formed through addition polymerization of propylene monomers C_3H_6 [28]. Its repeating monomer unit is shown in figure 2.5. PP is also a thermoplastic and polyolefin. PP has a lower density, a higher softening point, higher rigidity, and higher hardness than PE. PP's properties can vary due to the isomerism the methyl group (CH_3) imposes [33]. PP is used for many different applications, typically food packaging (yoghurt pots, margarine pots, sweet and snack wrappers), microwave-proof containers, carpet fibres, garden furniture, medical packaging and appliances, luggage, kitchen appliances and pipes [32].

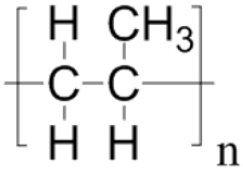

Figure 2.5: Chemical structure of PP. [34]

Polyvinyl chloride, PVC

PVC is a thermoplastic polymer made up of vinyl chloride monomers (VCMs), C_2H_3Cl, as shown in figure 2.6. The VCM is produced by combining chlorine (Cl) and ethylene C_2H_4 [35]. The two previously mentioned polymers, PE and PP, are considered crystalline (even though they still contain amorphous regions), whereas PVC is an amorphous polymer. This is due to the halogen Cl having high electronegativity and therefore a polarizing effect [36]. PVC is produced through addition polymerization of VCMs [37].

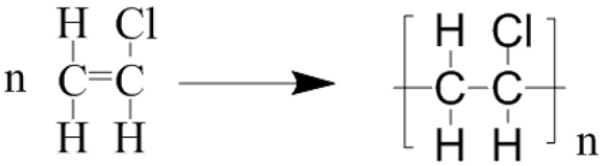

Figure 2.6: Chemical structure of PVC. [38]

PVC is, by itself, a rigid plastic, but with plasticizer additives, it can become flexible. Because of the chlorine, the plastic exhibits chemical stability and is significantly less prone to oxidation compared to polyolefins [36]. PVC is used in many applications

such as window frames, profiles, flooring, pipes, cable insulation, garden hoses, and inflatable pools [26].

Polyethylene terephthalate, PET

PET is a thermoplastic polyester, with ester groups (R-CO-OR) present in the polymer backbone. Depending on how it is cooled during production, it can be either amorphous or semi-crystalline [39]. It is produced by combining ethylene glycol ($C_2H_6O_2$) and terephthalic acid ($C_6H_4(CO_2H)_2$) or ethylene glycol and dimethyl-terephthalate ($C_6H_4(COOCH_3)_2$) through condensation polymerization. The two different reaction pathways result in the same polymer but with different condensation by-products [40]. Figure 2.7 shows the two pathways and the resulting polymer PET.

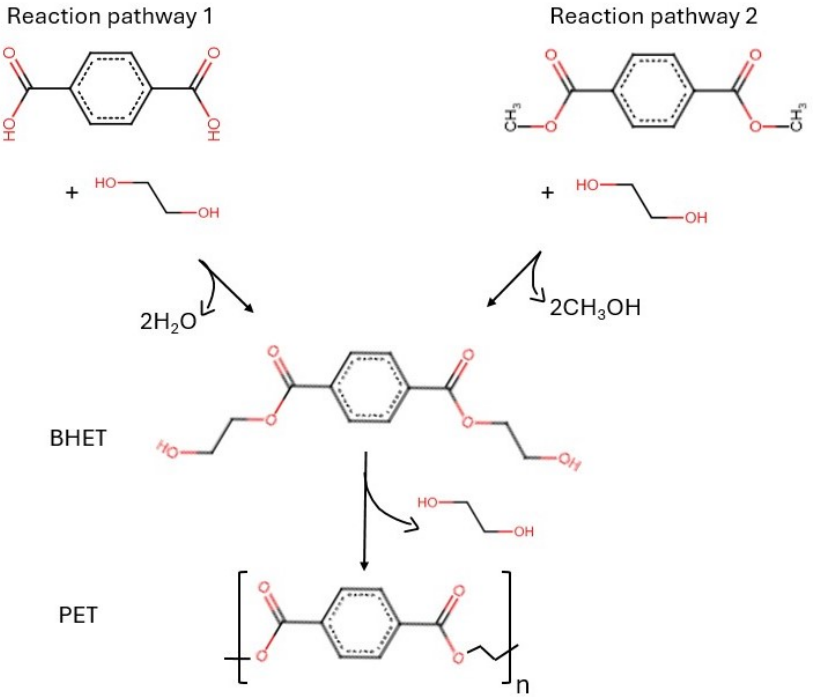

Figure 2.7: Polymerization and chemical structure of PET.

PET is commonly used for plastic bottles [26]. PET bottles are different from the other fractions that make up MPW as they are often separate from other waste streams and recycled to a high extent. In Sweden, like many other countries, there is a deposit return scheme (*pant* in Swedish) in place that specifically separates PET from other plastic waste streams, which allows for a high degree of mechanical recycling [41]. However, issues with downgrading through mechanical recycling remain, driving ongoing research for chemical recycling of PET [42].

2.1.3 Tetra Pak's Packaging Material

Tetra Pak offers a range of paper-based packaging, of different sizes and geometries, for food products. The anatomy of Tetra Pak carton material is shown in figure 2.8. The primary material used is paperboard, making up on average 75 wt% of the packaging. The remaining part is 20 wt% protective layers of polymers (LDPE), approximately 5 wt% aluminium [43]. As mentioned in the introduction, 178 billion packages were sold in 2024. The annual material sourcing, for the same year, was 2.2 million tonnes of paperboard, 145 000 tonnes of aluminium, and 700 000 tonnes of polymer [9].

Figure 2.8: Anatomy of an ambient Tetra Pak packaging material. [9]

The outermost LDPE layer protects the package from moisture. The following layer of paperboard gives the carton its strength and rigidity. In the aseptic packages, the LDPE layer on the inside of the paperboard adheres the aluminium foil (alufoil) to the paperboard. The aluminium foil protects the product against light and oxygen, provides additional stiffness, and enables induction sealing. The alufoil is coated with an adhesive PE layer, adhering the protective innermost LDPE layer, which in turn works to seal the package (protection from leakage) and protects the food product inside. The alufoil and polymer layers are often referred to as polyAl, especially in circumstances regarding the

product's end of life. The carton caps and closures are usually made of HDPE and PP [9].

Tetra Pak's packages are used for food, and when the consumer has consumed the food, the package is discarded. In places where waste management systems are in place, these packages are collected from households and sent to recycling/waste treatment facilities. Most of the collected cartons are sent to paper mills, where the paperboard fibres are separated from the polyAl by using a pulper. Recovery of fibres is a developed and established recycling pathway, but not available in all locations. Tetra Pak works continuously with investments in and development of recycling facilities and their availability around the world. The polyAl is extracted from the pulp in the paper mill and is then sent to a selected polyAl recycler if possible. The polyAl recycler processes the polyAl using mechanical recycling methods, which often include washing, drying, shredding and pelletizing. Chemical separation of aluminium and polymer can be included in the recycling process. The recycled polyAl material is not reused for food packaging, rather it is used to produce for example plastic pallets, crates, cable drums, bird feeders, furniture and construction applications [44]. As mentioned previously, there are downsides to mechanical recycling. This, combined with fossil resources being finite, is driving the need for circularity in plastic production and use, explaining Tetra Pak's increased attention to chemical recycling.

2.1.4 Plastic Feedstock Production

Synthetic plastics dominate the global plastics market, with bio-based plastics making up a very small share. The description of plastic feedstock production will therefore be limited to synthetic plastic feedstock. Synthetic plastics are derived from three different fossil-based sources: natural gas, coal, and crude oil.

Crude oil is pumped up from underground reserves and is a liquid mixture, containing some solid and gaseous fractions, of primarily hydrocarbons of various sizes. In addition to the hydrocarbons, there are small fractions of other organic compounds and metallic compounds. The gaseous phase is dissolved in the liquid phase and consists of light alkane hydrocarbons (CH_4, C_2H_6, C_3H_8 or C_4H_{10}) [12]. The solid phase is also dissolved in the liquid phase and made up of waxes (high molecular weight hydrocarbons) [45]. The crude oil composition depends on extraction location, but the number of different hydrocarbons in a specific crude oil is often found to be around 350 [46].

Crude oil is processed in oil refineries where the different hydrocarbons are separated through fractional distillation. Before distillation, contaminants such as water, inorganic salts, suspended solids, and water-soluble trace metal contaminants are removed through desalting. This is often an integrated part of the crude oil distillation unit [46]. The fractional distillation separates the different hydrocarbons depending on their molecular weight and boiling point. At the top of the distillation column, the temperature is cooler ($< 25°C$) and at the bottom it is considerably hotter ($\sim 350°C$). This temperature

gradient allows separation of hydrocarbon vapour fractions, as depending on their size they will condense at different levels in the column. Lighter hydrocarbons have lower boiling temperatures and these vapour fractions therefore flow to the top of the column. Heavier hydrocarbons have higher boiling temperatures, meaning they condense at lower levels in the column. Solids (the heaviest hydrocarbons) have the highest boiling temperature and remain at the bottom of the column. Typically, outflow from a fraction distillation column would be (in order of lightweight to heavy fractions): petroleum gas (primarily propane and butane [47]), naphtha, paraffin (kerosene), diesel, fuel oil, lubricating oil and bitumen. The different fractions all have different applications, with plastic production using primarily naphtha and petroleum gas [12]. Figure 2.9 shows the various hydrocarbon fraction ranges. PP, PE and PVC are all derived from cracked naphtha [12].

	Number of carbons	Boiling point range	Uses
Gases	1–4	0–30°C	Bottled and natural gas
Naphthas	5–10	30–180°C	Gasoline
Kerosenes	10–16	180–260°C	Kerosene for home heaters, jet fuel
Gas oils	16–60	260–350°C	Diesel fuel, feedstock for cracking
Lubricants	>60	350–575°C	Motor oil, feedstock for cracking
Fuel oil	>70	>490°C	Candles, fuel oil for ships and power stations
Asphalt	>80	>580°C	Roofing tar, road tar

Figure 2.9: Petroleum fractions and their carbon-atom-ranges. Reproduced with permission [48].

Naphthas are hydrocarbons with 5-10 carbon atoms. As mentioned, these are extracted primarily through crude oil distillation but can also be extracted from natural gas condensation (for example, pentane C_5H_{12}). By thermally cracking naphtha in a steam cracker, i.e., heating it to very high temperatures ($\sim 800°C$), causing it to decompose in the presence of water vapour, the naphtha hydrocarbons are split into major intermediates. The major intermediates consist of olefins (for example, ethylene and propylene) and aromatics (including benzene, toluene and xylene) [12]. Olefins are the main feedstock in PP, PE, and PVC plastic production. Aromatics are also used as feedstock for production of other plastics. They are for example used in PET and PS production. Mixtures of benzene, toluene and xylene are called BTX. The building blocks of PET are tereph-

thalic acid or dimethyl-terephthalate and ethylene glycol. Ethylene glycol $C_2H_6O_2$ is produced by oxidation and hydrolysis of ethylene. Xylene (C_8H_{10}) is a benzene ring with two methyl groups, also known as dimethylbenzene. The methyl groups' positions allow three xylene isomers: para-xylene, ortho-xylene and meta-xylene. Para-xylene is the building block for terephthalic acid which is produced by oxidation of para-xylene. Dimethyl-terephthalate is produced through further reaction of terephthalic acid and methanol [40].

Coal can be used as a source for plastic production feedstock through a process called coal-to-liquid (CTL) production. The first step of CTL is gasification of coal, which produces syngas [49]. Gasification is described in section *2.2.1.2 Gasification*. Syngas, or synthesis gas, is a versatile gas that can be used for multiple purposes, including fuel in electricity production or as feedstock in chemical production industries. It consists primarily of hydrogen (H_2) and carbon monoxide (CO), but also includes carbon dioxide (CO_2), methane (CH_4), nitrogen (N_2), water vapours (H_2O), other hydrocarbons and condensible compounds [50]. Syngas can in principle, be made from any hydrocarbon feedstock. Following the gasification step, the syngas (containing H_2 and CO) can be processed in a Fischer-Tropsch process which produces liquid hydrocarbons. The Fischer-Tropsch process is a series of chemical reactions that occur in the presence of a metal catalyst at elevated temperatures and pressure. It produces liquid hydrocarbons (C_nH_{2n+2}) in the gasoline-range (C_6-C_{12}) and diesel-range (C_{10}-C_{28}), i.e., naphtha, kerosene and some gas oils [51].

Methanol is not only used as feedstock in PET production but can be used as a feedstock to produce olefins or gasoline, which in themselves can be used as feedstock in plastic production. This is done through either a process called methanol-to-olefins (MTO) or a process called methanol-to-gasoline (MTG). MTO/MTG are processes that convert methanol into a mixture of hydrocarbons (olefins, aliphatics and aromatics) in a rather narrow range (gasoline range) up to C_{10} through a series of chemical reactions [52]. From MTO, ethylene and propylene can be produced. In the petrochemical industry, methanol is primarily produced from syngas, which in turn is obtained primarily from either gasification of coal or steam reforming of natural gas [53]. However, MTO is interesting as it is possible to produce methanol from biomass, offering a green alternative to plastic production using methanol [54].

Natural gas can be used to produce feedstock for PE [55], PP [56] and, as mentioned above, PET [40] production. The composition of natural gas varies depending on reservoir location, similar to crude oil composition, but is primarily made up of methane (70-90%). The remaining 30-10% consists of the hydrocarbons ethane, propane, butane, pentane and some non-hydrocarbon contaminants [57]. The ethane (C_2H_6) is separated from the other gas components and then thermally cracked, producing ethylene (C_2H_4). Thermal cracking means that the ethane is heated to very high temperatures [55], causing the bond configuration to change from a single bond to a double bond between the carbon atoms and eliminating H_2. Propane is also extracted for plastic feedstock production. Similarly to ethane, propane (C_3H_8) is cracked at elevated temperatures

producing propylene (C_3H_6) [56]. This is also how petroleum gases from crude oil fractional distillation are treated for plastic feedstock production.

As described, there are several ways to produce plastic feedstock but the primary feedstock type is naphtha, produced from the cracking of crude oil. This means that in order for a chemical recycling process for plastics to serve the purpose of increasing circularity in plastic production, the product outflow from the recycling process would preferably be naphtha. Processes producing syngas or lighter olefins (ethylene and propylene) would also be beneficial. This would allow products from chemical recycling to replace virgin fossil feedstock in existing petrochemical industries. Designing a chemical recycling process for plastics that produces naphtha could enable plastic-to-plastic recycling.

2.2 Chemical Recycling Processes

Chemical recycling of plastics can be divided into two main categories: solvolysis and thermolysis. Thermolysis is in simpler terms thermal decomposition. This category covers plastic recycling methods where heat is used to decompose plastics and fragment the polymers. The polymer fragments can be made up of smaller polymers, oligomers or monomers [7]. Solvolysis of polymers is the process of polymer decomposition through the use of solvents, resulting in either complete or partial depolymerization through chemical reactions between the solvent and polymer. Solvolysis is, in general, only suited for homogenous plastics and usually requires the polymer to contain heteroatoms [1]. There are different chemical recycling solvolysis processes for plastics and they differ in what type of solvent is used. This is reflected in the process names (hydrolysis, alcoholysis, methanolysis, glycolysis, and aminolysis) [1]. The solvent used depends on the plastic's composition, i.e., which polymer is the target for depolymerization and what the desired product is. Depending on the polymer and solvent, solvolysis can result in either complete depolymerization, producing a monomer feedstock available for re-polymerization, or partial depolymerization, producing other valued products [58].

Apart from these two main categories, there are currently a few chemical recycling methods considered more novel, where research is also being conducted [7]. These include photocatalytic methods, biotechnology, and electrochemistry. The photocatalytic methods encompass both photodegradation and photosynthesis depending on how the plastic waste is viewed (either as waste that you want to minimize or as a resource for chemical conversion). However, both pathways make use of chemical reactions driven by light, hence "photo" catalytic. The biotechnology methods also cover two areas: biological destruction and biological upcycling. Similar to photocatalytic methods, the difference lies in the desired outcome, where biological destruction aims to break down and degrade plastics, whereas biological upcycling uses plastic as a resource to create new desired compounds through biochemical reactions. The biotechnology

methods use microorganisms and enzymes in their recycling processes [7]. Lastly, the electrochemistry methods cover technologies where depolymerization is carried out through chemical reactions driven by electrical charge differences. Electrochemistry uses electrons as reagents and the reactions can be controlled in detail by controlling this supply. If the electrons are derived from renewable energy sources, such as wind and solar power, waste from the recycling process is further reduced as production of oxidant/reduction agents are avoided [59].

All of the aforementioned novel recycling methods face similar challenges, particularly with low conversion efficiencies, and can only be considered as emerging technologies. The novel methods show potential as sustainable processes in the future, partially due to their low energy consumption compared to the energy consumption required for the more mature technologies of thermolysis [7].

Within the field of plastic recycling, there are also different levels of recycling: primary, secondary, tertiary, and quaternary. Primary recycling refers to recycling of plastic material collected during the plastic production process, i.e., the recycling feedstock is made up of post-industrial, pre-consumer, uncontaminated single plastic waste. This recycling is viewed as a closed loop as it in simpler terms, recycles plastic scrap/excess product from the production process. Primary recycling is an established recycling path used in the industry. Secondary, tertiary and quaternary recycling refer to the recycling of post-consumer waste (PCW). Secondary recycling covers mechanical recycling. Tertiary recycling refers to chemical recycling producing value-added products (feedstock used for other purposes than plastic production) or feedstock for re-polymerization. This latter tertiary recycling is also known as plastic-to-plastic recycling, waste-to-plastic recycling or chemical recycling to monomer (CRM). An example of value-added product recycling is waste-to-fuel recycling. Quaternary recycling refers to energy recovery processes, also known as waste-to-energy (WTE) recycling [60].

As the aim of this thesis is to build a chemical recycling process model using CFD-DEM, both the solvolysis recycling methods and the third group of novel recycling methods are inappropriate. The solvolysis methods require significant chemistry knowledge and would entail modelling of detailed chemical kinetics. The novel recycling methods rely primarily on mechanisms outside of fluid mechanics. The remaining category thermolysis, is delved into further.

2.2.1 Thermolysis

The thermolysis process category includes the overarching methods of pyrolysis, gasification, and hydrocracking. These can in turn be combined or modified in different aspects, creating several different methods/subcategories all categorized as thermal or thermo-chemical decomposition treatments. There are not always clear distinctions between thermolysis processes. The three overarching methods are further explained in respective sections below. Figure 2.10 shows an overview of the primary chemical

recycling pathways for mixed plastic waste and the product outflows of the respective processes.

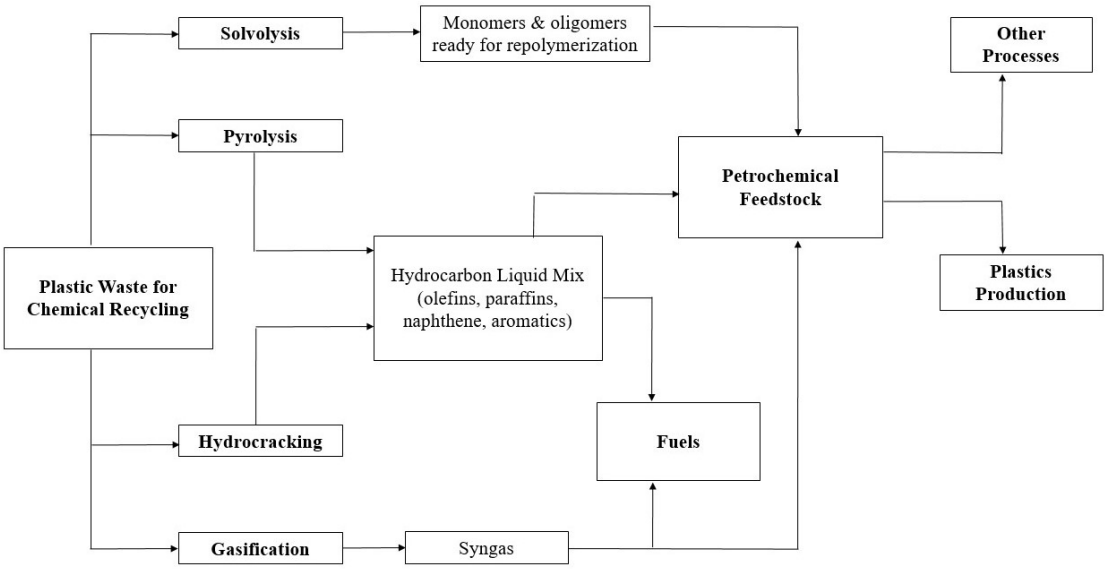

Figure 2.10: Chemical recycling pathways for plastic waste.

2.2.1.1 Pyrolysis

Pyrolysis is a thermal decomposition method for organic materials carried out by heating the materials in an anoxic environment. If the process was carried out in an oxic environment, it would be combustion or gasification, depending on the oxygen level. Exposing polymers to high temperatures in an anoxic environment causes the polymers to break down, producing a mixture of hydrocarbons. The high temperatures are necessary to break the endothermic covalent bonds within the polymer. The pyrolysis operating temperature depends on the process and feedstock, but typically temperature ranges of 300°C to 900°C are used. The oil product stream contains both liquid and gaseous fractions and can also include solid (char) fractions. The liquid products are condensible gases, whereas the gas products are non-condensible gases. The oil product is often referred to as pyrolysis oil or pyrolytic oil, and it is usually only the liquid fraction that is the desired product. When referring to pyrolytic oil, it can mean the entire product outflow, but in most cases it only refers to the liquid product. In this thesis, pyrolysis oil or pyrolytic oil will only refer to the liquid product stream. The pyrolytic oil can be treated further to achieve a feedstock that can be re-polymerized, similar to refining of crude oil or naphtha cracking [21]. The gas product stream can also be used in plastic-to-plastic recycling. Light hydrocarbon gases like propane and ethane, which can appear in the gas product stream depending on the parent polymer and the pyrolysis process, can be separated and used as feedstock in polyolefin production. Pyrolysis is a process method appropriate for plastic-to-plastic recycling, waste-to-fuel recycling, and waste-to-energy recovery [61].

Due to the high temperatures and energy required to break the endothermic polymer bonds, pyrolysis is considered an energy-intensive process. Additionally, further energy use is required for downstream treatment of pyrolytic oil to produce monomeric feedstock used for re-polymerization. The high temperatures permit the use of contaminated plastics in pyrolysis, allowing treatment of mixed plastic waste feedstock. Contaminations typical for post-consumer plastic waste are food, dirt, oil residues, printing ink, aluminium laminates (present in polyAl), etc. The level of contamination will affect the product yield, with a higher degree of contamination producing more tar and char [21]. These undesired by-products are further explained in section *2.2.1.2 Gasification*.

A general pyrolysis process setup consists of a feeding section, a reactor unit and product collection units with product separation functions and purification. As mentioned, pyrolysis produces liquid and gaseous hydrocarbon fractions. It also produces the solid fraction char, especially if the waste feedstock contains inorganic molecules. Char causes reactor fouling, but is in some pyrolysis processes a desired product. The products from pyrolysis evidently depend on the parent polymer or polymers involved. Product yield and composition can also be affected by tailoring certain process parameters. This allows tuning of the process to desired needs. The two main process parameters that have the most significant impact on product selectivity are temperature and reactor type. Other key process parameters are for example pressure and residence time [21].

Temperature controls breaking of the endothermic covalent bonds between polymer constituents. With high enough temperatures, enough energy is supplied to overcome the enthalpy of the otherwise stable bonds within the polymer. In general, polymers with more stable bonds such as polyolefins (C-C and C-H bonds) require higher pyrolysis temperatures whereas those with weaker bonds, i.e., polymers containing heteroatoms (C-X bonds) require lower pyrolysis temperatures. Plastics are, as stated, not made up entirely of polymers but also additives. Most of the additives will evaporate during pyrolysis, but some affect the chemical kinetics and mechanisms of the polymer decomposition, requiring modification of pyrolysis temperature. Tailoring of the process temperature can as mentioned impact product composition and yield. Generally, higher pyrolysis temperatures will result in a larger gaseous product fraction (smaller hydrocarbons) and lower pyrolysis temperatures will promote a larger liquidus product fraction (larger hydrocarbons) [21].

The cracking, or degrading, of the polymer backbone (i.e. the main hydrocarbon chain) depends on the polymer involved. Polyolefins (such as PE and PP) degrade primarily through random chain scission. The C-C bonds break at random points throughout the polymer backbone, producing a mix of smaller hydrocarbons of different lengths. For example, pyrolysis of HDPE produces a pyrolytic oil made up of a mix of waxes, paraffins and olefins. The pyrolytic oil from pyrolysis of polyolefins can be further refined through hydrotreatment (a reaction process with hydrogen used in oil refineries) to produce a feedstock appropriate for re-polymerization. Other plastics, such as PS, experience end-chain scission when pyrolysed and are thereby depolymerized directly into the constituent monomers. Polymers containing heteroatoms, such as PET or PVC,

complicate the pyrolysis process and are not ideal feedstock. Pyrolysis is an anoxic environment process and introducing a feedstock with polymers containing oxygen, such as PET, is not ideal. Polymers containing halogens need to go through a dehalogenation pre-process treatment as the halogens otherwise can go on to form hazardous and toxic compounds in the pyrolysis process. This does not mean that pyrolysis is not possible for polymers containing heteroatoms, only that the process design becomes more complex. The resulting product stream for these types of polymers differs in quality and application (usually fuels) compared to those derived from polyolefins, especially for those containing halogens. Pyrolysis of heteroatom-containing polymers can also produce corrosive compounds, complicating the process further. Polyolefins are therefore a more ideal feedstock for pyrolysis [21].

Within the pyrolysis category there are several methods and reactor types, however the main variation lies in whether the process uses heat to crack the polymers or if the process combines heat and catalysts to crack the polymers. The former method is known as thermal pyrolysis or thermal cracking, and the latter is known as catalytic pyrolysis or catalytic cracking. Catalytic pyrolysis uses catalysts, which lower the activation energy required for polymer scission. Consequently, catalysts reduce energy required for cracking [60]. One of the major limitations in scalability of pyrolysis for chemical recycling of plastics is its high energy requirement to achieve the necessary high temperatures for depolymerization. Some of the main areas of pyrolysis research is on how to decrease necessary operating temperatures, improving heat transfer and methods for improving product value and product selectivity [21]. Catalytic pyrolysis is one method of decreasing the energy requirement, others worth mentioning are plasma and microwave assisted pyrolysis. Most pyrolysis processes occur in an inert gas medium but it is possible to use other media. One such pyrolysis method, with advantages for pyrolysis of heteroatom containing polymers or contaminated plastic waste, hydrothermal liquefaction.

Catalytic Pyrolysis

Introducing catalysts in plastic pyrolysis processes has shown to decrease pyrolysis temperature and increase the quality of the pyrolytic oil yield [60]. Catalysts make the reaction processes more controllable and can be used as a tool to achieve increased product yield, quality and selectivity [60]. Some sources report that the pyrolytic oil yield is increased in catalytic cracking compared to thermal cracking[60], whereas others report a decrease in liquid oil yield, although with improved quality, and an increase in the gaseous fraction [61].

Depending on the plastic being pyrolysed and aim of the pyrolysis (desired product selectivity for example), the choice of catalyst will vary. In catalytic processes, either homogeneous catalysts (same phase as reactants) or heterogeneous catalysts (different phase to reactants) are available. Heterogeneous, usually solid, catalysts are more common in industrial applications as they are easier to separate and recover. Depending

on the catalyst's properties, it will interact differently with the polymer feedstock. This adds to the list of key process parameters that can be tailored to suit the design purpose [21]. The catalyst properties of interest in pyrolysis are acidity/basicity, porosity, crystallinity and BET surface area (the latter three particularly relevant for solid catalysts). For solid heterogeneous catalysts the polymer cracking is initialised at the catalyst's external surface. The resulting cracked hydrocarbons are then selectively drawn into the catalyst's pores. The porous structure of the catalyst will promote selective movement of polymer molecules and further catalytic cracking occurs on the catalyst's internal surfaces. This selectivity of the catalyst's textural properties causes formation of lighter hydrocarbons, i.e. pyrolytic gaseous products, to form primarily inside the pores and heavier oils or waxes to form on the catalyst's external surface. Porosity (pore size and volume), crystallinity and BET surface area all affect this textural selectivity of the catalyst. Depending on the catalysts chemical composition and structure, different reaction pathways will be possible, contributing to product selectivity. The choice of catalyst must however also be tailored to the chemical composition of the intended plastic waste. [61]

Microwave assisted pyrolysis

Microwave assisted pyrolysis is a method for electric-heated pyrolysis where the plastic waste is mixed with a highly microwave-absorbent dielectric material. The dielectric material absorbs the microwave energy, causing its molecules to vibrate which generates thermal energy. The thermal energy is transferred to the surrounding plastic through conduction. As the plastic is mixed with the dielectric material, this method allows a more even heat distribution, more rapid heating, lower residence time and an increase in control of the process [60]. Plastics have low thermal conductivity, causing low rates of heat transfer through the feedstock and consequently longer residence times for pyrolysis. The microwave assisted pyrolysis not only offers improved heat distribution and heating rates but is also more energy efficient as the microwave energy is transferred directly to the feedstock polymers and not wasted in heating the surrounding area of the pyrolysis chamber. Insufficient knowledge of the dielectric properties of plastic waste streams, especially mixed plastic waste streams, remains a challenge for microwave assisted pyrolysis [21]. The microwave's penetration depth is also quite limited. It only penetrates a few centimetres into the plastic, limiting it's applicability in handling large volumes of plastic waste [23].

Hydrothermal liquefaction

Hydrothermal liquefaction (HTL) is a pyrolysis method where the reaction medium is subcritical or supercritical water (SCW), rather than an inert gas medium [21]. At these conditions, water's physical and chemical properties are altered, making it a good solvent for organic compounds. The use of supercritical water or subcritical water

depends on the polymer feedstock undergoing depolymerization. Subcritical water can be used to depolymerize polymers containing heteroatoms (like PET) whereas supercritical water is needed for depolymerization of polyolefins. For both sub- and supercritical water, the water's dipole moment is decreased to the extent it can dissolve apolar organic polymer compounds. Subcritical water is sufficient for depolymerization of heteroatom polymers. The water retains some of it's polarity, allowing it to hydrolyse the polarised heteroatom bonds. However, the stronger C-C bonds in polyolefins require harsher conditions, i.e. supercritical water for depolymerization [62]. HTL is viewed as a promising method for plastic-to-plastic recycling as it increases liquid oil yield, decreases coke formation and water has the ability to react with organic contaminants present in the plastic waste whilst simultaneously cleaning the hydrocarbon liquid oil yield from these contaminants as they remain in the aqueous phase [63]. One challenge with HTL is the corrosive effect of SCW [21].

2.2.1.2 Gasification

Gasification is a process similar to pyrolysis, with the difference being higher process temperatures (700°C-1500°C) and a reactive environment. Gasification converts the plastics (or other organic solid materials) into a gaseous mixture (syngas). The elevated process temperatures, compared to pyrolysis, consequently entail a higher energy requirement [21]. In addition to syngas, tar and char is also produced [7]. Gasification does not use an inert environment like pyrolysis, instead a reactive environment is used. A simplified distinction between pyrolysis, gasification and combustion is the increasing amount of oxygen present. Pyrolysis occurs in an anoxic environment, gasification occurs with substoichiometric oxygen (significantly lower than stoichiometric) and combustion occurs with stoichiometric or excess oxygen present [64]. However, emphasis on *simplified* is key here as oxygen is not the only gasifying agent used to partially oxidize the organic solids in gasification processes. Typical gasifying agents used are air, oxygen, steam or CO_2, all used in controlled substoichiometric amounts [7].

The two by-products, tar (gaseous/liquid phase) and char (solid phase), formed during gasification are generally undesired. Tar consists of condensible higher molecular weight hydrocarbons, predominantly aromatics, and is present in the gaseous phase, thereby polluting the syngas. Tar decreases the syngas quality as it limits downstream use of syngas due to, for example, fouling or clogging of instruments. Its formation is inevitable in gasification but efforts to decrease tar formation are ongoing. The tar formation will depend on gasification process parameters (such as temperature and gasifying agent) and plastic waste composition. Often, the syngas produced must however still be cleaned to an extent depending on the downstream purpose. Tar appears as gaseous phase in syngas and condenses into fine droplets downstream. With lower concentrations of tar in the syngas the dew point of the tar is lowered, allowing lower operating temperatures without

condensation of the tar. Consequently this also allows lower operating temperatures for downstream processes using said syngas [65].

Char is a carbon-rich solid material that forms from the incomplete thermal degradation of the solid organic waste. It is present in both pyrolysis and gasification. Char also contains inorganic material, if this is present in the waste feedstock. Production of char in gasification (and pyrolysis) is undesired as it acts as a residue that needs to be removed and decreases efficiency explained by the lower conversion. Char production is usually low for gasification of plastics as polymers generally have high volatile content. However, this material property of high volatile content in polymers contributes to increased tar formation [60].

The commonly used gasifying agents are air, oxygen, steam or CO_2. Air gasification is considered a more simple and cheaper method out of the four, but generally produces lower quality syngas. This is due to the N_2 present in air which dilutes the syngas. One downside of air gasification is the formation of the potent atmospheric pollutant NO_x [21]. Oxygen gasification produces higher quality syngas than air gasification. There are methods using oxygen enriched air as gasifying agent and methods using pure oxygen as gasifying agent. Pure oxygen gasification produces higher quality syngas but requires oxygen separation from air, significantly increasing the process cost [60]. Steam gasification uses water vapour (steam) as gasifying agent and produces syngas with higher hydrogen content and higher heating value. Syngas with higher hydrogen content is sought after for certain downstream syngas purposes. Steam gasification is more resource intensive (energy and cost) as it includes the production of steam. The fourth common gasifying agent is CO_2. This gasifying agent is primarily used in carbon capture and carbon utilization applications [7].

In addition to these four more common gasifying agents there are other types of gasification, for example hydrogasification (hydrogen as gasifying agent) and plasma gasification. Hydrogasification is of interest as a gasification method that decreases the toxic by-products (dioxins) in methane production [66]. Plasma gasification proceeds at even higher temperatures (1500°C-5000°C) and produces higher quality syngas with lower tar levels [60].

2.2.1.3 Hydrocracking

Hydrocracking is a cracking method where hydrogen is used to break the C-C bonds in the polymer, cracking it into lighter sought-after hydrocarbons. It uses an inert hydrogen rich gaseous environment. In hydrocracking, hydrogenation (also known as hydrogenolysis) occurs first followed by thermal cracking. The hydrogenolysis is the reaction process where hydrogen is added to unsaturated bonds in the polymer chain, making these saturated. Saturated bonds are in turn more susceptible to thermal cracking, allowing a lower process temperature (typically 250°C–450°C[7]) for thermal cracking of the polymers. Hydrocracking uses catalysts, often transition metal catalysts

[67]. The addition of hydrogen in the cracking process is advantageous as it produces a high-quality liquid product, requiring little further processing before use as fuel or feedstock in chemical production [7]. Hydrogen is however expensive, with cost remaining an obstacle for industrial implementation of hydrocracking [60]. It is an extension of pyrolysis and is useful as it removes present heteroatoms [23].

2.3 Life Cycle Assessments of Thermolysis Recycling Methods

As described above, there are several process pathways possible for chemical recycling of plastic waste. The selection of process is not trivial and depends on feedstock composition and desired product output. In order to select which process type to proceed with in this thesis work, a comparative analysis using seven life cycle assessment (LCA) papers was carried out. One of the papers was a review paper on LCAs of chemical recycling of plastic waste, three papers investigated pyrolysis, two papers investigated gasification and one paper on hydrocracking was used.

In the review paper "*Developments in the life cycle assessment of chemical recycling of plastic waste – A review*" [68], Davidson et al. carried out a two part review of the LCA field for chemical recycling. The first part consisted of reviewing the development of LCA's for chemical recycling over the past decade by investigating the frequency of research outputs. The second part, of more interest to this thesis, consisted of a critical review of published LCA studies on chemical recycling of plastic waste. Davidson et al. identified 13 published LCA studies, each modelling at least one chemical recycling method. However, only 9 of these were analysed further as they fulfilled the three requirements posed:

1. The LCA contains one or more chemical recycling processes (gasification, pyrolysis, depolymerization, hydrocracking) model.
2. The LCA considers a MPW or single plastic waste stream as the main process stream of interest.
3. The LCA follows the principles of ISO 14040.

From Davidson et al.'s analyses, pyrolysis (7 papers) was shown to be the most frequently modelled chemical recycling method in LCA studies, followed by solvolysis/depolymerization (3 papers), hydrocracking (2 papers) and gasification (2 papers). Analysing conclusions from these 9 LCA studies shows that mechanical recycling usually performs better, from an environmental perspective, than chemical recycling and that any recycling process performs better than incineration, which in turn performs better than landfill. However, even though mechanical recycling was seen to perform better than chemical recycling from an environmental perspective, chemical recycling was seen to produce higher quality products with a wider range of applications [68]. The

authors emphasize the need to combine these two recycling methods in plastic waste management systems. Within the chemical recycling options, pyrolysis was determined to be the best option from an environmental perspective. The authors note a potential bias as plastic pyrolysis has been studied far more extensively than other chemical recycling methods, resulting in greater data availability for LCAs [68].

The conclusions drawn by Davidson et al. indicate pyrolysis as the preferred process option for chemical recycling of plastic waste. To validate and better understand this analysis, additional literature was consulted, including studies not covered in Davidson et al.'s review.

Pyrolysis LCAs

Jeswani et al. [69] carried out an LCA study comparing chemical recycling of MPW (PE+PP+PS) via pyrolysis with established mechanical recycling and energy recovery options, based on existing commercial facilities. The study evaluated the life cycle environmental impacts from three different perspectives: waste, product and a combination of waste and product. From the waste perspective, MPW was pyrolysed, converting it into a naphtha-cracker feedstock and the functional unit was 1 ton of MPW. The waste perspective compared pyrolysis with energy recovery from waste plastics via MPW incineration and combustion of refuse-derived fuel (RDF). For the product perspective, pyrolysis was used as an alternative process for the production of virgin-grade plastic, where the functional unit was defined as the production of 1 ton of virgin-grade LDPE plastic granulate. Here the authors compared LDPE production from pyrolysis of MPW with LDPE production from virgin naphtha. For the third perspective, Jeswani et al. combined the product and waste perspectives, including both the production of virgin mixed plastics and their end-of-life treatment as MPW. The three end-of-life treatment alternatives studied were plastic material recovery, through either mechanical (lower grade mixed-plastics granulate) or chemical recycling (producing virgin-grade LDPE granulate), and energy recovery (incineration and RDF). The functional unit for the third perspective was defined as the production of 1 ton of mixed virgin plastics and their end-of life treatment.

The results from their waste perspective LCA study showed that chemical recycling of MPW via pyrolysis had a lower climate change impact and life cycle energy use than energy recovery from MPW. However, pyrolysis did not perform better in most other impact categories. The results from the product perspective showed a similar pattern where production of 1 ton virgin grade LDPE granulates from pyrolysis of MPW had a 124% lower climate change impact than production from virgin fossil naphtha. They also account for a lower life cycle energy use, human health and freshwater ecotoxicity impact for chemical recycling of MPW to LDPE than for LDPE from virgin naphtha. The other impact categories show a significantly higher impact from the chemical recycling pathway over the virgin naphtha due to a lack of related credits for energy recovery and avoided incineration. The results from the combined perspective

suggest that chemical recycling has a 7% higher climate change impact than mechanical recycling and a 42% lower impact than the energy recovery option. The authors carry out sensitivity analyses, where interesting points to note are how the energy mix and mechanical recyclate quality have an effect on impact categories which in turn influence comparisons between alternatives [69]. The mechanical recyclate quality is discussed explicitly as LCAs often do not take into account the degradation of plastic quality with mechanical recycling. Jeswani et al. conclude that assuming mechanically recycled plastic replaces a virgin alternative is not plausible or acceptable. When taking into account a degrading plastic quality for mechanical recycling, the results show that climate change impact and energy use for pyrolysis and mechanical recycling of MPW are similar. The authors conclude that identifying a best option from their LCA studies will depend on which impact category is assessed.

In a third paper, Das et al. [70] carried out an LCA for pyrolysis of plastic waste for fuel production (P2F) and LDPE production (P2P) in an attempt to determine which is a better use of pyrolysis product from a life cycle perspective. In their study, naphtha was the main product in the P2F process whereas for P2P, the naphtha was further converted to ethylene which was then polymerized for production of LDPE. These further processing steps consume energy, water and emit greenhouse gases, leading the authors to question if a circular plastic production, where waste plastics are chemically recycled to produce new plastics, is more environmentally beneficial than converting plastic waste to fuels. Das et al. compared P2P and P2F in both EU and U.S. contexts for both cradle-to-gate and cradle-to-grave system boundaries, including an assessment of fossil fuel consumption for products derived from waste plastics versus those produced from virgin fossil resources. By comparing an EU and U.S. contexts, the effect of regional differences (such as electricity mix, water availability/scarcity and waste management methods) on the LCA results was also demonstrated, showing that the better use of pyrolysis product depends on the regional conditions. In a U.S. context, their results showed that for a cradle-to-gate frame, P2F had lower GHG emissions than P2P. In the EU context for cradle-to-gate, P2P was lower emitting than P2F. This was explained by a much higher LDPE yield in an EU context, affecting credit allocation in LCA calculations. However, when the system's boundary was expanded to cradle-to-grave, P2P had lower emissions than P2F in both the U.S. and EU contexts as combustion of the naphtha fuel drives up GHG emissions in the P2F case. The study also showed that naphtha (as fuel) and LDPE produced from recycled plastic waste were less GHG intensive than the conventional derivation of these products from virgin fossil sources. They showed that, from a product perspective (1 MJ naphtha or 1 kg LDPE), both P2P and P2F achieved lower GHG emissions than their respective baselines (virgin fossil sources) in both the EU and U.S. contexts, with P2P offering the largest reduction. Looking into other impact categories than GHG emissions, the authors presented that fossil fuel consumption, water consumption and waste generation were higher for P2P than for P2F. They also showed that solid waste and terrestrial ecotoxicity impacts were lower for P2P and P2F pathways than current waste management systems in place,

particularly in the U.S. context, where landfill is the main waste management for plastic waste. Conclusively, their study showed three main points of interest for this thesis:

1. with a cradle-to-grave system boundary, P2P showed reduced GHG emissions compared to P2F in both EU and US contexts.
2. P2P is lower emitting than the current waste management practice.
3. Both P2P and P2F product routes are lower emitting than conventional virgin production.

The results from an LCA study on ethylene monomer recovery via pyrolysis of PE by Somoza-Tornos et al. [71] indicate similar results. Somoza-Tornos et al. carried out a process simulation, set in an EU context, coupled with LCA, assessing both economic and environmental impacts. The environmental impact study consisted of two parts. First, they compared the environmental impact of pyrolysis with a "business as usual" (BAU) case for ethylene production from virgin fossil derived naphtha. Secondly, the authors compared the environmental impact of pyrolysis as an end-of-life treatment with landfill and incineration (treatment of 1 kg of PE waste as a functional unit). The process simulation computed 2.17 kg of waste PE for the production of 1 kg ethylene, 0.2 kg of methane, 0.4 kg of propylene and 0.3 kg of benzene. Their economic analyses showed that the total cost of production was 0.386 €/kg ethylene, half the cost of the BAU process (0.835 €/kg ethylene), indicating a highly competitive cost. In the environmental impact assessment, similar results were observed with pyrolysis, showing clear advantages in environmental performance over BAU. Pyrolysis had a reduced impact of 87% on human health, 89% on ecosystem quality, and 164% on resource scarcity compared to BAU. The authors environmental assessment of the three different end-of-life processes (pyrolysis, incineration and landfill) showed pyrolysis as the better performing of the three, largely explained by the revalorization of PE waste into multiple valuable by-products (methane, propylene and benzene). Somoza-Tornos et al.'s findings showcase chemical recycling via pyrolysis as a viable and beneficial process option.

The three LCA papers and the LCA review show the environmental benefits of pyrolysis as a waste management method for plastic waste. All three LCA studies discuss the effect of increasing circularity in the plastics economy via pyrolysis compared to the other two conventional end-of-life waste treatments (landfill and incineration). Somoza-Tornos et al. demonstrated the economic benefits of a more circular plastic production, an important incentive for advancing the industry toward circularity.

Gasification LCAs

In line with Davidson et al.'s findings, the number of relevant studies available on other chemical recycling processes than pyrolysis for plastic waste was significantly lower. To the knowledge of this thesis's author, no papers investigating gasification of MPW for monomer recovery or plastic feedstock recovery could be found. However, by

combining the conclusions from H. Khoo [72] and Afzhal et al [73], an impression of gasification for plastic-to-plastic recycling with regards to its potential and limitations could be gathered.

H. Khoo [72] carried out an LCA study on waste management alternatives for the plastic waste in Singapore. They reviewed the effects of different waste management process combinations from an LCA perspective, comparing each scenario to a reference case of the current plastic waste management. In the reference case, 7.24% of plastic waste was mechanically recycled and the rest was sent to waste to energy (WTE) recovery. As land scarcity is an issue in Singapore, the author addresses normalization and weighting of LCA results in regards to scales/sizes of valorization or waste treatment technologies. Eight different waste management scenarios with various fractions of mechanical recycling, WTE, pyrolysis and/or gasification for Singapore's entire plastic waste stream were investigated. MPW used in the study was composed of 40% PE, 17% PVC, 12% PP, 4% PS, 4.8% PET, and 22.2% other mixed fractions. Interesting for this thesis was comparing the effects of including pyrolysis versus gasification in plastic waste management. The results from the study showed that including gasification in the waste management treatment caused a pattern of peaks in the two impact categories acidification and particulate matter. Impact on these categories were also evident from pyrolysis, though not as significant as those generated by gasification. Gasification was seen to have a lower climate change impact than pyrolysis. The study also found that gasification processes generated more solid waste destined for WTE, while the scenario with the largest share of pyrolysis produced the least amount of annual solid waste. The waste management scenario with a higher degree of pyrolysis showed larger generation of valuable fuel recovery from plastics than for the scenario with more gasification. Looking at total impact with normalized and weighted scores, the author concluded the scenario with the highest potential degree of pyrolysis (combined with mechanical recycling and WTE) was the preferred option for plastic waste management in Singapore. The author also reported a larger land area requirement for gasification plants compared to pyrolysis plants [72]. From the presented results, weaknesses of gasification compared to pyrolysis for chemical recycling of plastic waste were indicated.

Afzal et al. [73] carried out a techno-economic analysis (TEA) and LCA of MPW gasification for methanol and hydrogen production. As described in section *2.1.4 Plastic Feedstock Production*, methanol serves as an intermediate in plastic production, arguably making Afzal et al.'s study relevant to the LCA analysis.

Afzal et al. [73] assessed two gasification pathways where the syngas was used to produce either methanol or hydrogen. They assessed two different feedstock types, MPW (50% PE+50%PP) and MSW, comparing these to existing fossil-fuel derived pathways for methanol and hydrogen production. The study found that MSW gasification had lower syngas yields than MPW gasification, having a very notable effect on cost/impact allocation per kg methanol or hydrogen. Only the results regarding MPW gasification compared to fossil fuel derived methanol and hydrogen from Afzal et al.'s paper are summarized further. From the TEA, the authors concluded that minimum selling price

(MSP) for methanol was 0.70$/kg and for hydrogen was 3.41$/kg whereas the average market price for fossil fuel derived methanol and hydrogen was 0.30$/kg and 1.15$/kg respectively. The authors identified the feedstock cost as the main driver of MSP for methanol and hydrogen produced from MPW. To achieve cost parity with existing fossil fuel derived pathways, the MPW feedstock price needs to be reduced. The authors used a cradle-to-gate system boundary and U.S. specific data when possible (otherwise global). It should be kept in mind that system boundaries have an effect on resulting impacts, as seen in the study by Das et al. [70]. Afzal et al. found that the total supply chain energy use for methanol and hydrogen from MPW gasification was reduced compared to the fossil fuel pathway by 52% and 56% respectively. This was mainly due to the natural gas feedstock for the fossil fuel pathway being counted as an upstream burden compared to plastic waste, having no associated upstream burden. The GHG emissions of MPW derived methanol and hydrogen were 166% and 36% larger respectively, than GHG emissions from the current virgin fossil fuel pathway. This increase in GHG emissions is explained by the fuel/energy input required for additional endothermic processing steps required when using MPW as a feedstock, compared to natural gas. For example, syngas production from natural gas uses one reformer whereas syngas from MPW feedstock uses three in Afzal et al.'s study. The authors acknowledge that alternate process configurations and energy sources could lower the GHG emissions for MPW gasification pathways. The percentage increase should not be mixed up with absolute values, where GHG emissions from both MPW-hydrogen and fossil-hydrogen are significantly higher than for MPW-methanol and fossil-methanol.

GHG emissions are not the only impact category examined by Afzal et al. [73]. The authors find that MPW-methanol had a lower impact than fossil-fuel-methanol in several categories such as acidification, fossil fuel depletion, ozone depletion and smog formation but a higher impact in the categories ecotoxicity, eutrophication, particulate formation and water use. MPW-hydrogen was found to have lower impact than fossil-hydrogen in categories such as carcinogenics, eutrophication, fossil fuel depletion, particulate formation and smog production but higher impact in categories such as acidification, ecotoxicity, ozone depletion and water use. The authors mention that some of these differences fall within estimated uncertainty ranges. Conclusively, Afzal et al. found that MPW gasification for methanol and hydrogen production resulted in a net increase of GHG emissions, with a larger increase for methanol production, but that it at the same time could be a promising approach to decreasing environmental impacts in several other impact categories. The cradle-to-gate system boundary should be kept in mind when comparing GHG emissions for fossil derived methanol and hydrogen versus MPW derived methanol and hydrogen.

The results from H. Khoo's paper [72] combined with Afzal et al.'s paper [73] and the previously mentioned pyrolysis LCA papers indicate that pyrolysis may be the preferred option over gasification for plastic-to-plastic recycling when aiming to increase plastic circularity and decrease environmental impact. Considering that Afzal et al. [73] showed MPW-methanol struggling to compete with fossil-methanol regarding minimum

selling price, and that Somoza-Tornos et al. [71] showed MPW-pyrolysis products to have a highly competitive cost with fossil-fuel derived products, gives further reason to believe pyrolysis may be the preferred process option for plastic-to-plastic recycling of MPW.

Hydrocracking LCA

In order to assess hydrocracking's potential as a chemical recycling method for plastic-to-plastic recycling of MPW, an LCA by Al-Salem et al. [74] was consulted. Their study was a two part LCA of waste management scenarios for handling PSW as a fraction of MSW in the Greater London area. In the first part of the study, the authors carried out an LCA for the current MSW management strategy, consisting of material recovery and incineration, and compared it to an engineered reference scenario where all PSW was sent to landfill. The results for part one of their study showed that the current waste management system performed better in all impact categories compared to the landfill option. The impact categories reviewed, in both part one and two of their study, were acidification potential (AP), eutrophication potential (EP), global warming potential (GWP) and photochemical ozone creation potential (POCP). More attention was paid to GWP and AP as these are, according to the authors, considered the most significant and better understood impact categories in waste management LCA studies. In the second part of the study, the authors investigated low temperature pyrolysis (LTP) and hydrogenation (VCC) as two alternative thermo-chemical treatments (TCT) for PSW management, comparing them to a Materials Recovery Facility (MRF). The authors assumed that products from the TCT plants and material from MRF could substitute commercial products. For the low temperature pyrolysis, valuable petrochemicals, e.g. gases (C_3-C_4), liquid fractions (naphtha), waxes (atmospheric residue) and heat (steam) was recovered. For the hydrogenation process, syncrude (synthetic crude oil) and e-gas (comparable to natural gas) were recovered. Three different product substitution factors (SF) where assessed (0%, 50% and 100%) and a functional unit of 1000 tonnes per annum (tpa) PSW was used. The PSW composition for the LTP was set to 83% polyolefins (PE + PP), 2% PVC and 15% PS whereas the PSW composition for the hydrogenation was set to 90% polyolefins (PE+PP) and 10% PVC. These values were based on feed criteria of the low temperature pyrolysis and the hydrogenation reactor [74].

From the LCA results, it was clear that the environmental impact of each waste management method depends on the market's ability to replace commercial petrochemical products with those recovered through the recycling process. For the case of substitution factor=100%, the three alternative waste management methods were shown to have the following orders of impact:

- AP: Low temperature pyrolysis > Hydrogenation > Mechanical recycling
- EP: Mechanical recycling > Low temperature pyrolysis > Hydrogenation

- GWP: Hydrogenation > Mechanical recycling > Low temperature pyrolysis
- POCP: Hydrogenation > Mechanical recycling > Low temperature pyrolysis
- Depletion of fossil resources: Hydrogenation >> Mechanical recycling > Low temperature pyrolysis

Focusing on AP and GWP, the study showed that hydrogenation and low temperature pyrolysis had overall larger negative impacts for these categories compared to mechanical recycling. They also concluded that pyrolysis was more environmentally friendly in terms of GHG emissions whereas hydrocracking was more environmentally friendly in terms of EP. Hydrogenation had a significantly higher POCP impact (almost 5 times larger than low temperature pyrolysis) and impact on depletion of fossil resources (where low temperature pyrolysis showed negative impact and mechanical recycling showed very small positive impact), both explained by the supply of natural gas to the hydrogenation process [74].

Determining a preferred option between hydrogenation and pyrolysis is not straight forward based on the results presented by Al-Salem et al. [74] as this would depend on which impact category was valued more. Hydrogenation can however be viewed as an extension of pyrolysis, where the main difference lies in the inert gas medium used for the process. It can therefore be argued that development of pyrolysis can be viewed as development of hydrocracking, as the underlying process is the same.

Conclusion from LCAs

Based on the LCA analysis for the three chemical recycling options (pyrolysis, gasification and hydrocracking), pyrolysis is indicated as the preferred option for plastic-to-plastic recycling of MPW and therefore selected as the appropriate process for further investigation using CFD-DEM.

2.4 Pyrolysis Reactors

In order to investigate pyrolysis for plastic recycling using CFD-DEM modelling, a simulation setup of a pyrolysis reactor needs to be constructed. There are several different reactor types available. Reactor types are either batch or continuous reactors, depending on how they process feedstock. Batch reactors are operated in batch-mode, where a set amount of feedstock is loaded into the reactor and the reactor is then sealed. A complete pyrolysis cycle is run before the reactor is emptied and a new batch is loaded. The continuous reactor operates with a continuous pyrolysis process and feedstock loading. Some of the most common reactor types are fixed bed reactors, fluidized bed reactors (most common for plastic pyrolysis [21]), rotary kilns and auger/screw reactors. Reactors vary not only in regards to feedstock loading, but also method of heating, mixing, residence time etc. [75]. For catalytic pyrolysis, the reactor type affects

which catalysts can be used [21]. A short description of the most common reactor types is given below.

Fixed bed reactor

The fixed bed reactor is a simple reactor design where the feedstock is placed in a fixed bed and heated from the outside. This type of reactor is slow as heat penetrates a stationary mass [75]. Due to slow heat transfer, the temperature distribution throughout the feedstock mass varies, causing spatially uneven thermal cracking. For pyrolysis of plastic, this type of reactor is especially slow as plastic has low thermal conductivity. As there is no mixing in the reactor, the use of catalysts is very limited [21].

Fluidized bed reactor

Fluidized bed reactors make use of the fluidization operation and can be run in continuous mode. In fluidization, a liquid or gas is passed through a bed of solid particles, causing it to have fluid-like properties. In order to achieve fluidization, the liquid or gas must be passed through at a high enough velocity. When the velocity is high enough, the particle drag compensates for the bed weight and the bed expands with the particles suspended in the fluid. At this state, the solid particles can be described as floating and having fluid-like properties, i.e. a fluidized state is achieved [76]. Fluidized bed reactors have very good mixing rates, good heat and mass transfer and short residence time of volatiles, limiting the formation of undesired by-products. However, this reactor type faces issues with de-fluidization due to agglomeration [23].

Rotary kiln reactor

Rotary kiln reactors are constructed using a rotating cylinder. The feedstock is fed into the rotating cylinder and is continuously mixed due to the rotation. This reactor type typically has faster heating than the fixed bed reactor but slower heating than fluidized bed reactors. Rotary kilns can handle a wide variety of feedstock types and sizes and can be operated in both batch and continuous mode [75].

Screw/Auger reactor

Screw/auger reactors are usually a tubular design with a rotating screw inside that pulls the feedstock through the auger. As the screw rotates, it moves the feedstock material through the heated tube, allowing this pyrolysis reactor to operate in continuous mode. The rotation rate of the screw and length of reactor are both controlled, which allows more precise control of residence time. This reactor setup also allows for selective zone heating, further increasing control over the process [21].

2.5 Thesis Scope and Justification

The project scope does not include gathering of experimental data of a pyrolysis process, rather validation of the CFD-DEM model is carried out using a pre-existing benchmarking case. Determining specifics of the pyrolysis CFD-DEM modelling setup is primarily governed by modelling feasibility and finding a satisfactory benchmarking case for validation of simulation setup.

The benchmarking case selected for validation of the CFD-DEM model is a two-part study carried out by Zhang et al. [77][78]. The first paper is an experimental study on pyrolysis of mixed plastic waste in a rotating furnace. The authors studied the effects of filling ratio of heat carriers and the effect of different plastic waste types on the product yield and composition [77]. The second paper is a numerical CFD-DEM study looking at the heat transfer for plastic waste pyrolysis in a rotary furnace, where the authors used their first paper to validate their CFD-DEM model. The authors compared the influence of heat carrier loading and furnace rotation speed on the pyrolysis of plastic waste [78].

The benchmarking case was selected based on modelling feasibility (simple reactor type) and available relevant data for CFD-DEM simulations of MPW pyrolysis. A rotary kiln reactor provides a good balance between reactor complexity and heat transfer efficiency, directly correlated to both modelling feasibility and industrial relevance. Rotary kilns offer more efficient heat transfer compared to fixed-bed reactors due to internal mixing induced by rotation, while avoiding the operational challenges of fluidized beds, such as de-fluidization. Within the scope of a master's thesis, this reactor type represents a practical compromise being sufficiently complex to capture realistic industrial behaviour yet remains a simple reactor model to build.

The selected mixed plastic waste composition for the CFD-DEM modelling includes PE, PP and polyAl. This plastic waste composition was selected based on the fact that PE and PP make up the largest fractions of mixed plastic waste, both in Sweden and globally, they require no pre-treatment such as dehalogenation prior to pyrolysis (as required for PVC), and they do not contain heteroatoms. As this thesis project is in collaboration with Tetra Pak, polyAl is also included. It is primarily mixing and heating of the plastic particles that is investigated, especially how plastic particle heating is affected by including polyAl in the plastic waste mix. Due to the interspersed aluminium, with higher thermal conductivity than the polymers, polyAl could potentially improve heating of the plastic waste by acting as a heat carrier in the plastic granular mix.

3 CFD-DEM Theory

CFD-DEM modelling uses a Lagrangian-Eulerian multiphase approach where the governing equations for the continuous fluid phase are written in Eulerian form and the governing equations for the dispersed particle phase are written in Lagrangian form. The continuous phase governing equations are modified using volume fractions and source terms to take into account the dispersed particle phase. Using this Lagrangian-Eulerian approach resolves the fluid flow on a fixed grid whilst simultaneously enabling individual tracking of dispersed particles. Depending on the number of particles in the dispersed phase, a set of Lagrangian governing equations can be solved for each individual particle or a statistical approach can be used where the total number of particles instead are represented by a smaller amount of computational parcels. In CFD-DEM, the particle phase is modelled using DEM particles. DEM particles are preferred when particle density is high and inter-particle interactions are significant. In this thesis, the heat transfer in the particle-dense region and inter-particle heat transfer is of interest, making DEM particles a suitable choice for the Lagrangian phase. The Eulerian and Lagrangian phase interactions can be coupled as either one-way or two-way. With one-way coupling, only the continuous phase influences the dispersed phase whereas with two-way coupling the dispersed phase also influences the continuous phase. The phase interactions for two-way coupling are displacement of the continuous phase by the dispersed phase and heat, mass and momentum transfer between the phases. The software used for the CFD-DEM model was Star-CCM+ [79].

3.1 Eulerian Phase

The governing equations include the continuity equation (eq. 3.1), momentum balance equation (eq. 3.2) and energy balance equation (eq. 3.3) shown below. The governing equations are written for incompressible flow, relevant for this thesis, where $\mathbf{v}$ is the velocity vector [u, v, w] in [x, y, z] direction and ρ is the fluid density [79].

Continuity equation

The continuity equation ensures mass conservation and as there is no mass transfer between the phases, there is no source term from the particle phase to the continuous phase [79].

$$\nabla \cdot (\rho \mathbf{v}) = 0 \tag{3.1}$$

Momentum equation

The momentum balance equation conserves momentum by applying Newton's second law to a fluid continuum and is shown in equation 3.2. The momentum balance equation is written in conservative form as appropriate for the finite volume method. Newton's second law states that the rate of change of momentum is equal to the sum of the forces acting on the fluid. In equation 3.2, $\boldsymbol{\sigma}$ is the stress tensor containing the surface stresses on the fluid volume, $\mathbf{f}_b$ is the body force vector containing the body forces acting on the fluid volume V and $\mathbf{S}_V$ is the momentum transfer source term between the particle phase and continuous phase within the cell volume. The stress tensor includes the normal and shear stresses imposed on the fluid volume surfaces and can be expanded into a pressure term (normal stress) and viscous stress tensor (shear stress). The body force vector contains body forces like gravity [79].

$$\frac{\partial(\rho\mathbf{v})}{\partial t} + \nabla \cdot (\rho\mathbf{v} \otimes \mathbf{v}) = \nabla \cdot \boldsymbol{\sigma} + \frac{\mathbf{f}_b}{V} + \mathbf{S}_V \tag{3.2}$$

Energy Equation

The energy equation conserves energy, following the first law of thermodynamics. Equation 3.3 shows the energy equation in conservative form where e is the internal energy of the fluid (see equation 3.4), $\mathbf{S}_E$ is the source term for energy transfer between the phases and $\mathbf{q}$ is the heat flux vector accounting for heat conduction [79]. The internal energy is given by equation 3.4. The heat flux is given by Fourier's law, see equation 3.5, where k is the thermal conductivity of the fluid [79].

$$\frac{\partial(\rho e)}{\partial t} + \nabla \cdot (\rho e\mathbf{v}) = -\nabla \cdot \mathbf{q} + \mathbf{S}_E \tag{3.3}$$

$$e = c_p T \tag{3.4}$$

$$\mathbf{q} = -k\nabla T \tag{3.5}$$

3.2 Lagrangian Phase

The Lagrangian phase governing equations for DEM particles are described below and formulated for a single particle, see equations 3.6, 3.8 and 3.23. In this thesis, the flow is considered laminar and each DEM particle therefore has a deterministic trajectory [79].

Mass conservation

For this thesis, mass transfer between the phases was neglected in order to reduce complexity, as can be seen in equation 3.6 where m_p is the particle mass [79].

$$\frac{dm_p}{dt} = 0 \tag{3.6}$$

Momentum conservation

The particle DEM phase has both rotational and translational movement. Rotational movement is accounted for by the angular momentum balance equation (eq.3.7) and translational movement is accounted for by the linear momentum balance equation (eq. 3.8) [79].

The angular momentum balance equation is shown in equation 3.7, where $\mathbf{I}_p$ is the particle's moment of inertia, ω_p is the particle angular velocity, $\mathbf{M}_b$ is the drag torque and $\mathbf{M}_c$ is the contact torque which arises from the rolling resistance. There are three different rolling resistance methods implemented in Star-CCM+ and applied in this thesis is the simplest force proportional method [79].

$$\mathbf{I}_p \frac{d\boldsymbol{\omega}_p}{dt} = \mathbf{M}_b + \mathbf{M}_c \tag{3.7}$$

The linear momentum balance equation of a particle is described by equation 3.8, where $\mathbf{v}_p$ is the instantaneous particle velocity, $\mathbf{F}_s$ is the resulting surface force vector on the particle's surface and $\mathbf{F}_b$ is the particle's body force vector. The resultant $\mathbf{F}_s$ represents the momentum transfer from the continuous phase to the particle [79].

$$m_p \frac{d\mathbf{v}_p}{dt} = \mathbf{F}_s + \mathbf{F}_b \tag{3.8}$$

The relevant surface force vector contributions and body force vector contributions for this thesis are the drag force $\mathbf{F}_d$, the gravity force $\mathbf{F}_g$ and the contact force $\mathbf{F}_c$, see equations 3.9 and 3.10 [79].

$$\mathbf{F}_s = \mathbf{F}_d \tag{3.9}$$

$$\mathbf{F}_b = \mathbf{F}_g + \mathbf{F}_c \tag{3.10}$$

The drag force is defined in equation 3.11, where C_d is the drag coefficient, A_p is the projected area of the particle and $\mathbf{v}_s$ is the particle slip velocity calculated as the instantaneous particle velocity subtracted from the instantaneous velocity of the continuous phase ($\mathbf{v}_s$=$\mathbf{v}$-$\mathbf{v}_p$). Star-CCM+ offers three methods for defining the drag coefficient. For this thesis the Gidaspow Drag Coefficient method, see equation 3.12 and 3.13, is used as it is suitable for high particle density regions, which in this case occurs at the bottom of the reactor and investigation of the heat transfer within this

region is of interest. Re_p is the particle Reynolds number described in equation 3.27, ϵ is the void fraction, ϵ_{min} is the cutoff void fraction and w is the Wen-Yu exponent [79].

$$\mathbf{F}_d = \frac{1}{2} C_d \rho A_p |\mathbf{v}_s| \mathbf{v}_s \tag{3.11}$$

$$C_d = \frac{4}{3}(150\frac{1-\epsilon}{\epsilon Re_p} + 1.75), \qquad \text{if} \quad \epsilon < \epsilon_{min} \tag{3.12}$$

$$\text{otherwise} \quad C_d = \begin{cases} \frac{24(1+0.15\cdot Re_p^{0.687})}{\epsilon Re_p}\epsilon^{1-w}, & \text{if } \epsilon Re_p \leq 1000 \\ 0.44, & \text{if } \epsilon Re_p > 1000 \end{cases} \tag{3.13}$$

When modelling DEM particles specifically, the Lagrangian phase momentum equation includes a contact force vector term in the resulting body force vector. This contact force vector accounts for the inter-particle and particle-boundary interactions of the DEM particles. The contact force is accumulated for all of the particle's contact points and applied as a body force, see equation 3.14, where $\mathbf{F}_{cm}$ is a contact model force [79].

$$\mathbf{F}_c = \sum_{contacts} \mathbf{F}_{cm} \tag{3.14}$$

Star-CCM+ offers three contact force model descriptions for DEM particles and for this thesis the Hertz-Mindlin No Slip Contact Model is used. The Hertz-Mindlin model is a non-linear spring-dashpot model with a normal and tangential force component, both containing a non-linear spring and damping contribution, see equation 3.15. Equations 3.16 and 3.17 show the normal and tangential forces, both present in equation 3.15, and their respective components (spring stiffness K and damping N). Here, d is the overlap at the contact point, ν_n and ν_t are the normal and tangential velocity components of the relative sphere surface velocity at the contact point, $C_{n\,rest}$ and $C_{t\,rest}$ are the normal and tangential coefficients of restitution (measures elasticity of a collision), $N_{n,damp}$ and $N_{t,damp}$ are the normal and tangential damping coefficients [79].

$$\mathbf{F}_{contact} = F_n \mathbf{n} + F_t \mathbf{t} \tag{3.15}$$

$$F_n = -K_n d_n - N_n \nu_n \qquad \begin{cases} K_n = \frac{4}{3} E_{eq} \sqrt{d_n R_{eq}} \\ N_n = \sqrt{(5 K_n M_{eq})} N_{n,\mathrm{damp}} \\ N_{n,\mathrm{damp}} = \frac{-ln(C_{n\,rest}}{\sqrt{\pi^2 + \ln(C_{n\,rest})^2}} \end{cases} \tag{3.16}$$

$$F_t = \begin{cases} -K_t d_t - N_t \nu_t, & \text{if } |K_t d_t| < |K_n d_n| C_{fs} \\ \dfrac{|K_n d_n C_{fs} d_t|}{|d_t|}, & \text{otherwise} \end{cases} \quad \text{where} \quad \begin{cases} K_t = 8 G_{eq} \sqrt{d_n R_{eq}}, \\ N_t = \sqrt{5 K_t M_{eq}}\, N_{t,\mathrm{damp}} \\ N_{t,\mathrm{damp}} = \frac{-ln(C_{t\,rest})}{\sqrt{\pi^2 + \ln(C_{t\,rest})^2}} \end{cases} \tag{3.17}$$

In equations 3.17 and 3.16 the following variables are used: R_{eq} is the equivalent radius, M_{eq} is the equivalent particle mass, E_{eq} is the equivalent Young's modulus, G_{eq}

is the equivalent shear modulus and C_{fs} is the static friction coefficient. The equivalent variables are calculated for the bodies in contact, which in this case is either particle-particle contact or particle-wall contact. Equations 3.18-3.21 show how these equivalent variables are calculated for particle-particle contact and particle-wall contact [79].

$$R_{eq} = \begin{cases} R_{eq_{ji}} = \frac{1}{\frac{1}{R_j} + \frac{1}{R_i}} \\ R_{eq_{wi}} = R_i \end{cases} \tag{3.18}$$

$$M_{eq} = \begin{cases} M_{eq_{ji}} = \frac{1}{\frac{1}{M_j} + \frac{1}{M_i}} \\ M_{eq_{wi}} = M_i \end{cases} \tag{3.19}$$

$$E_{eq} = \begin{cases} E_{eq_{ji}} = \frac{1}{\frac{1-\nu_j^2}{E_j} + \frac{1-\nu_i^2}{E_i}} \\ E_{eq_{wi}} = \frac{1}{\frac{1-\nu_w^2}{E_w} + \frac{1-\nu_i^2}{E_i}} \end{cases} \tag{3.20}$$

$$G_{eq} = \begin{cases} G_{eq_{ji}} = \frac{1}{\frac{2(2-\nu_j)(1+\nu_j)}{E_j} + \frac{2(2-\nu_i)(1+\nu_i)}{E_i}} \\ G_{eq_{wi}} = \frac{1}{\frac{2(2-\nu_w)(1+\nu_w)}{E_w} + \frac{2(2-\nu_i)(1+\nu_i)}{E_i}} \end{cases} \tag{3.21}$$

For linear elastic isotropic materials with Poisson's ratio $\nu \leq 0.45$, Young's modulus E and the shear modulus G are related as described by equation 3.22 [79].

$$G = \frac{E}{2(1+\nu)} \tag{3.22}$$

Energy conservation

Lagrangian particles are considered internally homogenous and have a low internal thermal resistance, a low Biot number, giving the equation for energy conservation for a particle as shown in equation 3.23. In equation 3.23, Q_t is the convective heat transfer to the particle from the continuous phase and Q_s is a heat source term covering heat conduction between particles and between particles and solids [79].

$$m_p c_p \frac{dT_p}{dt} = Q_t + Q_s \tag{3.23}$$

The convective heat transfer to a particle is described by equation 3.24, where A_s is the particle's surface area, h is the heat transfer coefficient of the particle, T is the surrounding continuous phase temperature and T_p is the particle's temperature [79].

$$Q_t = hA_s(T - T_p) \tag{3.24}$$

The heat transfer coefficient is determined based on the particle Nusselt number, Nu_p, which for spherical particles in Star-CCM+ is determined by the Ranz-Marshall correlation. Equation 3.25 shows the definition of the particle Nusselt number, where k is the thermal conductivity of the continuous phase and D_p is the particle diameter. Equation 3.26 is the Ranz-Marshall correlation, applicable up to particle Reynolds number $\mathrm{Re}_p \simeq 5000$. Pr is the continuous phase Prandtl number, defined by equation 3.28. The particle Re number is defined according to equation 3.27, where ρ is the continuous phase density and μ is the continuous phase dynamic viscosity, making the Ranz-Marshall correlation only applicable to a viscous continuous phase [79].

$$Nu_p \equiv \frac{hD_p}{k} \quad \Rightarrow \quad h = \frac{Nu_p k}{D_p} \tag{3.25}$$

$$Nu_p = 2(1 + 0.3Re_p^{1/2} Pr^{1/3}) \tag{3.26}$$

$$Re_p \equiv \frac{\rho |\mathbf{v}_p| D_p}{\mu} \tag{3.27}$$

$$Pr = \frac{\nu}{\alpha} = \frac{c_p \mu}{k} \tag{3.28}$$

There is not only heat transfer between the continuous and particle phase, but also conductive heat transfer between particles and between particles and the heated kiln chamber walls. The particle-particle conductive heat transfer, from particle i to particle j, is described by equation 3.29. Here, k is the equivalent thermal conductivity of the two particles (see equation 3.30) and r_c is the contact area radius. The conductive heat transfer is related to the particle energy balance equation as a source term [79].

$$q_{ij} = 4r_c k (T_j - T_i) \tag{3.29}$$

$$\frac{1}{k} = \frac{1}{k_i} + \frac{1}{k_j} \tag{3.30}$$

The conductive heat transfer from wall to particle *i* is described by equation 3.31. The walls are set to have a fixed temperature [79].

$$q_{iw} = 4r_c k_i (T_w - T_i) \tag{3.31}$$

The contact area radius, equation 3.32, depends on which bodies are in contact as the equivalent radius is modified according to equation 3.18. The contact area radius equation includes the contact overlap *d* [79].

$$r_c = \sqrt{dR_{eq}} \tag{3.32}$$

The particle Nusselt number measures the efficiency of heat transfer through a fluid layer (to the particle in this case) when convection is added, i.e. it is the ratio of

total heat transfer (convection+conduction) through the fluid layer to the static scenario when only conduction is present. The Nusselt number is used to measure heat transfer enhancement due to convection, if Nu = 1 then heat transfer is through pure conduction. The heat transfer coefficient h measures the rate of heat transfer between a fluid and a solid surface ($[W/m^2K]$). The Biot number, see equation 3.33, measures the ratio of the convective heat transfer at the solid surface to the thermal conductivity within the solid. It is a non-dimensional number and a low Biot number indicates low internal resistance to conduction and thereby small internal temperature gradients. In equation 3.33, L_c is the characteristic length of the solid body (in this case spherical particle). [80].

$$Bi = \frac{h \cdot L_c}{k_p} \tag{3.33}$$

Star-CCM+ treats DEM particles as internally homogenous, applying lumped system analysis [79]. Temperature of a body at time step t using lumped system analysis is described by equation 3.34, where T_∞ is the ambient temperature, T_i the initial temperature and b is the constant described by equation 3.35 [80].

$$\frac{T(t) - T_\infty}{T_i - T_\infty} = e^{-bt} \tag{3.34}$$

$$b = \frac{h}{\rho \cdot c_p \cdot L_c} \tag{3.35}$$

Thermal diffusivity, see equation 3.36, is a material property that measures the ratio of heat conduction to heat storage in a material. If the thermal diffusivity is high, then heat diffuses fast through the material. If it is low, the material absorbs and stores most of the heat. In equation 3.36, k_p is the particle thermal conductivity, ρ is the particle material density and c_p is the particle material's specific heat [80].

$$\alpha = \frac{heat\ conduction}{heat\ storage} = \frac{k_p}{\rho \cdot c_p} \tag{3.36}$$

3.3 Phase Coupling

The coupling of governing equations is carried out by scaling the governing fluid flow equations through volume partitioning and accounting for source terms. For two-way coupling mass, momentum and heat transfer is carried out in both directions (continuous to dispersed phase and dispersed to continuous phase) through source terms. For one-way coupling there is mass, momentum and energy exchange only in one direction, from the continuous phase to the dispersed particle phase. In this case, the continuous phase is not aware of mass, momentum or heat transfer to the dispersed phase. For example, when one-way coupling is used for colder DEM particles that are dispersed in a hotter gas phase, there is no heat loss from the continuous phase to the dispersed phase even

though the dispersed phase experiences a temperature increase. Instead, the temperature field of the continuous phase is used to calculate heat transferred to the dispersed phase without said heat actually being lost from the continuous phase, thereby maintaining the temperature field. In two-way coupling however, the heat absorbed by the dispersed phase is accounted for as a loss from the continuous phase [79].

The dispersed Lagrangian phase displaces the continuous phase by taking up volume in the domain. This displacement is accounted for by the volume fraction ϕ_c and is calculated for each cell in the discretized domain. The volume fraction for the Lagrangian phase is the fraction of the cell volume of which the particles take up. The local volume fractions are interpreted as void spaces by the continuous phase, decreasing the available volume η for the continuous phase to occupy. The volume fraction for each phase is related through equation 3.37 [79].

$$\phi_c = 1 - \eta \tag{3.37}$$

As the dispersed phase reduces the volume that is occupied by the continuous phase, this consequently reduces the area over which fluxes for the fluid phase are calculated. Volume partitioning of the mesh cells is used to calculate the volume fractions for each phase. Each phase takes up a volume of the cell's total volume V, see equation 3.38. The subscript k for the continuous phase applies if there is more than one continuous phase [79].

$$V = \sum_k V_k^F + \sum V^{DEM} \tag{3.38}$$

The available volume fraction for the continuous phase in a cell, η is calculated through equation 3.39 [79].

$$\eta = \frac{\sum V^F}{V} \tag{3.39}$$

The continuity, momentum and energy equation of the continuous phase are scaled using η, see equation 3.40-3.42. Here, the governing equations are described for a control volume V (i.e. grid cell) with a surface area A. The term s_{int} is an internal source term which arises from modelled interactions, $\mathbf{I}$ is the identity tensor, E is the total energy (internal and kinetic energy), H is the total enthalpy and $\mathbf{T}$ is the viscous stress tensor [79].

$$\frac{\partial}{\partial t}\int_V \eta dV + \oint_A \eta\rho\mathbf{v}\cdot d\mathbf{a} = 0 \tag{3.40}$$

$$\frac{\partial}{\partial t}\int_V \eta\rho\mathbf{v}dV + \oint_A \eta\rho\mathbf{v}\otimes\mathbf{v}\cdot d\mathbf{a} = -\oint_A \eta p\mathbf{I}\cdot d\mathbf{a} + \oint_A \eta\mathbf{T}\cdot d\mathbf{a} + \int_V \eta\mathbf{f}_b dV + \int_V s_{int}dV \tag{3.41}$$

$$\frac{\partial}{\partial t}\int_V \eta\rho E dV + \oint_A \eta\rho H\mathbf{v}\cdot d\mathbf{a} = -\oint_A \eta\mathbf{q}\cdot d\mathbf{a} + \oint_A \eta\mathbf{T}\cdot\mathbf{v}d\mathbf{a} + \int_V \eta\mathbf{f}_b\cdot\mathbf{v}dV + \int_V s_{int}dV \tag{3.42}$$

Applying the divergence theorem gives the governing equations on differential form (recognised from section 3.1) with the volume fraction scaling included, see equation

3.43-3.45. In the momentum equation, the viscous stress tensor $\mathbf{T}$ and the pressure term $p\mathbf{I}$ are combined in the stress tensor $\boldsymbol{\sigma}$. In the energy equation, only the internal energy is included as the kinetic energy is handled in the momentum equation. As the flow is incompressible, the viscous work term and pressure work term are neglected and the total enthalpy term only includes the internal energy contribution, see equation 3.46 where pV is the pressure volume term [79].

$$\nabla \cdot (\eta\rho\mathbf{v}) = 0 \tag{3.43}$$

$$\frac{\partial(\eta\rho\mathbf{v})}{\partial t} + \nabla \cdot (\eta\rho\mathbf{v} \otimes \mathbf{v}) = \nabla \cdot (\eta\boldsymbol{\sigma}) + \frac{\eta\mathbf{f}_b}{V} + \mathbf{S}_V \tag{3.44}$$

$$\frac{\partial(\eta\rho e)}{\partial t} + \nabla \cdot (\eta\rho e\mathbf{v}) = -\nabla \cdot (\eta\mathbf{q}) + \mathbf{S}_E \tag{3.45}$$

$$H = e + pV \tag{3.46}$$

Source terms

The rate of momentum transfer from the continuous phase to a single particle has previously been stated in equation 3.8 as $\mathbf{F}_s$. The two-way coupled momentum equation for the continuous phase includes the source term field $\mathbf{S}_V$, as shown above. This source term represents the rate of momentum transfer from all particles in a cell c to the continuous phase within that cell and is for unsteady simulations calculated according to equation 3.47 (discrete form for one cell). Here, δ is the Dirac delta function which filters out the parcels π not present in the cell, n_π is the number of particles represented by parcel π, and t_p is the particle residence time within the cell, during the global time step Δt. Parcels are collections of particles, a method that Star-CCM+ uses to reduce computational cost for particle tracking [79].

$$\mathbf{S}_V = -\frac{1}{\Delta t}\sum_{\pi}\sum_{\delta t_p} n_\pi \mathbf{F}_s \delta t_p \tag{3.47}$$

The rate of energy transfer due to convection, Q_t, from the continuous phase to a single particle was described previously in equation 3.24. The two-way coupled energy equation for the continuous phase includes the source term field $\mathbf{S}_E$, as shown above. This source term represents the rate of energy transfer from all particles in a cell c to the continuous phase within that cell and is for unsteady simulations calculated according to equation 3.48 (discrete form for one cell). This equation also includes a term representing the mechanical work ($\mathbf{F}_s \cdot \mathbf{v}_p$) due to drag forces on the particle, i.e. the particle and fluid do equal and opposite work on each other [79].

$$\mathbf{S}_E = -\frac{1}{\Delta t}\sum_{\pi}\sum_{\delta t_p} n_\pi (Q_t + \mathbf{F}_s \cdot \mathbf{v}_p)\delta t_p \tag{3.48}$$

Both the source terms $\mathbf{S}_V$ and $\mathbf{S}_E$ are applied in the continuous phase equations. The continuous phase's effect on the DEM particles is accounted for by solving the DEM phase equations by using the temperature, velocity and pressure fields of the continuous phase.

3.4 Solver

Two different segregated flow solver procedures where applied in this thesis, steady state and unsteady state. Initially, a steady state solver (solution only advancing in space) was used to converge the flow field prior to particle injection. At particle injection, the solver was switched to an implicit unsteady solver, advancing the solution in both space and time. Implicit time integration uses both the known flow field at the current time step and the unknown flow field at the future time step to calculate the flow field at the future time step. This makes the implicit time integration unconditionally stable, allowing larger time steps than an explicit scheme.

Both the steady and unsteady solver used the SIMPLE algorithm as the segregated flow solver. SIMPLE is one of the pressure-velocity coupling algorithms available for segregated flow in Star-CCM+. The segregated flow solvers first solve the discretized mass and momentum equations separately and then iteratively solve these for the velocity field ([u v w]) and pressure field (p). SIMPLE starts by solving the discretised momentum equations for the intermediate velocity field **v***. The intermediate mass fluxes are calculated using **v*** followed by solving the pressure correction equation from **v***. The pressure field is updated based on the pressure correction equation. The updated pressure field is then used to update the velocity field, ensuring it satisfies the continuity equation. Remaining transport equations such as the energy balance equation is solved using the updated pressure and velocity field. The updated velocity field may now no longer satisfy the momentum equation, which re-initiates the SIMPLE loop. In this manner, the SIMPLE algorithm solves the segregated flow through pressure-velocity coupling.

Figure 3.1 shows a flow chart of the interpreted CFD-DEM solver procedure for two-way coupling in Star-CCM+. The SIMPLE steps are highlighted in light blue. Coupling of the flow field from the CFD solver to the DEM solver is illustrated with a $-\ \cdot\cdot-$ line. The source term coupling from the DEM phase to the fluid phase is illustrated with a dotted line. The solid black line illustrates the coupling of particle position, calculated by the DEM solver, to the CFD solver for calculating volume fractions. It can also be noted in figure 3.1 that the DEM-solver uses an internal particle time step, sub-stepping within the global time-step. This is due to the physics of DEM particle motion being dependent on three time scales, which ever is smallest sets the limiting particle time-step necessary in order to capture said physics.

The first restriction for DEM particle motion is the Rayleigh wave propagation time τ_1. This is because it is assumed that the force acting on a particle is only affected by the

particle's immediate neighbours during a single time-step duration. Rayleigh waves are surface acoustic waves, arising from localised impact, that travel along the surface of a solid. In order for the assumption of surface forces to hold, the particle time-step needs to be limited to the time it takes for the Rayleigh wave to propagate across the particle's surface to its opposite side. The wave propagation is dependent on the particle's material properties as these affect the wave speed $V_{Rayleigh}$. The Rayleigh wave propagation time for spherical particles is calculated according to equation 3.49. Here, $V_{Rayleigh}$ is the Rayleigh wave speed and R is the sphere radius. The maximum particle time-step should not be larger than $t_{scale} \cdot \tau_1$ where t_{scale} is a user-defined time-scale (default value is $t_{scale} = 0.4$) [79].

$$\tau_1 = \pi \frac{R}{V_{Rayleigh}} \tag{3.49}$$

The second criterion limiting the time-step for moving DEM particles is the impact duration time τ_2. The impact duration time for two elastic spherical particles, assuming Hertz contact theory, is calculated according to equation 3.50. The impact duration time is dependent on the material properties of the particles. Here, R is the particle radius, E is Young's modulus, ρ is the particle's density, ν is the Poisson's ratio and v_{impact} is the normal impact velocity. The maximum particle time-step should not be larger than $0.1 \cdot \tau_2$ [79].

$$\tau_2 = 2.94\left(\frac{5\sqrt{2}\pi\rho}{4}\frac{1-\nu^2}{E}\right)^{\frac{2}{5}}\frac{R}{\sqrt[5]{v_{impact}}} \tag{3.50}$$

The third criterion limiting DEM particle time-step is a geometric condition to limit particles moving too far within the global time step as this can result in missing contacts. This is called the particle transit time. The DEM particles are constrained to take at least 10 time-steps to move the full length of the radius. Particle transit time τ_3 for spheres is calculated according to equation 3.51 where R is the particle radius and $v_{particle}$ is the particle's speed. The maximum particle time-step should not be larger than $0.1 \cdot \tau_3$ [79].

$$\tau_3 = \left(\frac{R}{v_{particle}}\right) \tag{3.51}$$

The final particle time-step is determined based on which of the three criterion has the smallest required time-step, i.e. which out of $t_{scale} \cdot \tau_1$, $0.1 \cdot \tau_2$ or $0.1 \cdot \tau_3$ is the smallest. Generally, it is most often τ_1 that is the limiting factor [79].

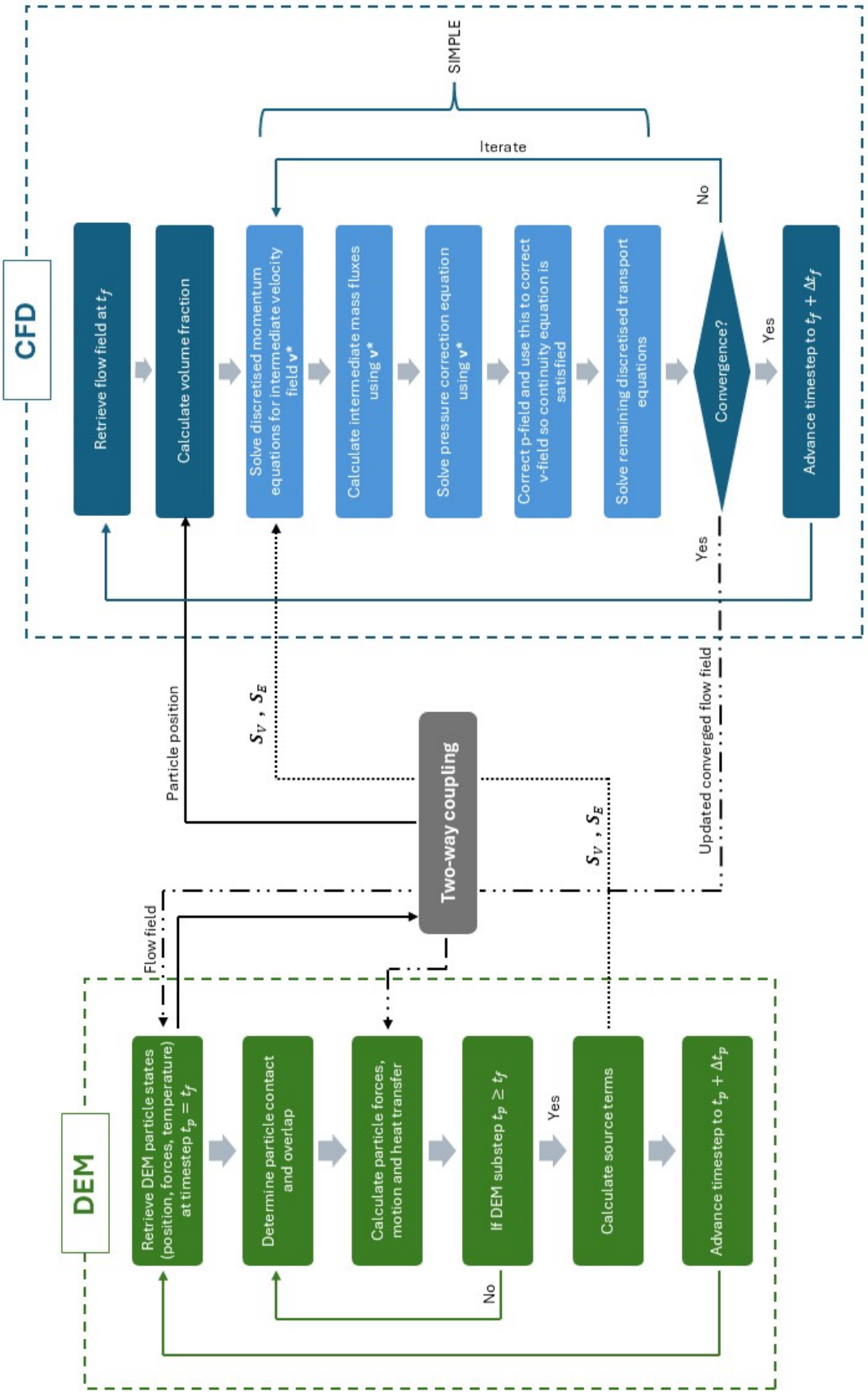

Figure 3.1: Flow chart of the solver procedure for the CFD-DEM simulation with two-way coupling.

3.5 Mesh

In CFD it is always important to select an appropriate mesh cell size based on the scale of the physics phenomena that the simulation aims to capture. For CFD-DEM simulations, it is also important to consider mesh cell size in relation to particle size. For DEM simulations, it is recommended to have a grid size 3-5 times larger than the smallest particle radius [81]. There are two reasons why grid size needs to be considered in relation to particle size. Firstly, it is important with regards to the particle contact detection calculation. By tracking the dispersed particles, the CFD-code can mark the grid cells containing particles as active and employ contact detection for the particles within those cells. For spherical particles, contact is detected if the distance between two particles is less than the sum of their radii. If contact is detected, the contact forces are then calculated. This is computationally more efficient than running a CFD-DEM code that checks each particle's distance against every other particle in the computational domain. If the particles are larger than the cell, this efficiency is reduced as the particle is tracked over multiple cells.

Secondly, if particles span over multiple grid cells, this can have an effect on the interpolation of fluxes at the cell faces and introduce errors. The continuous phase flow parameter values are stored in the cell centre for each cell. The flow field values are unknown for the cell faces and found through interpolation between the cell centre values each side of the cell face. If the particle spans over multiple cells, then the momentum acting on the particle from the continuous phase can vary for each cell. This will have an effect on the resulting surface force vector $\mathbf{F}_s$ acting on the particle.

The mesh's grid size combined with the physical processes present in the simulation impact the time step size that can be applied in the unsteady solver. The Courant-Friedrich-Levi (CFL) condition is a stability criterion used to ensure numerical stability, see equation 3.52. For explicit methods, the CFL condition is strict. Implicit methods are however, as previously mentioned, less sensitive to numerical instabilities, and may therefore tolerate a higher Courant number (C>1). The CFL condition ensures that the numerical solution does not advance the simulation faster (Δt) than the physical phenomenon can propagate (u) through the domain (Δx).

$$C = \frac{u\Delta t}{\Delta x} \leq 1 \;\Rightarrow\; \Delta t \leq \frac{\Delta x}{u}, \text{ (Numerical speed} \leq \text{Physical propagation speed)} \quad (3.52)$$

3.5.1 Mesh Quality

The mesh needs to be of high quality in order for the solution of the discretized governing equations to converge, be accurate and stable. If the mesh has bad quality, then the fluxes and gradients on the cell faces can become inaccurate due to difficulties with interpolation. This results in incorrect flow fields. A mesh of high quality runs more efficiently and can allow larger time steps. To assess mesh quality, the following five

mesh metrics can be used; aspect ratio, face validity, cell quality, skewness angle and volume change [79].

The aspect ratio is in general the ratio of the cell's longest length to its shortest length and should ideally have the value 1. For tetrahedral cells the aspect ratio is the ratio of the maximum edge length and the cell's internal sphere radius. The polyhedral mesher uses tetrahedral cells that are then converted into polyhedral cells. A high aspect ratio indicates a less symmetric cell, leading to a directional bias when calculating gradients and fluxes. A symmetric cell minimizes interpolation anisotropy between cells. In Star-CCM+ the field function *Cell Aspect Ratio* can be used to identify skewed or stretched cells, where 1 is the ideal value and values closer to zero indicate highly stretched cells [79].

Face validity measures how the cell's face normals are directed in relation to the cell centroid. For a good cell the face normals point outwards and for a bad cell (i.e. skewed cell) the cell normals point inwards toward the cell centroid. The ideal face validity value is 1 as this means all the face normals point outwards. Face validity values below 1 are considered bad and values below 0.5 represent a negative volume cell which is not allowed [79].

Cell quality is a metric that uses both the relative geometric distribution of the cell centroids of the face neighbour cells and the orientation of the cell faces to measure the cell's quality. A cell quality of 1 is a perfect cell and values less than 1.0e-05 are considered bad cells. The metric is based on a hybrid of the Gauss method and least-squares method for cell gradient calculation [79].

Skewness angle indicates the orthogonality of the mesh and is an important metric for calculation of diffusion on the grid. The optimal skewness angle is 0°, representing an orthogonal grid. Skewness angles larger than 85° are considered bad and values larger than 90° can lead to serious convergence issues as diffusion terms become unbounded [79].

Volume change describes the ratio of a cell's volume to its largest neighbour's volume. A volume change value of 1 means that the cell has equal or larger volume than its neighbours. Large differences in volume between neighbouring cells can cause inaccuracies and instabilities in the solver. Cell volume changes of 0.01 or smaller are considered bad cells and should be avoided [79].

4 Method

The simulation setup is based on the simulation setup used by Zhang et al. in their experimental [77] and numerical [78] study on pyrolysis of plastic waste, which this thesis aims to use for validation of the numerical setup. The base-line simulation setup developed is described in section *4.1 Simulation Setup*. Section 4.2 describes the methodology of the conducted mesh sensitivity study and section 4.3 describes the method of validating the numerical setup. Finally section 4.4 describes the methodology for the investigative CFD-DEM simulations on pyrolysis of MPW. All simulations were carried out in Star-CCM+ version 2506.

Working with CFD-DEM and finding a simulation setup which converges, is accurate and efficient, is an inherently iterative process. The base-line simulation setup was developed in parallel as the mesh sensitivity study and validation process. Some simulation setting choices were made based on findings from this iterative process, which are further described as results in section 5.3 *Insights from the Simulation Setup Development*. Further iterative model development was carried out during the CFD-DEM simulations for MPW pyrolysis, primarily focusing on attempting to decrease computational time.

4.1 Simulation Setup

The rotary kiln geometry was created in the Star-CCM+ CAD tool, see figure 4.1, with the drum dimensions given by Zhang et al. [78]. The internal drum diameter was set to 300 mm and width to 65 mm. Figure 4.1 includes the inlet pipe, outlet pipe and the particle injection plane. The material of the drum was set to UNSS30200 Stainless Steel.

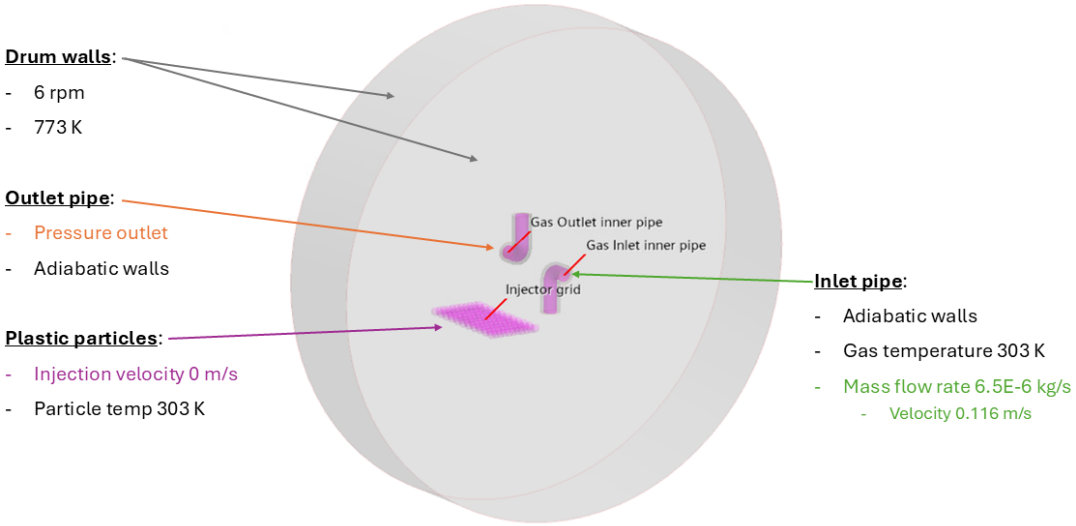

Figure 4.1: Geometry and boundary conditions of the setup.

The temperature was set to a constant value of 773 K for the drum walls with a wall relative rotation of 6 rpm based on Zhang et al.'s experimental paper [77]. The inlet and outlet pipes were set to adiabatic walls. Temperature of the particles at injection was set to 303 K, aligning with the temperature of the inert N_2 gas coming in through the inlet pipe. The mass flow rate of the inert gas was determined from the volume flow rate of 350 ± 10 ml/min given by Zhang et al. [77]. Particle injection rate was set to 2000 particles/s, starting from 0.5 s and stopping at 1.5 s, with a particle diameter of 2.5 mm and particle injection velocity of 0 m/s. Spherical particles were used (volume ≈ 8.2 mm^3).

Table 4.1 shows the physics models used in the setup. The second and third columns show the selected Lagrangian Multiphase models and the Multiphase Interaction models used. Heat transfer through radiation was omitted from the model setup. Impact from radiation on heat transfer on this type of setup was determined negligible based on previous experience.

Table 4.1: Physics models, Lagrangian Multiphase models and Multiphase Interaction models used.

Physics models	**Lagrangian Multiphase models**	**Multiphase Interaction models**
DEM	Constant Density	Conduction Heat Transfer
Gas	DEM Particles	Hertz-Mindlin
Gradients	Drag Force	Rolling Restistance
Gravity	Drag Torque	
Ideal Gas	Solid	
Implicit unsteady	Spherical Particles	
Lagrangian Multiphase	Temperature	
Laminar	Two-way	
Multiphase Interaction		
Segregated Flow		
Segregated Fluid Temperature		
Solution Interpolation		
Three Dimensional		

The gas model was set to Nitrogen (N_2) with the default material properties, as shown in table 4.2.

Table 4.2: Nitrogen gas material properties.

Dynamic viscosity, μ	1.78837e-5 Pa/s
Molecular weight	28.0134 kg/kmol
Specific heat, c_p	1040.76 J/(kg K)
Thermal conductivity, k	0.0255984 W/(m K)

Three different plastic materials were defined, each under *solid* in the Lagrangian Multiphase models. The material properties of each plastic are stated in table 4.3. The material property data for LDPE was taken from Zhang et al. [78] and material property data for polyAl was provided by Tetra Pak. For PP, material property data was found through two different sources ([82] [32]). Due to confidentiality, the material data for polyAl cannot be disclosed in table 4.3, however the relative size of selected properties are noted.

Table 4.3: Material properties used for the three plastics; LDPE, PP and polyAl.

	LDPE	PP	PolyAl
Density, ρ	900 kg/m^3	886 kg/m^3[82]	$\rho_{PP} < \rho_{PE} < \rho_{polyAl}$
Poisson's ratio, ν	0.39	0.42 [83]	-
Specific Heat, c	1000.0 J/(kg K)	1764.0 J/(kg K) [82]	$c_{p,\,PE} < c_{p,\,PP} < c_{p,\,polyAl}$
Thermal Conductivity, k	0.200 W/(m K)	0.137 W/(m K) [82]	$k_{PP} < k_{PE} < k_{polyAl}$
Shear modulus, G	100 MPa	457.74 MPa [83]	-
Young's Modulus, E	278 MPa	1300 MPa [83]	-

In order to mimic the setup used by Zhang et al. [77], a steady flow field with developed boundary layers was calculated before injecting the particles. Therefore, an initial simulation using a steady state solver was run to get a fully developed flow field fast, followed by switching the solver to an implicit unsteady solver when the particles were injected. The steady state flow field was saved and used as initial conditions for all simulations. Volume sourcing was activated for the implicit Lagrangian solver. Both solvers used the SIMPLE algorithm as described previously in section *3.4 Solver*.

4.2 Mesh Sensitivity Study

The mesh sensitivity study was carried out using three different meshes with varying base cell size; coarse mesh (7.5 mm base size), medium mesh (5 mm base size) and fine mesh (2.5 mm base size), see figures 4 and 5 in the Appendix. To resolve the flow through the inlet and outlet pipes, a smaller base cell size was used for these regions and maintained constant for the three different mesh sizes. Only the base cell size in the drum region was varied for the mesh sensitivity study as the physics of interest occur within this region. The surface remesher, polyhedral mesher and prism layer mesher were used for all three meshes.

The prism mesh layer was set to fixed settings, remaining constant for all three meshes. This, to avoid particle centroids existing within the prism layer as the simulation setup predominantly involves the plastic particles rolling along the drum walls at the bottom of the drum. Omitting the prism layer was considered, however it was included in order to resolve the thermal boundary layer. The prism layer total thickness was set to 1.25 mm, avoiding DEM centroids from lying within the prism layer.

The mesh sizes were selected based on the theory for appropriate mesh size for DEM-simulations, as described in section *3.5 Mesh*, in combination with considering with the size of the rotary kiln. Recommended grid size, is as previously stated, 3-5 times larger

than the smallest particle radius. The base cell sizes were selected considering this range, however with selected grid cell sizes being on the smaller end of the spectrum. The smallest base cell size was set to the same size as the particle diameter, in attempt to avoid cells (excluding prism layer cells) smaller than the plastic particles. The mesh settings used are stated in table 4.4.

Table 4.4: Automated mesh settings used.

Mesher Controls	
Base Size	2.5 mm / 5 mm / 7.5 mm
Volume growth rate	1.1
Number of prism layers	4
Prism layer total thickness	1.25 mm
Prism layer stretching	1.2
Max tet size	100% relative to base
Custom cell size pipes	1.0 mm
Custom prism layer thickness pipes	0.33 mm

The time step used was set to a specified field function different for each mesh, originally in attempt to satisfy the CFL condition. The time step field functions were setup using three different size time steps; one time step pre particle injection, a second time step during particle injection and particle ”falling”, and a third time step during particle ”rolling”. Falling, referring to the time interval when particles were injected at the injection plane and falling to the bottom of the rotary kiln. Rolling, referring to the time at which all particles have fallen down and instead are rolling along the kiln walls.

Particle velocity was measured for respective movement (falling and rolling) for the medium mesh. Based on the grid size and particle velocity, the time step satisfying the CFL condition ($C \leq 1$) was calculated. The calculated time step was used as a reference for setting a larger time step, increasing the Courant number. As implicit solver is used, the CFL condition is not strict. The new increased Courant number for falling and rolling was then used uniformly for the three meshes, scaling the time step to scaled mesh size. The determination and calculation of time steps for the three different mesh sizes (fine, medium, coarse) is shown below.

Medium mesh

$$\begin{aligned} u_{\text{falling}} &= 2.2\,\text{m/s} \\ u_{\text{rolling}} &= 0.6\,\text{m/s} \end{aligned} \Rightarrow \begin{aligned} \Delta t_{\text{falling, CFL}} &\leq 0.000227\,\text{s} \\ \Delta t_{\text{rolling, CFL}} &\leq 0.0083\,\text{s} \end{aligned}$$

$$\begin{aligned} \Delta t_{\text{falling, selected}} &= 0.01\,\text{s} \\ \Delta t_{\text{rolling, selected}} &= 0.5\,\text{s} \end{aligned} \Rightarrow \begin{aligned} C_{\text{falling}} &= \frac{2.2\,\text{m/s} \cdot 0.01\,\text{s}}{5\,\text{mm}} = 4.4 \\ C_{\text{rolling}} &= \frac{0.6\,\text{m/s} \cdot 0.5\,\text{s}}{5\,\text{mm}} = 60 \end{aligned}$$

Fine mesh

$$\begin{aligned} C_{\text{falling}} &= 4.4 \\ C_{\text{rolling}} &= 60 \end{aligned} \Rightarrow \begin{aligned} \Delta t_{\text{falling}} &= \frac{4.4 \cdot 2.5\,\text{mm}}{2.2\,\text{m/s}} = 0.005\,\text{s} \\ \Delta t_{\text{rolling}} &= \frac{60 \cdot 2.5\,\text{mm}}{0.6\,\text{m/s}} = 0.25\,\text{s} \end{aligned}$$

Coarse mesh

$$\begin{aligned} C_{\text{falling}} &= 4.4 \\ C_{\text{rolling}} &= 60 \end{aligned} \Rightarrow \begin{aligned} \Delta t_{\text{falling}} &= \frac{4.4 \cdot 7.5\,\text{mm}}{2.2\,\text{m/s}} = 0.015\,\text{s} \\ \Delta t_{\text{rolling}} &= \frac{60 \cdot 7.5\,\text{mm}}{0.6\,\text{m/s}} = 0.75\,\text{s} \end{aligned}$$

The time step field functions used in Star-CCM+ for the mesh sensitivity study are summarized in table 4.5. Particle injection proceeds at 0.5 s and from iterative development it was noted that by 2.5 s all particles had settled to rolling motion. For the mesh sensitivity study, only PE particles were injected in order to use obtained results to validate the simulation setup. The physical time simulated for the mesh sensitivity was set to 15 s.

Table 4.5: Time step field functions used for mesh sensitivity study.

Fine	\$Time < 0.5 ? 0.1: < 2.5 ? 0.005 : 0.25
Medium	\$Time < 0.5 ? 0.1: < 2.5 ? 0.01 : 0.5
Coarse	\$Time < 0.5 ? 0.1: < 2.5 ? 0.015 : 0.75

4.3 Validation

The simulation setup was validated using the results from the mesh sensitivity study and comparing these to the published results from Zhang et al.'s paper *Numerical investigation on the heat transfer of plastic waste pyrolysis in a rotary furnace* [78].

The data for average temperature of plastics with no heat carrier loading was used for validation. Zhang et al. used PE particles. All mesh sensitivity simulations and validation simulation were run using the default value of 20 000 max DEM substeps.

4.4 CFD-DEM Simulations of MPW Pyrolysis

Investigative simulations on MPW pyrolysis for different waste composition were run using the validated simulation setup and selected mesh from the mesh sensitivity study. Three initial cases (case 1.0, 2.0 and case 3.0) were run for 100 s using default value (20 000) for max DEM substeps. Case 1.0, was an extension of the validation case with only PE particles being injected. Case 2.0, used a combination of PE and PP particles and case 3.0 used a combination of PE, PP and polyAl particles, see table 4.6.

Table 4.6: Particle combinations used in CFD-DEM simulations of MPW pyrolysis.

Simulation case	**MPW composition**
Case 1.0	2000 PE
Case 2.0	1000 PE + 1000 PP
Case 3.0	670 PE + 670 PP + 670 polyAl

After completing the mesh sensitivity study and validation, further thought was given to the total thickness of the prism layer. The total thickness was changed to 1.15 mm for the remaining three cases in order to fully avoid particle centroids within or on the face of the prism layer cells.

The plastic materials were defined by using a pre-existing material (Rubber Arlon Thermabond 99180T010) but with modified material properties, according to table 4.3, for each plastic.

Whilst working with simulation case 1.0, 2.0 and 3.0 further simulation cases of interest were developed. Firstly, the current computational speed was noted as quite slow and further simulations within the time frame of the thesis would be limited unless the computational speed was increased. In attempt to increase computational speed, versions of case 1.0-3.0, dubbed cases 1.1-3.1, were run using max DEM substeps set to 1000 instead of the default value 20 0000.

A further two cases, case 4 and 5, were set up to supplement cases 1.0-3.0 with regards to heat transfer for different particle compositions. Case 4 and 5 used the same setup as case 1.0 but with PP and polyAl particles instead of PE particles, respectively. Cases 4 and 5 were run after cases 1.1-3.1. Based on results found from cases 1.1-3.1 it was decided to revert back to the default value of max 20 000 DEM substeps.

Table 4.7 shows a summary of the investigative simulation cases run for MPW pyrolysis.

Table 4.7: Summary of simulation cases run for MPW pyrolysis.

Simulation case	**Particles**	**max DEM substeps**
Case 1.0	2000 PE	20 000
Case 1.1	2000 PE	1000
Case 2.0	1000 PE + 1000 PP	20 000
Case 2.1	1000 PE + 1000 PP	1000
Case 3.0	670 PE + 670 PP + 670 polyAl	20 000
Case 3.1	670 PE + 670 PP + 670 polyAl	1000
Case 4	2000 PP	20 000
Case 5	2000 polyAl	20 000

4.5 Potential Sources of Error

Preferably, validation of the numerical setup would have been carried out using more data sets. The validation paper [78] looks at cases with different heat carrier loading. However, due to time constraints only the case with no heat carrier loading was used for validation. Ideally, validation through experimental data for the three cases (PE, PE+PP and PE+PP+polyAl) should have been carried out but resources for this were not available.

The plastic materials were defined by using a pre-existing material and only changing the material properties. Creating new materials for each plastic in the material database would be the correct method. This was compromised initially as a simplification and later not corrected due to time constraints. Further, heat conductivity was set to a constant value in Star-CCM+. However, as mentioned in section *2.1.1.2 Polymer Heat Conductivity* the heat conductivity of polymers decreases with increasing temperature. This effect is not considered and could be viewed as a source of error.

There were some queries that arose from the iterative development of the simulation setup regarding the DEM time step and resolving of particle interactions, further explained in section *5.3 Insights from the Simulation Setup Development*. If the hypothesis of particle interactions not being resolved properly, is correct, this would be a source of error.

As noted, working with CFD-DEM is an iterative process and the information regarding appropriate mesh size for DEM simulations was found after the mesh sensitivity cases had been started. The selected mesh sizes for the mesh sensitivity study were considered with regard to their base cell size (length), not the cell volumes. Appropriate mesh size for DEM simulations should perhaps be considered using the cell volume size in relation to particle size rather than the particle length and base cell length.

5 Results

Results from the mesh sensitivity study and validation of the simulation setup are described in section 5.1. Noteworthy findings from the iterative work of developing the simulation setup are summarized in section 5.3. Results from the investigative CFD-DEM simulations of MPW pyrolysis are described in section 5.2. Figures of the steady state flow field used as initial conditions for all simulations can be found in the appendix, see figures 1-3.

5.1 Mesh Sensitivity Study and Validation

Particle injection is specified in Star-CCM+ through a particle injection rate. The injection rate is affected by the time step, causing some variation in number of particles injected. Resulting mesh data, including particle count, for the three meshes is shown in table 5.1. See figures 4 and 5 in the appendix for the three different meshes.

Table 5.1: Mesh data for the three meshes; coarse, medium and fine.

	Coarse	**Medium**	**Fine**
Base cell size	7.5 mm	5 mm	2.5 mm
Cell count drum	66 324	113 503	448 130
Average cell volume, drum	387 mm^3	130 mm^3	18 mm^3
Particle count	2155	1957	2189
Total solver elapsed time	21.6 hours	32.5 hours	46.2 hours

Figure 5.1 shows the average particle temperature measured for the three meshes and includes data from the validation paper. Only slight differences are observed between the meshes and all three correlate to an adequate extent with the data for average particle temperature from the validation paper, thereby validating the simulation setup. The slope of the fine mesh's average particle temperature appears to fit the slope of the data from the validation paper better. When looking into other parameters such as average particle Nusselt number, see figure 5.2, and average particle velocity, see figure 6 in the appendix, a noticeable difference for the coarse mesh compared to both the medium and fine mesh can be observed.

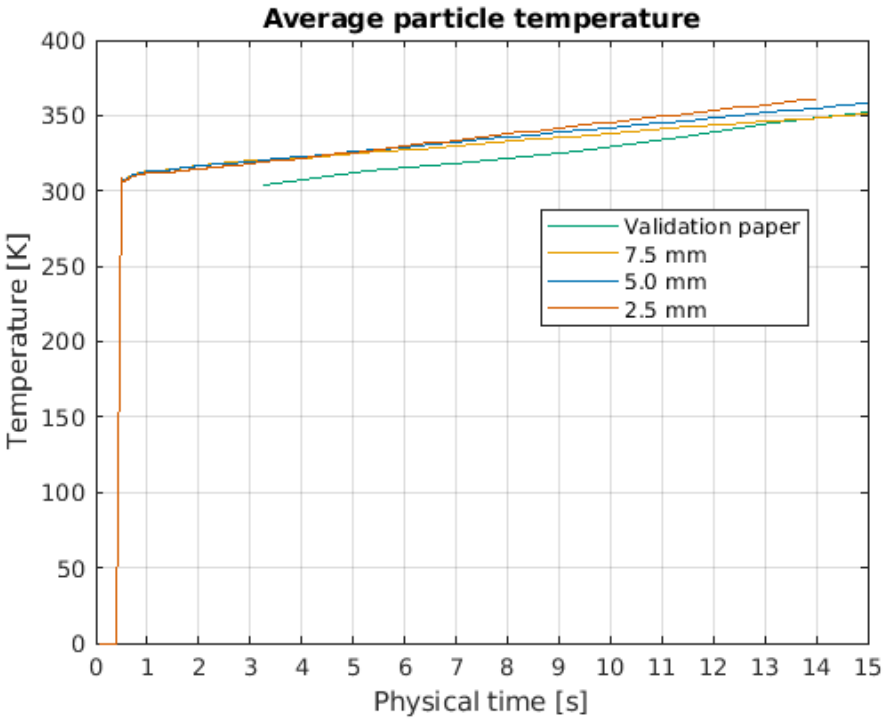

Figure 5.1: Average particle temperature for the three meshes and data from the validation paper [78].

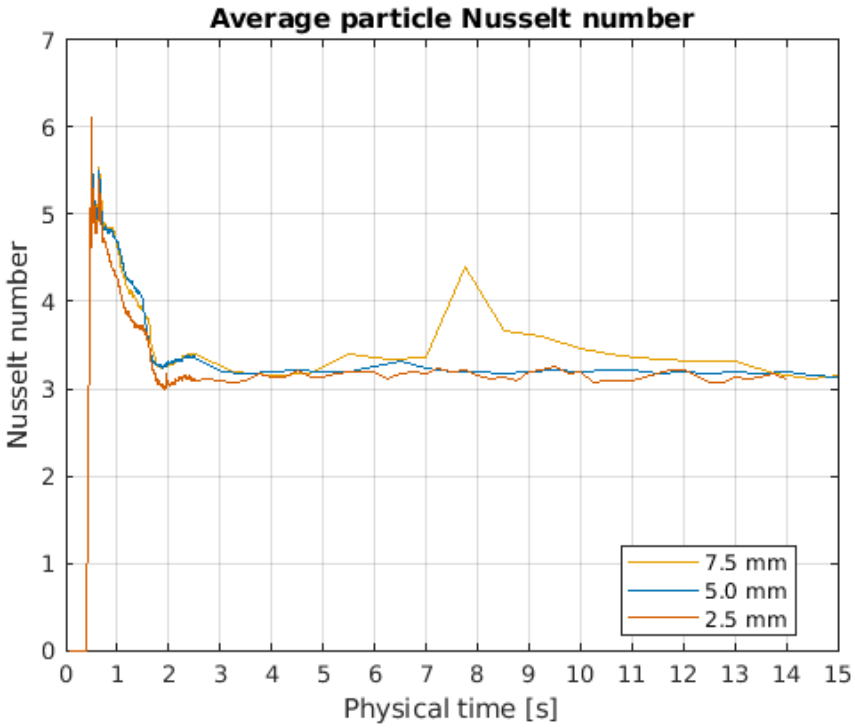

Figure 5.2: Average particle Nusselt number for the three meshes.

The results from figure 5.1, 5.2 and 6 (in the appendix) indicate that the coarse mesh is too coarse. The fine mesh corresponds best to the validation paper data, however the run time using this mesh is too long. Therefore, the medium mesh was selected for the following investigative CFD-DEM simulations of MPW pyrolysis. Figure 5.3 shows the medium mesh on a cross section of the rotary kiln, with the gas inlet and outlet pipes visible. The automated medium mesh was found to have high enough mesh quality and no further adjustments were needed. Figures 8-11 in the appendix show the mesh metrics aspect ratio, cell quality, skewness angle and volume change for the medium mesh.

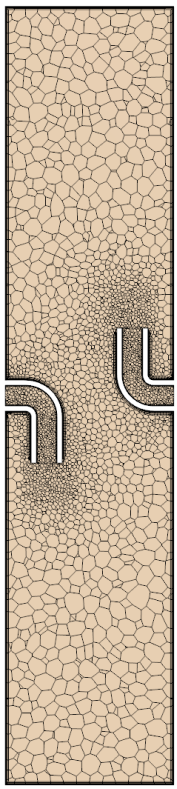

Figure 5.3: Medium mesh.

5.2 CFD-DEM Simulations of MPW Pyrolysis

All simulation cases in table 4.7 were run using the medium mesh with the time step as stated in table 4.5. The resulting particle injection for each case is shown in table 5.2. Total elapsed solver time for each case can be found in table 1 in the appendix, where particle interaction can be seen to have an effect on the simulation run time. Computational time increases when different particle types are present and with increased allowed max DEM sub-step. The max DEM substep was also seen to have an effect on total number of injected particles. Cases 1.1, 2.1 and 3.1, with max DEM substeps set to 1000, did not achieve the targeted 2000 total particle count, see table 5.2. It is therefore not only the global time step that affects particle injection, as seen in the mesh sensitivity study, but also modifications of the DEM solver.

Table 5.2: Particle count for cases 1.0-5.

Case number	**Total**	**PE**	**PP**	**polyAl**
Case 1.0	2160	2160	-	-
Case 1.1	1937	1937	-	-
Case 2.0	2162	1083	1079	-
Case 2.1	989	515	474	-
Case 3.0	2168	723	723	722
Case 3.1	990	318	329	343
Case 4	2166	-	2166	-
Case 5	2154	-	-	2154

The energy required for heating up the different particle types, i.e. the volumetric heat capacity C_{vol}, was calculated using $C_{vol} = \rho \cdot c_p$ and is shown in table 5.3. The table also includes the thermal diffusivity α, calculated using equation 3.36. Neither values for polyAl can be disclosed due to confidentiality, however the relative size can be disclosed. Values for solid aluminium [84] and N_2 gas [85] are also included for further discussion in chapter *6 Discussion*. The calculated volumetric heat capacity shows that out of the plastic materials, PE requires the least amount of energy to heat up and polyAl requires the most. The thermal diffusivity shows that PE could act as a heat carrier better than polyAl. It should be noted that both the volumetric heat capacity and thermal diffusivity are calculated for the materials at room temperature atmospheric conditions. As DEM does not resolve the particles internally, thermal diffusivity cannot be used to analyse the results from the CFD-DEM simulations. It is however useful for discussion purposes.

Table 5.3: Calculated C_{vol} and α of PE, PP and polyAl.

Material	C_{vol}	α
PE	900.0 kJ/m^{3}K	0.222 mm^2/s
PP	1563 kJ/m^{3}K	0.088 mm^2/s
polyAl	PE < PP < polyAl	$\alpha_{PP} < \alpha_{polyAl} < \alpha_{PE}$
Aluminium	2485 kJ/m^{3}K	91 mm^2/s
N_2	1.301 kJ/m^{3}K	19.7 mm^2/s

5.2.1 Case 1

Figure 5.4 shows the average, minimum and maximum particle temperature for the PE particles in case 1.0 and 1.1. The figure includes the average, minimum and maximum PE particle temperature from the validation paper's case with 0% heat carrier loading. Noticeable in figure 5.4 is that both simulation case 1.0 and 1.1 calculate lower particle temperatures than the numerical data from the validation paper, however case 1.1 is significantly lower. Case 1.0 shows a similar heating pattern to that of the validation paper, following a logarithmic curve shape, whereas case 1.1 appears linear. Particle temperature disparity between the cases and validation paper increases over time, resulting in approximately 60 K temperature difference at 100 s between case 1.0 and the validation paper. Case 1.1 shows a completely different particle heating trajectory with significantly lower calculated temperatures. The results produced for heating of PE particles when setting max DEM substeps to 1000 are therefore deemed inaccurate.

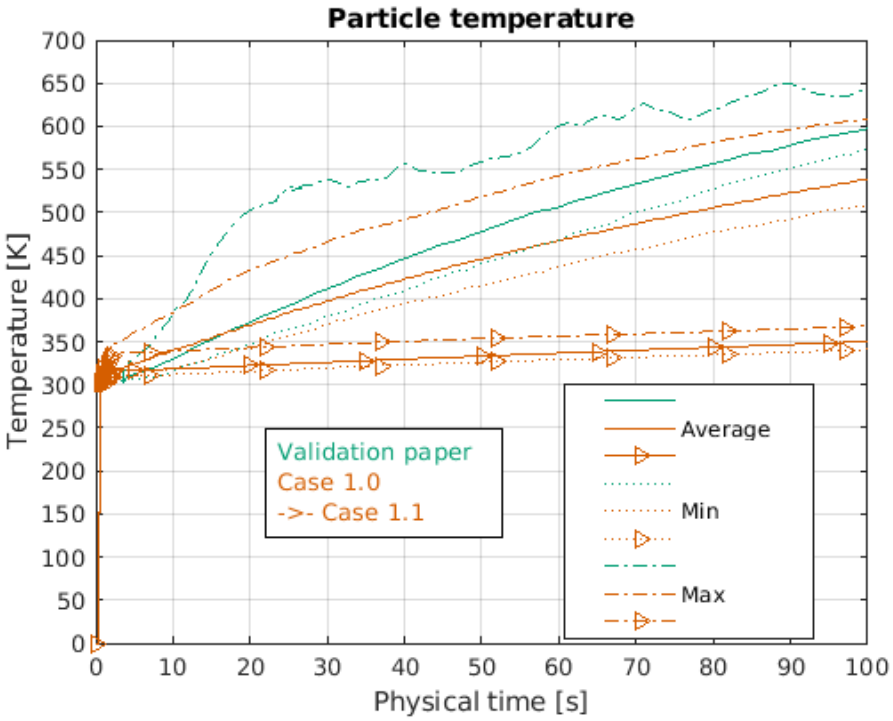

Figure 5.4: Average, min and max PE particle temperature for case 1.0, 1.1 and data from the validation paper ([78]).

Figure 5.5a shows the average particle Nusselt number for the PE particles in case 1.0. Using equation 3.25, the corresponding average particle heat transfer coefficient was calculated and is shown in figure 12 in the appendix. Using the calculated particle average heat transfer coefficient and equation 3.33, the corresponding Biot number was calculated and is shown in figure 5.5b. The results in figures 5.5a and 12 in the appendix show a slow decrease in Nusselt number and heat transfer coefficient, indicating a slight decrease in convective heat transfer efficiency. The average particle Nusselt number is relatively low, indicating that convection does not enhance heat transfer to the particles much. The particle average Biot number is low, which is reasonable as Star-CCM+ assumes DEM particles are internally homogenous.

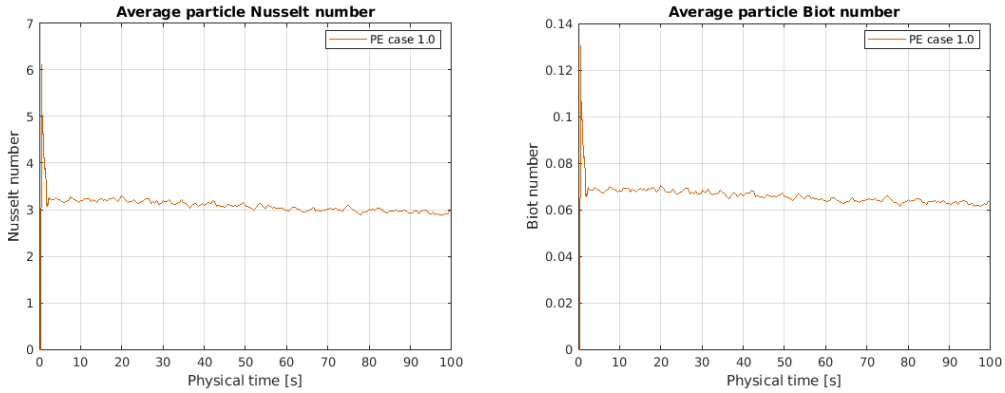

(a) Nusselt number

(b) Biot number

Figure 5.5: Average particle Nusselt number and Biot number for the PE particles in case 1.0.

The presence of the injected particles is visible in the the temperature field of the gas phase, as shown in figure 13 in the appendix, forming a slightly cooled region at the bottom of the reactor compared to the initial condition temperature field (figures 2-3 in the appendix).

5.2.2 Case 2 & 4

Figure 5.6 shows the average particle temperatures, for both PE and PP particles, for case 2.0, 2.1 and 4, including the data set for average PE particle temperature from the validation paper. The same occurrence, as noted in figure 5.4, can be observed here when comparing case 2.1 and 2.0. Case 2.1, with significantly fewer max DEM substeps, calculates inaccurate particle heating.

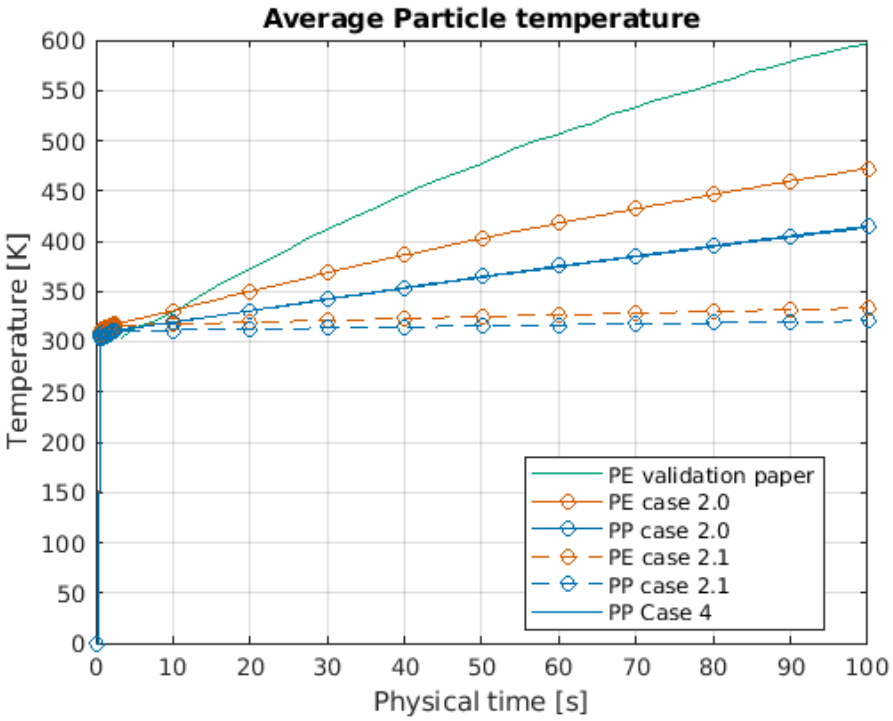

Figure 5.6: Average particle temperature for PE and PP particles in case 2.0, 2.1 and 4, including data from the validation paper ([78]).

Figure 5.7 shows average particle temperatures, excluding the inaccurately calculated temperatures of case 2.1, for PE and PP particles. Figure 5.7 shows that PE particles heat up faster than PP particles as expected, based on the volumetric heat capacities in table 5.3. The heating of PE particles is decreased when mixed with PP. It is difficult to see the plotted line for PP particles case 4 in figure 5.7 as it is very close to the plotted line for PP particles case 2.0. The difference between the two cases is small but visible in the zoomed in version of figure 5.7, see figure 5.8. The zoomed in figure shows that PP particles are heated slightly faster when mixed with PE particles (case 2.0) than when solely PP particles are present (case 4). PP particles need to absorb more heat in order to increase in temperature, as noted by the higher volumetric heat capacity, compared to PE. The PE particles increase in temperature with less energy, allowing them to heat up faster. The PE particles are therefore hotter than PP, at any given time, driving heat transfer through conduction from PE to PP when in contact. This could explain the slower heating of PE particles, if PP is absorbing thermal energy from them. The average particle temperature difference, ≈ 1 K, noted for PP particles (compare case 2.0 and 4) could be explained by the heat transferred from hotter PE particles, indicating a heat carrier effect. However, the difference is small and may fall within the numerical uncertainty of the simulation.

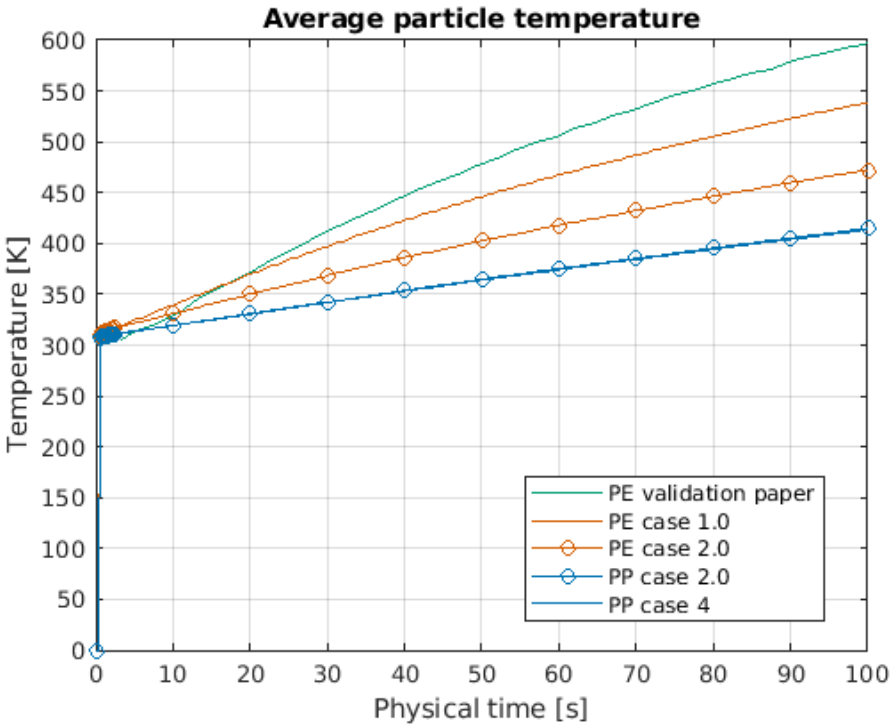

Figure 5.7: Average particle temperature for case 1.0, 2.0, 4 and data from the validation paper ([78]).

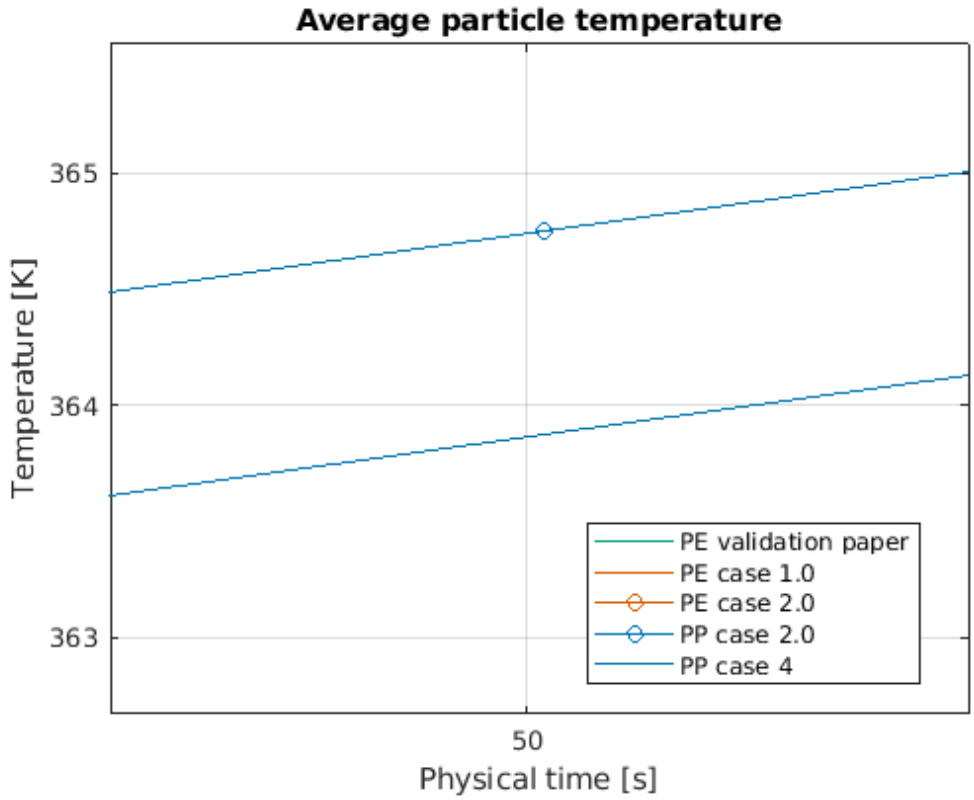

Figure 5.8: Zoomed in versions of figure 5.7 showing the difference between case 2.0 and 4.

Figure 5.9a shows the average particle Nusselt number for PE and PP particles in case 1.0, 2.0 and 4. The corresponding average heat transfer coefficients are shown in figure 14 in the appendix. Figure 5.9a shows the particles to have a very similar particle average Nusselt number, slightly decreasing over time, again indicating that convection does not enhance heat transfer to the particles significantly. Figure 5.9b shows the particle's average Biot number, calculated using the particle's average h (figure 14 in the appendix). PP particles have a larger Biot number compared to PE particles, however still small enough to allow lumped system analysis (uniform internal heating).

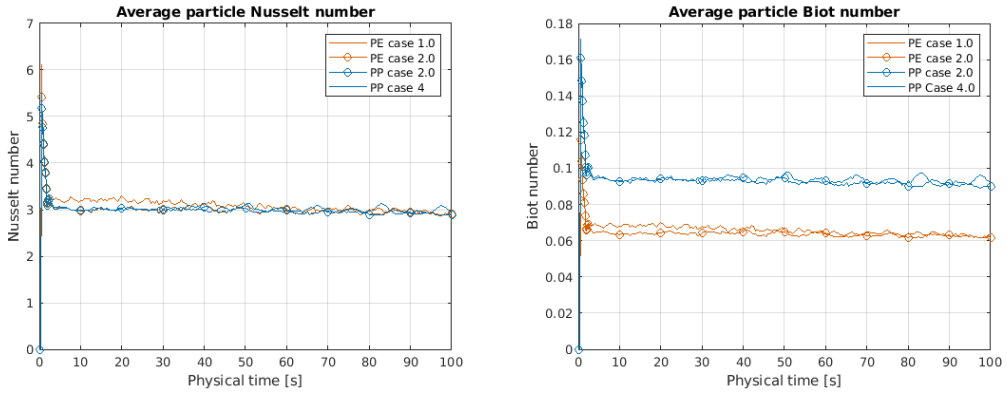

(a) Nusselt number

(b) Biot number

Figure 5.9: Average particle Nusselt number and calculated average particle Biot number for particles in case 1.0, 2.0 and 4.

Particle mixing within the reactor for case 2.0 was uniform, as shown in figure 15 in the appendix. Similarly to case 1.0, the presence of the injected particles is visible when looking at the gas temperature field, see figure 16 the appendix.

5.2.3 Case 3 & 5

Figure 5.10 shows the particle's average temperature for case 3.0, 3.1 and 5, including data for PE particles from the validation paper. The calculated average particle temperatures for case 3.1 are, as found for case 1.1 and 2.1, inaccurate due to the significantly lower temperatures and different heating pattern (more linear than logarithmic).

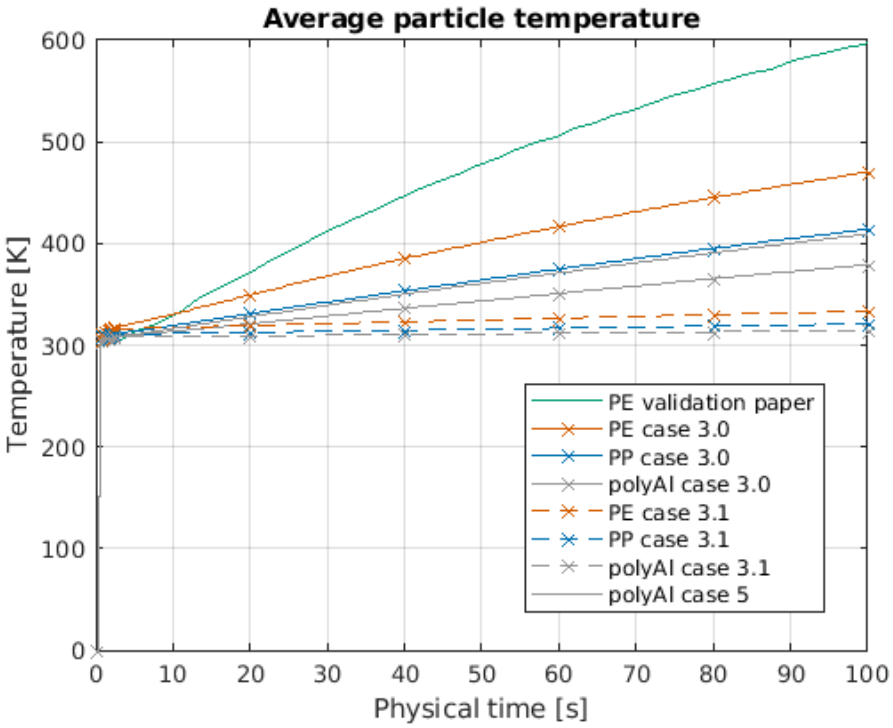

Figure 5.10: Average particle temperature for PE, PP and polyAl particles in case 3.0, 3.1 and 5, including data from the validation paper ([78]).

Figure 5.11 shows the average particle temperature for cases 1.0, 2.0, 3.0, 4 and 5, including the average PE particle temperature from the validation paper. The overall heating rate of the three particle types is as expected from the volumetric heat capacity in table 5.3. PE heats up fastest as this particle type requires the least amount of energy to increase in temperature, followed by PP, and polyAl heating up slowest. PolyAl has a higher noticeably higher volumetric heat capacity than PP, however there is very little difference in heating of sole PP (case 4) and sole polyAl (case 5). Following the observed heating pattern for sole PE (case 1.0) compared to sole PP (case 4), heating of only polyAl particles should be noticeably slower than PP.

The heating rate of polyAl particles is shown to decrease when mixed with other particle types (case 3.0) compared to sole heating of polyAl (case 5), see figure 5.11. Noticing a difference between heating of PP particles in case 2.0 and case 3.0 is difficult in figure 5.11, however when zooming in a small difference can be distinguished, see figure 5.13. Similarly, PE case 2.0 and PE case 3.0 are difficult to distinguish in figure 5.11, but visible when zooming in as shown in figure 5.12.

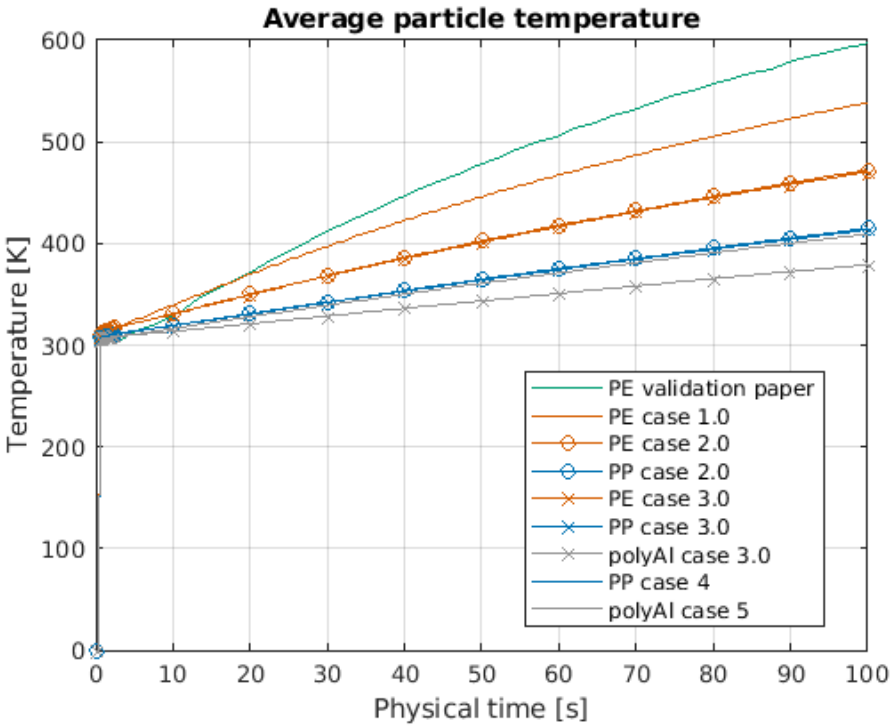

Figure 5.11: Average particle temperature for case 1.0, 2.0, 3.0, 4, 5 and data for heating of PE particles from the validation paper ([78]).

The heating rate for PE case 3.0 compared to case 2.0 is slightly lower, with a 2 K difference measured throughout, see figure 5.12. This could be explained by hotter PE particles conducting heat to other colder particle types. As shown in figure 5.13, PP particles in case 3.0 are slightly hotter than in case 4 but colder than compared to case 2.0. This could indicate that polyAl is absorbing this ”lost” heat from both PE and PP as analysed in the previous section, however polyAl’s particle heating is lower in case 3.0 than case 5. The observed temperature difference for PP particles is also very small, and could lie within the numerical uncertainty of the simulations, rather than being a result of particle heat transfer interaction. The temperature differences observed for PE particles is also small enough to potentially be due to numerics rather than reflecting present physics.

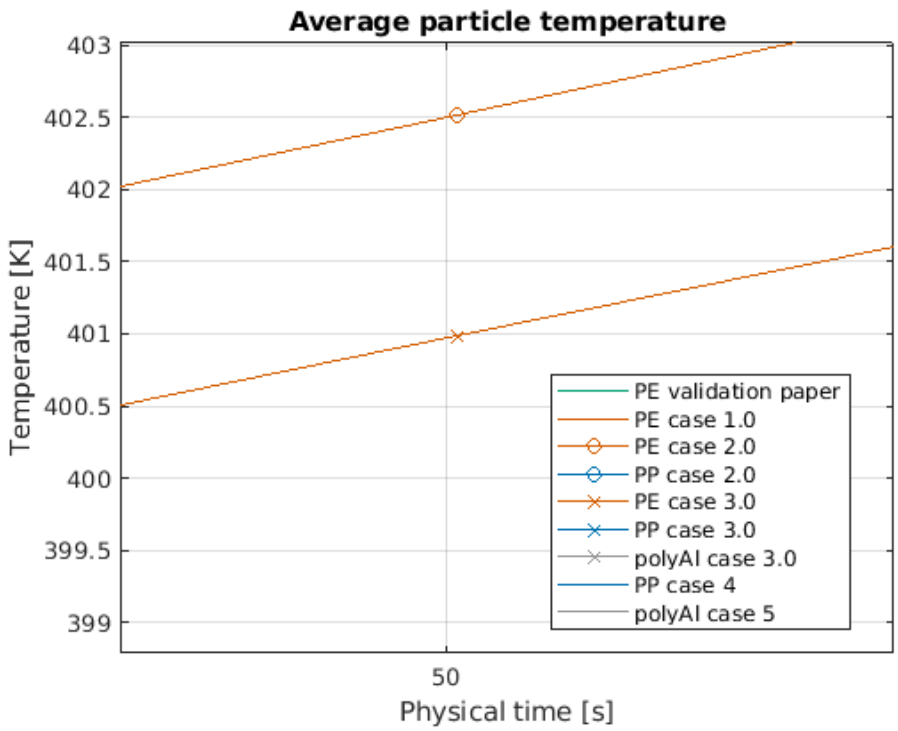

Figure 5.12: Zoomed in versions of plot shown in figure 5.11 showing the difference between PE case 2.0 and 3.0.

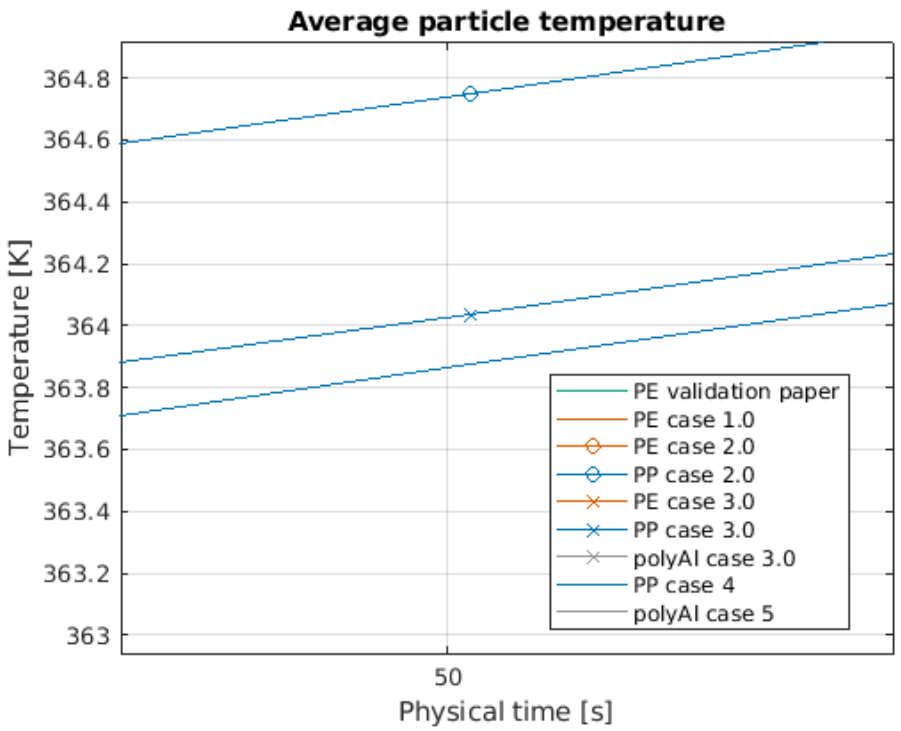

Figure 5.13: Zoomed in versions of plot shown in figure 5.11 showing the difference between PP case 2.0, 3.0 and 4.

Figure 5.14a shows the average particle Nusselt number for case 1.0, 3.0, 4 and 5. Again, the same trend can be observed with a small decrease in Nusselt number over time, with the exception for case 5. The corresponding calculated heat transfer coefficients are shown in figure 17 in the appendix and were used to calculate the average particle Biot numbers shown in figure 5.14b. PolyAl has a noticeably lower Biot number than both PP and PE particles, indicating that internal temperature gradients are even smaller for polyAl particles.

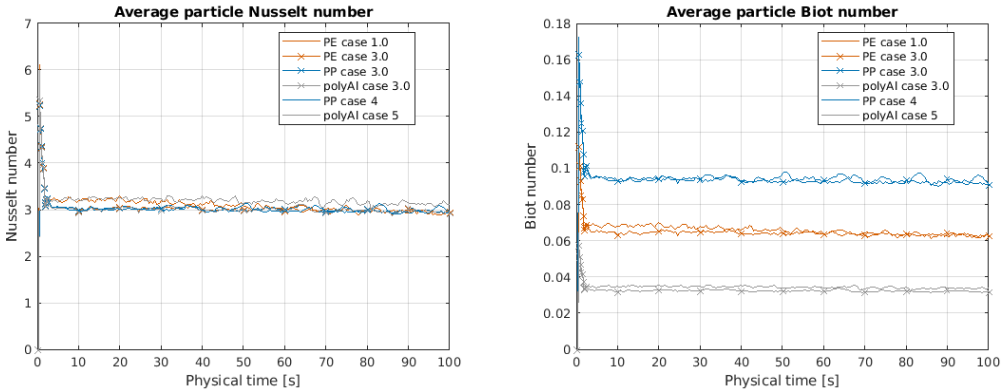

(a) Nusselt number

(b) Biot number

Figure 5.14: Average particle Nusselt number and calculated average particle Biot number for particles in case 1.0, 3.0, 4 and 5.

Particle mixing within the reactor for case 3.0 was uniform, as shown in figure 18 in the appendix. Similarly to case 1.0 and 2.0, the presence of the injected particles is visible when looking at the gas temperature field, see figure 19 the appendix. Also included in the appendix are plots of the average particle temperatures for each particle type, see figures 20-22. The particle average temperature for each particle type at 100 s is summarized in table 5.4 below to illustrate the difference in temperatures between the cases.

Table 5.4: Approximate particle average temperature at 100 s for case 1.0, 2.0, 3.0, 4 and 5.

PE	case 1.0	538 K
	case 2.0	472 K
	case 3.0	470 K
PP	case 2.0	415 K
	case 3.0	414 K
	case 4	413 K
polyAl	case 3.0	379 K
	case 5	409 K

5.3 Insights from the Simulation Setup Development

When setting up the simulation model, the main issues encountered were to do with stability and computational time. Running a simulation in parallel on more than one node can increase computational speed, a method often used for computing flow fields. However, flows including DEM particles have limitations regarding number of nodes that can be used relative to the number of present DEM particles. During the iterative setup development it was discovered that the simulation was only stable if run on a single node (with one node having 64 cores). Star-CCM+ recommends the number of processors, i.e. cores, used for DEM should be determined by dividing the number of DEM particles by 1500. As the setup uses 2000 particles the simulation should only be run using one core according to these recommendations. The mesh sensitivity, validation and case 1.0 simulations were run using 64 cores as the Star-CCM+ recommendation was only found after some time. For case 2.0 and 3.0 the number of cores used was varied throughout the simulations in an attempt to decrease computational run time. Running on 1-2 cores slowed down the computation but running on 4 cores showed increased computational speed. Due to time constraints, this was not investigated further. The remaining cases (1.1, 2.1, 3.1, 4 and 5) were all run on 4 cores.

Another insight from the setup development was found when investigating the effect of using one-way or two-way coupling. Initially two-way coupling was applied but in an attempt to reduce the computational time, one-way coupling was tested. This was however found to produce a significant difference in heating of the particles, with one-way coupling heating the particles unreasonably fast. This was determined to be due to the continuous phase not registering a heat loss even though the dispersed phase was absorbing this heat. Figure 23 in the appendix shows the significant difference in particle average temperature for one-way and two-way coupling.

Originally when running simulations it was noted that the DEM-sub step was maxed out (default 20 000 sub steps) for nearly all particles each iteration, indicating that particle interaction was perhaps not being resolved. Assuming that this was causing some error, further simulations with a significantly decreased max DEM substep were also tested to try and reduce run time. The trail of thought here was that if the high level of substepping produced error, it might be worth trying a much lower level of substepping as well, as the already existing error might not increase too much in relation to gained computational speed. Therefore, a significantly lower max DEM substep value of a 1000 was tested. However, this produced completely inaccurate results indicating further that particle interaction is important in calculating heat transfer to the particles. The error found when running with default 20 000 max substeps was smaller and more acceptable. The applied 20 000 max substeps in case 1.0 was reached for all particles, indicating that the solver was struggling to resolve particle interactions properly. This could potentially explain the lower average particle temperature of PE particles in case 1.0 compared to the data for PE particles from the validation paper, which presumably used a simulation setup

that was able to resolve particle interactions. If particle interactions, i.e. contact and collision with other particles and walls, are not resolved then this should cause inaccurate calculations of heat conduction through particle contact and consequently affect particle heating. The inability to resolve particle interactions is expected to be because of the time step applied. Efforts to understand how (and if) the global time step constrains the internal DEM time step were made, however due to time constraints these efforts were limited and results from this cannot be reported. Further work regarding this is needed and perhaps the DEM solver needs a significantly smaller time step, than the current time step used, to resolve particle movement and interactions. This could potentially lead to both an increase and decrease in computational time for the simulations. If the DEM solver needs less substeps to resolve particle interactions sufficiently, this could decrease computational time. However, a smaller time step would mean more time increments for simulating 100 s, which would most likely increase computational time. Altair state that a typical time step for DEM simulation is in the range 1e-4 to 1e-6 s, significantly smaller than the time step applied [81].

6 Discussion

6.1 Simulation Setup Validity

The mesh sensitivity and validation was carried out for a shorter simulation time than that of the MPW pyrolysis cases. This was due to the low computational speed. Initially, the simulation setup was determined valid when the simulation was run for 15 s physical time. However, it was later noted that there was a significant particle temperature discrepancy between case 1.0 and the corresponding data from the validation paper when the simulation was run for 100 s physical time. Ideally, all cases would have been run for 300 s physical time, as used in the validation paper. At time step 100 s, the average particle temperature measured approximately 540 K for case 1.0 and 600 K for the validation paper, a 60 K temperature difference, indicating an inaccurate simulation setup. In order to achieve accurate results the setup needs to be validated. Work on this would only be realistically possible if the computational run time first is noticeably decreased, however the extensive run time may be because of an incorrect simulation setup. The current runtime is leading to development of the model being impractical and improving the simulation setup in order for it to be accurate is necessary. Time step optimization, number of allowed substeps in the DEM solver and finding a preferred approach for running the CFD-DEM simulations on available high performance computing (HPC) architecture would be suggested initial improvement areas for decreasing run time and working on accuracy. As mentioned in section *5.3 Insights from the Simulation Setup Development*, the time step is likely affecting the DEM solver's ability to resolve particle interactions, which could be causing inaccuracies.

6.2 CFD-DEM Simulations of MPW Pyrolysis

The aim of the investigative CFD-DEM simulations of MPW pyrolysis, as stated in section 2.5, was to investigate mixing and heating of plastic particles and focusing particularly on the effects of including polyAl. The hypothesis was that polyAl, due to the interspersed aluminium, could work as a heat carrier in the plastic granular mix and improve heating of the plastic waste particles. Pure aluminium has a higher thermal conductivity and diffusivity than the polymer types (PE and PP). The polyAl material was however seen to have a lower thermal diffusivity than pure PE particles but higher than PP. Due to DEM not resolving the particles internally, the effect of thermal diffusivity cannot be observed in the simulations. However, both calculated values of

volumetric heat capacity and thermal diffusivity indicate that PE would be a better heat carrier than polyAl.

The reported results show that the heating of PE and polyAl particles are affected when mixed with other particle types. PP particles do not exhibit a significant effect in heating pattern. The difference in PE heating could be explained by the interacting particle's different temperatures driving heat transfer from the PE particles. This effect should however show up for PP particles when mixed with polyAl, as PP has a lower volumetric heat capacity (reaches higher temperature faster than polyAl) and therefore should be losing heat to polyAl in the same way PE does when mixed with PP. Additionally, the difference in heating PP and polyAl (case 4 and 5) was expected to be larger due to the significant difference in volumetric heat capacity. This difference does not show up in the simulation results. The unexpected heating patterns exhibited by PP, combined with a noticeably longer computational time for case 4 compared to case 5 and case 1.0 could indicate inaccuracies in the setup or lack of understanding material behaviour of PP. The causes of the observed heating patterns are difficult to pin point as several factors may be interacting. Further simulations combining PE+polyAl and PP+polyAl are needed.

PolyAl has the highest thermal inertia and will not work as a heat carrier as it requires more energy to heat up, continuously maintaining a lower temperature than the other two particle types (until the system reaches equilibrium). If polyAl was pre-heated, or the pyrolysis was run in continuous mode, it could potentially act as a heat carrier. Due to aluminium's higher melting temperature, the plastics will melt first and solid aluminium will be present in a plastic fluid. If the pyrolysis process is run at a temperature lower than aluminium's melting point and it is run in a continuous or semi-batch mode (has to be stopped at some point to remove aluminium build up), then the solid dispersed aluminium could potentially work as a heat carrier. Aluminium requires a lot of energy to heat up, however once it reaches the ambient temperature and is hotter than incoming plastics, it could due to its high thermal diffusivity, act as a heat carrier. The solid aluminium would be smaller than incoming plastic particles which could be beneficial for mixing. It should be noted that this is speculative and requires further investigation.

The rotary kiln walls are prescribed a constant wall temperature. When the system increases in thermal load, i.e. when introducing particles with higher thermal inertia (PP and polyAl), more thermal energy from the walls is absorbed by the particles. In order to maintain the constant wall temperatures, the energy to the system increases, entailing that the total amount of energy in the system is different for the cases, complicating comparison between cases. If instead a constant heat flux was used as boundary condition, this might better show how the available, and limited, thermal energy would be distributed amongst the particle types over time. With the current setup, it is difficult to say how heat transfer changes between the cases and explain why PP's heating pattern is seemingly unaffected when mixed with other particles and why polyAl's heating rate decreases.

It should also be questioned how much difference in particle heating is to be expected when combining different particle types in the current setup. The particle loading in the reactor is low, creating little particle layering. Most particles are in contact with the wall at all times, with gas moving rather freely amongst the particles. This would suggest that most particles do not experience much environmental difference when mixed with other particle types, with the exception of conductivity between the particles. How much does respective particle type's thermal conductivity matter in conduction between particles? Perhaps the difference in particle-particle conduction is negligible as wall conduction and gas convection dominate. If particle loading was much higher, this would create a very different environment for heat transfer, with many particles not being in contact with the walls and gas movement in the granular mix being more restricted.

The internal mixing of particles was investigated using animations of compiled PNGs for the particle scenes as shown in figures 15 and 18 in the appendix. Particles were fully mixed in both cases (2.0 and 3.0). The particles have different density which could cause slightly different mixing patterns, such as heavier particles sinking, when a higher particle loading is applied. In order to investigate a more realistic mixing scenario, simulations with a larger filling ratio, suggestively 1/3 reactor volume filled with particles ($\approx$ 21 000 particles), should be run. A larger filling ratio would be applied in an industrial setting and simulations of this would give insight on potential upscaling issues. Increasing particle count is expected to increase computational time as more particle equations need to be resolved. There is also the possibility of a decreasing effect on computational time as particle movement would be more restricted with higher particle density, however this would most likely not outweigh the increase due to increased number of equations being solved. As mentioned in section 3.4, particle displacement is one of the limits on DEM time step.

A particle filling ratio of 1/3 reactor volume would represent a more realistic setup, even though it would still be on a lab-scale. This would showcase particle interactions expected on a larger scale and how mixing might be affected. Agglomeration of certain particle types in regions of the drum could affect overall heating of the granular mass, for example if one particle type was in contact with the heated walls to a higher extent.

Using a higher filling ratio would not only give insight on potential changes in particle mixing but also changes in heat transfer within the granular mass. Heating of the particles, when applying a larger filling ratio, is expected to be slower for two reasons; fewer particles are in direct contact with the heated walls and the heated inert gas becomes more "trapped" within the granular mass. Both of these factors would increase temperature gradients within the granular mass. Heat convection from the gas to particles would be affected by the gas becoming "trapped" within the granular mass. Once the hot gas has transferred heat to the particles it would not be able to escape the particle matrix as easily and gas residence time within the granular mass would increase. "New" hot gas would most likely struggle to penetrate the granular mass, leading to a thicker thermal boundary layer on the particles. The decreased replacement of gas surrounding the particles would decrease the Nusselt number. Another consequence of

longer residence time for gas is, as Zhang et al. [78] discuss in the validation paper, the occurrence of more undesired secondary reactions which affects product yields. Studying particle heating in this more thermally inert system with higher filling ratio, would be useful for further process development and design. Equally, potential mixing improvements in order to increase gas circulation within the granular mass could be uncovered.

The amount of energy required to heat the nitrogen gas is low compared to the particles ($C_{vol,\,N_2} = 1.3\ kJ/m^3K$), meaning that the amount of energy stored in the gas, which could be transferred to the particles, is smaller. However, the thermal diffusivity of the nitrogen gas ($\alpha_{N_2} = 19.7\,mm^2/s$) is higher than for the polymer's, indicating that heat is efficiently conducted through the gas. In order to gain a better understanding of the heat transfer within the domain a further simulation case with no gas present would ideally be run if possible. DEM simulations without a continuous phase can be run in Star-CCM+ using meshfree DEM, however this modelling method does not include heat transfer. It should be explored if this is possible in other softwares, for example EDEM. A simulation case with no gas present could illustrate how significant the respective forms of heat transfer (convection and conduction) are and if one dominates. Considering the inaccurate and fast particle heating calculated for one-way coupling, the heat transfer from gas to particle phase should perhaps not be underestimated. Not having a gas phase present would decrease the number of equations being solved and most likely increase computational speed. Understanding which heat transfer mechanism is dominant would be useful for process development.

Gaining a better understanding on the dominant form of heat transfer would also be important in regards to the issue of resolving particle interaction. If conduction is determined dominant, then resolving particle interaction is necessary as conduction occurs through contact. As stated previously, it may be the unresolved particle contacts causing the under-predicted particle average temperature in case 1.0 compared to data from validation paper. Unresolved particle contacts resulting in inaccurately calculated heat conduction would explain the inaccurate results for case 1.1, 2.1 and 3.1, which presumably calculates larger errors for particle interaction as max DEM substep was set to 1000 (compared to 20 000).

6.3 CFD-DEM as part of a Multi-Scale Process Model

Part of the thesis aim was to assess the potential of using CFD-DEM as a tool for developing chemical plastic recycling of MPW. From the literature survey it was found that available reactor setups for pyrolysis all involve multiphase flow where the dispersed particle phase is present to a high degree in the continuos phase. Eulerian particle models are generally more suited for sparsely dispersed particle flows where overall flow patterns and properties are of interest. Lagrangian particle models track individual particles and

are used when the microscopic behaviour (i.e. what happens to individual particles) is of interest, compared to the macroscopic level of Eulerian models. The dispersed particles are therefore appropriately modelled using a Lagrangian formulation. Suitable alternatives are either Lagrangian material particles or DEM particles. Lagrangian material particles have mass and volume and are the most general formulation of the Lagrangian dispersed particle phase. DEM particles are limited to solid particles and DEM was designed specifically for modelling particle-dense granular materials [79]. Behaviour of particles in regions with high particle density is dominated by particle-particle interaction (collision, friction, contact forces), which the DEM model is designed to resolve. The Lagrangian material particle model is designed to resolve fluid-particle interactions (for example drag and lift forces) in flows and are better suited for flows not dominated by particle-particle interactions. The choice of CFD-DEM therefore seems to be an appropriate tool when working with virtual modelling of chemical plastic recycling. The investigative MPW pyrolysis simulations show how phenomena such as heat transfer and mixing in a chemical recycling reactor unit can be studied using CFD-DEM. However, in order to develop a full-bodied process model, further virtual models are needed to complement the CFD-DEM simulations.

DEM uses individual discrete elements, representing the particles, that interact with each other. Gradients within the particle are not resolved as there is no internal discretization of the particles. The simulation setup used in this thesis gives insight on particle temperature and heat transfer to the particles but not on internal particle temperature gradients. Modelling heat transfer within a single plastic granulate might be of interest for investigation of polymer cracking if perhaps trying to find optimal shape and size of granulates to achieve more uniform cracking or heating. This could be of interest for developing pre-processing, i.e. which size and geometry should feedstock be in order to avoid inefficient heating, as plastics in general have low thermal conductivity. In order to model internal particle heat conduction a multi-physics tool like COMSOL would be useful, where a single particle can be discretised. Before delving into internal particle heat transfer it would be of interest to determine which form of heat transfer to the particles is dominant, convection or conduction. The thermal diffusivity of the materials would also become relevant when resolving internal heat transfer.

Further development of the model setup would also include adding a reaction kinetic model. One idea could be to use the tracked particle temperature data from the CFD-DEM simulations and apply these to a chemical reaction code where cracking reactions are described using Arrhenius equations, triggering chemical reactions when particles reach a certain temperature. In order to write a chemical reaction model code for this purpose, the product formation would have to be determined experimentally. This is further discussed in section *6.5 Suggested Future Work*.

Lastly, there is the aspect of phase change that occurs in pyrolysis and how or if this should be considered when aiming to build a full-bodied process model. Using thermoplastics in pyrolysis will lead to them melting, with PE having a melting point temperature around 105-140 °C [86](depending on the PE type) and PP around 200

°C [33]. From the literature survey it was not clear if, or to which extent, melting and cracking occur consecutively or simultaneously. However, there is clearly melting of thermoplastics during pyrolysis and using solid spherical particles to represent a liquidus plastic is questionable. It could be worth exploring if there is a significant difference in heating of plastics when modelled as solid spherical particles compared to a liquid phase. Most of the products produced in pyrolysis are found in the gas phase (condensible and non-condensible gases). This phase exchange is also not considered in the current setup. It might not be of any value creating virtual models that incorporate the different states, however it is an aspect that needs to be considered if aiming to build a full-bodied process model. The melting temperature of aluminium compared to plastics should also be considered. At higher temperatures, the plastic granular mass will have melted and there will be a multiphase flow with two fluid phases, gas and melted plastics, with a dispersed solid phase of aluminium particles. Eventually, the solid aluminium particles will also melt.

6.4 Challenges of MPW Pyrolysis

The main challenges of MPW pyrolysis as a recycling method mentioned frequently in literature, regardless of intended recyclate product, are related to issues with feedstock and the process' energy intensity [87]. Both these issues affect the economic viability of operating MPW pyrolysis plants [88]. It is the issue of energy intensity that makes the potential of polyAl as a heat carrier an interesting question to pose and investigate.

Issues related to the plastic feedstock are primarily to do with quality and availability. Feedstock for plastic waste pyrolysis is typically post consumer waste, i.e. a heterogenous and contaminated plastic feed. The feedstock not only varies in composition but also in the shapes and sizes of the plastics. Pyrolysis allows a higher degree of contamination in the feedstock than mechanical recycling, however contamination levels are still limited and pre-sorting is necessary. Contamination of the feed has an effect on product quality, product yield and operation maintenance. Biomass contamination is not necessarily problematic as co-feeding plastic waste and biomass in pyrolysis is possible, with ongoing research pushing improvements [87].

A consequence of the feedstock heterogeneity is the risk of present toxic substances that can form toxins in the reactor or otherwise be damaging to the reactor. Upstream sorting of the waste to identify feed content and remove undesired materials before pyrolysis is necessary, adding to process costs. Depending on reactor type and waste composition, the process setup can be more or less forgiving to feedstock varying in shape and size. Some reactor types, like rotary kilns, are more forgiving whereas fluidized beds require pre-processing (for example crushing and sieving) of the waste to ensure a uniform sized feed [87]. Plastic films are a common plastic waste product that often cause processing difficulties [73]. Acquiring a steady feed of sufficient quality and/or volume has previously been a challenging factor in developing plastic recycling

methods. However, recent changes in regulations on plastic waste export has increased the amount of plastic waste handled within the EU, hopefully decreasing the issue of unavailability [87].

Pyrolysis is an energy intensive process and necessary energy input is strongly linked to the relatively high operating temperatures used. Different temperature ranges, heating rates and residence times can all be used to modify product compositions and yields. These parameters have a strong correlation to the process' high energy demand and energy costs [89]. Depending on the energy source used, costs and environmental impact can vary. However, the energy intensity of pyrolysis, regardless of energy source, significantly impacts the process operation costs which has an effect on the products' minimum selling prices. Efficient and optimal heating is therefore an important design parameter and engineering challenge. It is not uncommon to integrate an internal energy loop in pyrolysis, where combustion of some products are used to fuel the pyrolysis reactor. If polyAl had turned out to work as a heat carrier this would be a good motive to include the polyAl material in the process and would aid heating, hopefully decreasing the required energy intensity and energy cost. This was however shown not to be the case and the results indicate that perhaps separating aluminium from polyAl as a pre-processing step might be preferred.

Energy requirement and costs is also increased when downstream product purification is necessary. There appears to be somewhat of a disagreement on if pyrolysis of plastic waste, for production of value added products, is viable or even technically possible due to contamination and waste heterogeneity. Some sources claim that it is ([90], [91], [92] among others) whereas others claim that product quality is far too low and the necessary downstream purification, if technically possible, renders MPW pyrolysis infeasible [93]. The topic on downstream purification of pyrolysis products was not covered in the literature survey due to time constraints. Identifying if pyrolysis as recycling method of MPW is possible on an industrial scale is not easy. Most experimental studies on pyrolysis of plastic waste were, in the literature survey, found to be carried out on a laboratory scale whereas studies on industrial scale appeared to be predominantly simulations, TEAs and LCAs. This gives reason to question how much is understood or known about the complications of scaling up endeavours and how this affects the pyrolysis process. For example, temperature control and uniform heat transfer at a larger scale is more technically challenging than at a laboratory-scale [89]. Perhaps some of the disagreement on feasibility of MPW pyrolysis stems from this possible knowledge gap. With this noted, there are several companies that have demonstrated working pilot scale or commercial pyrolysis plants treating plastics [21]. Enval Ltd [94] is a company that treats plastic aluminium laminates using pyrolysis, recovering aluminium and producing pyrolysis gas and oil. Sapporo Plastic Recycling had a fully commercial pyrolysis plant on the Hokkaido island for 15 years with the capacity of treating 50 tons MPW per day [95]. The plant was decommissioned due to financial issues [60].

In order for pyrolysis as a recycling method of plastic waste to be economically viable, there must be a market for the recyclate product. If the product is intended to replace a primary raw material, it must also be competitively priced. Required pre-treatment of feedstock increases process costs, however installations of pre-treatment units could decrease downstream purification costs. One potential advantage of pyrolysis, which could have a positive effect on the supply-demand relationship with the market, is the potential possibility of varying the product outflow by tuning the pyrolysis plant's process parameters (heating, residence time, feedstock composition etc.). This would ideally allow for some flexibility to product and feedstock market adaptations.

Pyrolysis as a method for plastic-to-plastic recycling also faces regulatory challenges. Using recycled plastic in food contact materials is very challenging due to strict EU regulations [96]. Regulations for pyrolysis of plastic waste and classification of pyrolysis-derived products varies, affecting industrial application and market adoption [89]. Replacing virgin fossil sourced materials with pyrolysis products appears to not only be a financial challenge but also having pyrolysis products recognised on the market.

With current efforts to develop sustainable industries and society, with improved recycling being a vital cornerstone of this, environmental impacts of new recycling methods cannot be ignored. The high energy demand of pyrolysis can have a large impact on sustainability and environment, where choice of energy source plays a significant role. There are also challenging environmental concerns regarding process emissions for pyrolysis (for example greenhouse gases and particulate matter) that need attention [89].

6.5 Suggested Future Work

This thesis was intended to be a first step in developing an accurate multi-scale numerical model for chemical recycling of mixed plastic waste where the aim was to create a setup that either included multi-physics integration or was extendable to include multi-physics at a later stage. As assessed in section *6.3 CFD-DEM as part of a Multi-Scale Process Model*, the current model setup does not include any multi-physics integration. This section contains suggestions on the immediate next steps to take towards achieving the envisioned full-bodied process model. The following discussion on future work presumes action to achieve a valid simulation setup, as discussed in section *6.1 Simulation Setup Validity*, has been completed successfully. The key areas recommended for immediate future research are investigation of material parameters (thermal conductivity of polymers and melting point of aluminium), experimental validation and ideally development of a suitable reaction model.

Firstly, the current simulation setup uses constant values of thermal conductivity for the different plastics. As noted in the literature survey, section *2.1.1.2 Polymer Heat Conductivity*, thermal conductivity is temperature dependent. The effect of assuming a constant value thermal conductivity, when in fact it varies with temperature, should be

investigated. If assuming a constant value thermal conductivity causes non-negligible inaccuracies in particle heating then a temperature dependent field function for thermal conductivity should be applied. Availability of data for such a field function for selected materials needs to be reviewed, if non-existent this would require further experimental work.

Secondly, further experimental work for validating a full-bodied numerical setup is needed. Specifically, experiments investigating the product yield and composition for MPW pyrolysis containing polyAl is needed. This would, as a suggestion, be carried out using gas chromatography. Currently, there is little known of pyrolysis products from pyrolysis of plastic and aluminium. During the literature survey only one paper was found on pyrolysis of plastic and aluminium [97]. Experimental work investigating the effect of including aluminium is needed, especially investigating how aluminium's melting point might affect product yield, product composition and operating temperature range. Aluminium has a melting point temperature of 660 K and pyrolysis processes usually operate between 300-900 K. It would be interesting to investigate how aluminium interacts with the cracking polymer molecules. If aluminium was determined to have a significantly negative effect on the process, then separation of plastic and aluminium for polyAl (as mentioned in section *2.1.3 Tetra Pak's Packaging Material*) might be a necessary pre-processing treatment.

Experimentally investigating product yield and composition for pyrolysis of MPW specifically containing aluminium is necessary if efforts are to be made in developing reaction kinetic models. Ideally, a full-bodied numerical model setup would include the ability to simulate reactive flows and therefore chemical reaction models are needed. If reaction models for pyrolysis of MPW were available, it could aid and allow process development and optimization through virtual modelling rather than expensive and limited experimental methods, particularly on an industrial scale. There are four issues to consider with regards to developing a chemical reaction model for MPW pyrolysis. The first issue is to determine which level of detail the reaction model should cover, i.e. how simple or complex can/should the model be. An increasingly complex model will notably increase computational demand. Further, the composition and contamination of the pyrolysis feedstock must be considered with regard to the reaction model. Both of these can vary considerably, which consequently could cause a variance in product yield and composition. Therefore it would be interesting to investigate if it is possible to develop a reaction model which allows for a certain level of variance of feedstock constituent and contamination levels. In connection to this it would be necessary to delve into available literature on contaminants and additives found in post-consumer plastic waste. Considering how much the pyrolysis process parameters can vary (feedstock composition, shape and size, contamination levels, pre-processing, reactor type etc.), and thereby affect product yield and composition, it could be quite challenging developing a useful reaction model.

As realised from section *6.4 Challenges of MPW Pyrolysis*, there remain several challenges with pyrolysis as a recycling method for MPW, which all require further research.

Some of these challenges can be worked on using CFD-DEM simulations, with efforts for improving heat transfer being especially relevant. CFD-DEM could also be a useful tool in developing pre-treatment processes (sorting, washing etc.). Creating a full-bodied multi-scale process simulation setup however, requires considerably more work.

7 Conclusions

There are many different chemical recycling process options for recycling of plastics being developed, with some process types only suited for very specific plastics. Based on the content found in MPW, the preferred chemical recycling option would be pyrolysis, especially if plastic-to-plastic recycling is the aim. Pyrolysis appears a promising recycling method for increasing circularity in the plastic sector, however several challenges remain. Primary concerns are high energy demand, as pyrolysis is a very energy intensive process, and feedstock issues related to quality (composition, contamination and shape/size uniformity). Using MPW as feedstock, the issues of feedstock quality are especially eminent.

The energy intensity of pyrolysis is strongly correlated to the applied temperature range. Generally, higher process temperatures increase the yield of smaller hydrocarbons whereas lower operating temperatures increase yield of larger hydrocarbons. For plastic-to-plastic chemical recycling, smaller hydrocarbon pyrolysis products in the naphtha range (C_5-C_{10}) are desired product outflow. Uniform heating, and consequently uniform cracking, with low residence time for intermediates are also important factors influencing product yield of smaller hydrocarbons. Non-uniform cracking and longer residence time increases undesired secondary reactions which in turn leads to higher char formation and increased yield of larger hydrocarbons.

The potential of using CFD-DEM as a tool for developing chemical recycling of MPW was tested by investigating the heating of plastic particles for different particle compositions. Specifically, the inclusion of polyAl particles was studied with the intent to investigate if the interspersed aluminium would cause the polyAl particles to act as heat carriers in the plastic granular mix, potentially improving heating of the simulated MPW. The other two particle types used were the two most common constituents found in MPW, i.e. polyethylene and polypropylene. PE was found to have the lowest volumetric heat capacity and the largest thermal diffusivity out of the three plastics, indicating that it is rather this material that has potential to act as a heat carrier. PolyAl requires the most energy, out of the three particle types, to heat up. This causes polyAl to, at all times, have a lower average particle temperature compared to PE and PP in a transient system. PolyAl will therefore increase the energy demand and run time of the pyrolysis process required, to reach targeted temperatures. As discussed in section 6.4 *Challenges of MPW Pyrolysis*, the energy intensity required for pyrolysis is one of the main challenges. Including polyAl will have a negative effect in this regard. It might therefore be of interest to separate the plastic and aluminium in polyAl in a pre-processing step. However, as speculated in section 6.2 *CFD-DEM Simulations of MPW Pyrolysis*, there

is potential for solid aluminium from polyAl to work as heat carrier in lower temperature pyrolysis processes when run in continuous or semi-batch mode.

The CFD-DEM model setup developed was deemed adequate to gain some insights, however improvements are needed in order to validate the setup. The time step used in the setup is suspected to be the cause of unresolved particle interactions (calculating inaccuracies in heat conduction through particle contacts) and causing excessive computational time.

The simulation setup developed for the CFD-DEM simulations showed good potential for using CFD-DEM as a tool in pyrolysis process development, especially for work aimed at developing and improving heat transfer. CFD-DEM is a good initial step in creating a full-bodied process model of pyrolysis for chemical plastic recycling. Further work to develop a multi-scale model should focus on developing chemical reaction models for pyrolysis of MPW including polyAl. In order for this to be possible, experimental work determining product yield must first be carried out as this is currently unknown. Further understanding of effects on including aluminium in the process is needed as well as how commonly found contaminations of MPW might affect heating and product yield.

Bibliography

[1] OECD. *Global Plastics Outlook: Economic Drivers, Environmental Impacts and Policy Options*. 2022. DOI: 10.1787/de747aef-en. URL: https://doi.org/10.1787/de747aef-en.

[2] J. G. Speight. "Chapter 14 - Monomers, Polymers, and Plastics". In: *Handbook of Industrial Hydrocarbon Processes*. Ed. by J.G. Speight. Boston: Gulf Professional Publishing, 2011, pp. 499–537. ISBN: 978-0-7506-8632-7. DOI: https://doi.org/10.1016/B978-0-7506-8632-7.10014-3. URL: https://www.sciencedirect.com/science/article/pii/B9780750686327100143.

[3] European Parliament. *Plastic waste and recycling in the EU: facts and figures*. 2024. URL: https://www.europarl.europa.eu/topics/en/article/20181212STO21610/plastic-waste-and-recycling-in-the-eu-facts-and-figures (visited on 08/08/2025).

[4] European Commission. *Packaging waste*. 2025. URL: https://environment.ec.europa.eu/topics/waste-and-recycling/packaging-waste_en (visited on 10/07/2025).

[5] Inc. A&C Plastics. *Medical Uses for Plastic Materials*. n.d. URL: https://www.acplasticsinc.com/informationcenter/r/medical-uses-for-plastic-materials (visited on 08/09/2025).

[6] PWR Pack. *The Ultimate Guide to Food Packaging Materials*. 2025. URL: https://www.pwrpack.com/pwr-insights/food-packaging-materials/ (visited on 08/09/2025).

[7] S. Chen and Y.H. Hu. "Advancements and future directions in waste plastics recycling: From mechanical methods to innovative chemical processes". In: *Chemical Engineering Journal* 493 (2024), p. 152727. DOI: 10.1016/j.cej.2024.152727.

[8] A. Rahimi and J.M. García. "Chemical recycling of waste plastics for new materials production". In: *Nature Reviews Chemistry* 1 (2017), p. 0046. DOI: https://doi.org/10.1038/s41570-017-0046.

[9] Tetra Pak. *Solutions*. Accessed: 2025-08-04. 2025. URL: https://www.tetrapak.com/solutions.

[10] G. W. Coates and Y. D. Y. L. Getzler. "Chemical recycling to monomer for an ideal, circular polymer economy". In: *Nature Reviews Materials* 5 (2020), pp. 501–516. DOI: 10.1038/s41578-020-0190-4. URL: https://doi.org/10.1038/s41578-020-0190-4.

[11] British Plastics Federation. *Plastics Additives*. n.d. URL: https://www.bpf.co.uk/plastipedia/additives/Default.aspx%5C#HeatStabilisers (visited on 09/01/2025).

[12] British Plastics Federation. *How Is Plastic Made? A Simple Step-By-Step Explanation*. n.d. URL: https://www.bpf.co.uk/plastipedia/how-is-plastic-made.aspx (visited on 09/01/2025).

[13] European Environment Agency. *Global bio-based plastics production capacity*. Published: 2024-04-18. URL: https://www.eea.europa.eu/en/circularity/sectoral-modules/plastics/global-bio-based-plastics-production-capacity (visited on 09/01/2025).

[14] TWI Global. *Thermoset vs Thermoplastic (What is the Difference?)* n.d. URL: https://www.twi-global.com/technical-knowledge/faqs/thermoset-vs-thermoplastic (visited on 09/01/2025).

[15] Plastics Europe. *How plastics are made*. 2025. URL: https://plasticseurope.org/plastics-explained/how-plastics-are-made/ (visited on 09/01/2025).

[16] M. Barón et al. "Glossary of class names of polymers based on chemical structure and molecular architecture (IUPAC Recommendations 2009)". In: *Pure and Applied Chemistry* 81.6 (2009), pp. 1131–1186. DOI: 10.1351/PAC-REC-08-01-30. URL: https://publications.iupac.org/pac/81/6/1131/index.html.

[17] LibreTexts Contributors. *16.2: Hydrocarbons*. 2021. URL: https://chem.libretexts.org/Courses/Nassau_Community_College/Principles_of_Chemistry/16%3A_Organic_Chemistry/16.02%3A_Hydrocarbons (visited on 09/04/2025).

[18] A. Queiroz et al. "Subcritical and supercritical water for chemical recycling of plastic waste". In: *Current Opinion in Green and Sustainable Chemistry* 25 (2020), p. 100364. ISSN: 2452-2236. DOI: https://doi.org/10.1016/j.cogsc.2020.100364. URL: https://www.sciencedirect.com/science/article/pii/S2452223620300535.

[19] William Professor Emeritus (Michigan State U.) Reusch. *Free Radical Polymerization*. 2015. URL: https://chem.libretexts.org/Courses/Purdue/Purdue_Chem_26100%3A_Organic_Chemistry_I_(Wenthold)/Chapter_08%3A_Reactions_of_Alkenes/8.7.Polymerization/Free_Radical_Polymerization (visited on 09/05/2025).

[20] S. Ray and R.P. Cooney. "Chapter 9 - Thermal Degradation of Polymer and Polymer Composites". In: *Handbook of Environmental Degradation of Materials (Third Edition)*. Ed. by Myer Kutz. Third Edition. William Andrew Publishing, 2018, pp. 185–206. ISBN: 978-0-323-52472-8. DOI: https://doi.org/10.1016/B978-0-323-52472-8.00009-5. URL: https://www.sciencedirect.com/science/article/pii/B9780323524728000095.

[21] K.M. Knauer, C. Higginson, and M. Lee. "Circular Plastics Technologies: Pyrolysis of Plastics to Fuels and Chemicals". In: *Physical Sciences Reviews* 9 (2024), pp. 1931–1953. ISSN: 2365-659X. DOI: 10.1515/psr-2022-0175. URL: https://www.osti.gov/servlets/purl/1984227.

[22] D.A. Purser, A.A. Stec, and T.R. Hull. "14 - Effects of the material and fire conditions on toxic product yields". In: *Fire Toxicity*. Ed. by Anna Stec and Richard Hull. Woodhead Publishing, 2010, pp. 515–540. ISBN: 978-1-84569-502-6. DOI: https://doi.org/10.1533/9781845698072.4.515. URL: https://www.sciencedirect.com/science/article/pii/B9781845695026500142.

[23] M. Seifali Abbas-Abadi et al. "Challenges and opportunities of light olefin production via thermal and catalytic pyrolysis of end-of-life polyolefins: Towards full recyclability". In: *Progress in Energy and Combustion Science* 96 (2023), p. 101046. ISSN: 0360-1285. DOI: https://doi.org/10.1016/j.pecs.2022.101046. URL: https://www.sciencedirect.com/science/article/pii/S0360128522000533.

[24] Y. Jia et al. "Effect of temperature and crystallinity on the thermal conductivity of semi-crystalline polymers: A case study of polyethylene". In: *Materials Chemistry and Physics* 287 (2022), p. 126325. ISSN: 0254-0584. DOI: https://doi.org/10.1016/j.matchemphys.2022.126325. URL: https://www.sciencedirect.com/science/article/pii/S0254058422006319.

[25] K. Funk, J. Milford, and T. Simpkins. "Chapter 19 - Waste not, want not: analyzing the economic and environmental viability of waste-to-energy technology for site-specific optimization of renewable energy options". In: *Bioenergy (Second Edition)*. Ed. by Anju Dahiya. Second Edition. Academic Press, 2020, pp. 385–423. ISBN: 978-0-12-815497-7. DOI: https://doi.org/10.1016/B978-0-12-815497-7.00019-1. URL: https://www.sciencedirect.com/science/article/pii/B9780128154977000191.

[26] H. Ljungkvist Nordin and A.K. Westöö. *Plast i Sverige: fakta och praktiska tips*. Kort version av "Kartläggning av plastflöden i Sverige" (SMED rapport nr 2019:01). ISBN: 978-91-620-8852-1; accessed on 2 September 2025. Naturvårdsverket (Swedish Environmental Protection Agency), 2020. URL: https://www.naturvardsverket.se/4ac391/globalassets/media/publikationer-pdf/8800/978-91-620-8852-1.pdf.

[27] S. K. Ghosh and P. Agamuthu. "Plastics in municipal solid waste: What, where, how and when?" In: *Waste Management & Research* 37.11 (2019), pp. 1061–1062. DOI: 10.1177/0734242X19880656. URL: https://doi.org/10.1177/0734242X19880656.

[28] K.M. Cantor and P. Watts. "1 - Plastics Materials". In: *Applied Plastics Engineering Handbook*. Ed. by Myer Kutz. Plastics Design Library. Oxford: William Andrew Publishing, 2011, pp. 3–5. ISBN: 978-1-4377-3514-7. DOI: https://doi.org/10.1016/B978-1-4377-3514-7.10001-7. URL: https://www.sciencedirect.com/science/article/pii/B9781437735147100017.

[29] S.M. Kurtz. "1 - A Primer on UHMWPE". In: *UHMWPE Biomaterials Handbook (Third Edition)*. Ed. by Steven M. Kurtz. Third Edition. Oxford: William Andrew Publishing, 2016, pp. 1–6. ISBN: 978-0-323-35401-1. DOI: https://doi.org/10.1016/B978-0-323-35401-1.00001-6. URL: https://www.sciencedirect.com/science/article/pii/B9780323354011000016.

[30] L.E. Helseth. *Polyetylen*. Store norske leksikon. Used figure of PE molecular structure. License: CC BY SA 3.0. 2025. URL: https://snl.no/polyetylen (visited on 06/01/2026).

[31] Adventpac. *LDPE and HDPE: Key Differences & Similarities*. 2020. URL: https://www.adventpac.com/resources/differences-between-ldpe-and-hdpe (visited on 09/02/2025).

[32] Plastics Europe. *Polyolefins*. 2025. URL: https://plasticseurope.org/plastics-explained/a-large-family/polyolefins/ (visited on 09/02/2025).

[33] Edinburgh Napier University British Plastics Federation. Colin Hindle. *Polypropylene (PP)*. n.d. URL: https://www.bpf.co.uk/plastipedia/polymers/PP.aspx (visited on 09/02/2025).

[34] S. Ore. *Polypropylen*. Store norske leksikon. Used figure of PP molecular structure. License: CC BY SA 3.0. 2025. URL: https://snl.no/polypropylen (visited on 06/01/2026).

[35] British Plastics Federation. *Polyvinyl Chloride (PVC)*. n.d. URL: https://www.bpf.co.uk/plastipedia/polymers/PVC.aspx (visited on 09/02/2025).

[36] European Council of Vinyl Manufacturers (ECVM). *PVC's physical properties*. n.d. URL: https://www.pvc.org/about-pvc-old/pvcs-physical-properties/ (visited on 09/02/2025).

[37] M. Worgull. "Chapter 9 - Polymer materials for hot embossing". In: *Hot Embossing (Second Edition)*. Ed. by Matthias Worgull. Second Edition. Micro and Nano Technologies. Elsevier, 2024, pp. 245–268. ISBN: 978-0-12-821193-9. DOI: https://doi.org/10.1016/B978-0-12-821193-9.00015-8. URL: https://www.sciencedirect.com/science/article/pii/B9780128211939000158.

[38] S. Ore, A. Stori, and L.E. Helseth. *Polyvinylklorid*. Store norske leksikon. Used figure of PVC molecular structure. License: CC BY SA 3.0. 2025. URL: https://snl.no/polyvinylklorid (visited on 06/01/2026).

[39] L. T. Sin and B. S. Tueen. "1 - Plastics and environmental sustainability issues". In: *Plastics and Sustainability*. Ed. by Lee Tin Sin and Bee Soo Tueen. Elsevier, 2023, pp. 1–43. ISBN: 978-0-12-824489-0. DOI: https://doi.org/10.1016/B978-0-12-824489-0.00006-4. URL: https://www.sciencedirect.com/science/article/pii/B9780128244890000064.

[40] M. T. Siraj et al. "12.47 - Eco-friendly food packaging innovations: A review of recent progress on recyclable polymers". In: *Comprehensive Materials Processing (Second Edition)*. Ed. by Saleem Hashmi. Second Edition. Oxford: Elsevier, 2024, pp. 693–709. ISBN: 978-0-323-96021-2. DOI: https://doi.org/10.1016/B978-0-323-96020-5.00077-7. URL: https://www.sciencedirect.com/science/article/pii/B9780323960205000777.

[41] Pantamera (Returpack AB). *Om pantsystemet*. n.d. URL: https://www.pantamera.nu/privatperson/fakta--statistik/om-pantsystemet (visited on 09/02/2025).

[42] T. Thiounn and R.C. Smith. "Advances and approaches for chemical recycling of plastic waste". In: *Journal of Polymer Science* 58.10 (2020), pp. 1347–1364. DOI: https://doi.org/10.1002/pol.20190261. eprint: https://onlinelibrary.wiley.com/doi/pdf/10.1002/pol.20190261. URL: https://onlinelibrary.wiley.com/doi/abs/10.1002/pol.20190261.

[43] F. Recupido et al. "Post-consumer recycling of Tetra Pak®: Starting a "new life" as filler in sustainable polyurethane foams". In: *Food Packaging and Shelf Life* 40 (2023), p. 101175. ISSN: 2214-2894. DOI: https://doi.org/10.1016/j.fpsl.2023.101175. URL: https://www.sciencedirect.com/science/article/pii/S2214289423001527.

[44] Tetra Pak. *Sustainability*. Accessed: 2025-10-07. 2025. URL: https://www.tetrapak.com/sustainability/focus-areas/circularity-and-recycling/recycled-products.

[45] J.G. Speight. "Chapter 1 - Heavy Oil, Extra Heavy Oil, and Tar Sand Bitumen". In: *Heavy Oil Recovery and Upgrading*. Ed. by James G. Speight. Gulf Professional Publishing, 2019, pp. 3–47. ISBN: 978-0-12-813025-4. DOI: https://doi.org/10.1016/B978-0-12-813025-4.00001-5. URL: https://www.sciencedirect.com/science/article/pii/B9780128130254000015.

[46] A.M. Aitani. "Oil Refining and Products". In: *Encyclopedia of Energy*. Ed. by Cutler J. Cleveland. New York: Elsevier, 2004, pp. 715–729. ISBN: 978-0-12-176480-7. DOI: https://doi.org/10.1016/B0-12-176480-X/00259-X. URL: https://www.sciencedirect.com/science/article/pii/B012176480X00259X.

[47] U.S. Energy Information Administration. *Crude oil distillation and the definition of refinery capacity*. 2012. URL: https://www.eia.gov/todayinenergy/detail.php?id=6970.

[48] P. Bodenes. "Study of the application of pulsed electric fields (PEF) on microalgae for the extraction of neutral lipids." Used figure 3 from thesis with permission from author. Theses. Université Paris Saclay (COmUE), May 2017. URL: https://theses.hal.science/tel-01540436.

[49] T. Goga et al. "A lifecycle-based evaluation of greenhouse gas emissions from the plastics industry in South Africa". In: *South African Journal of Science* 119.1/2 (2023). DOI: 10.17159/sajs.2023/13842. URL: https://doi.org/10.17159/sajs.2023/13842.

[50] Gas Data Limited. *Syngas: What is it, how is it made & where is it used?* 2023. URL: https://www.gasdata.co.uk/whats-on/syngas-what-is-it-how-is-it-made-where-is-it-used/ (visited on 08/21/2025).

[51] J.G. Speight. "Chapter 8 - Hydrocarbons from synthesis gas". In: *Handbook of Industrial Hydrocarbon Processes (Second Edition)*. Ed. by James G. Speight. Second Edition. Boston: Gulf Professional Publishing, 2020, pp. 343–386. ISBN: 978-0-12-809923-0. DOI: https://doi.org/10.1016/B978-0-12-809923-0.00008-4. URL: https://www.sciencedirect.com/science/article/pii/B9780128099230000084.

[52] M.R. Gogate. "Methanol-to-olefins process technology: current status and future prospects". In: *Petroleum Science and Technology* 37.5 (2019), pp. 559–565. DOI: 10.1080/10916466.2018.1555589. eprint: https://doi.org/10.1080/10916466.2018.1555589. URL: https://doi.org/10.1080/10916466.2018.1555589.

[53] J.P. Chakraborty, S. Singh, and S.K. Maity. "Chapter 6 - Advances in the conversion of methanol to gasoline". In: *Hydrocarbon Biorefinery*. Ed. by Sunil K. Maity, Kalyan Gayen, and Tridib Kumar Bhowmick. Elsevier, 2022, pp. 177–200. ISBN: 978-0-12-823306-1. DOI: https://doi.org/10.1016/B978-0-12-823306-1.00008-X. URL: https://www.sciencedirect.com/science/article/pii/B978012823306100008X.

[54] Vioneo. *Honeywell's Technology chosen by Vioneo for its Planned European Production of Fossil-Free Plastics*. 2025. URL: https://vioneo.com/news/honeywells-technology-chosen-by-vioneo-for-its-planned-european-production-of-fossil-free-plastics/ (visited on 09/08/2025).

[55] A-Pac Manufacturing. *Understanding the Connection Between Natural Gas and Industrial Production of Polyethylene*. 2024. URL: https://www.polybags.com/how-natural-gas-production-affects-the-resin-market/ (visited on 09/04/2025).

[56] Container & Packaging; Stephen Post. *Plastic 102: Exactly How Is It Made?* 2019. URL: https://www.containerandpackaging.com/resources/plastic-101-exactly-made (visited on 09/04/2025).

[57] J. Ochoa Robles, S. De-León Almaraz, and C. Azzaro-Pantel. "Chapter 2 - Hydrogen Supply Chain Design: Key Technological Components and Sustainable Assessment". In: *Hydrogen Supply Chains*. Ed. by Catherine Azzaro-Pantel. Academic Press, 2018, pp. 37–79. ISBN: 978-0-12-811197-0. DOI: https://doi.org/10.1016/B978-0-12-811197-0.00002-6. URL: https://www.sciencedirect.com/science/article/pii/B9780128111970000026.

[58] J.E. Lee et al. "Current methods for plastic waste recycling: Challenges and opportunities". In: *Chemosphere* 370 (2025), p. 143978. ISSN: 0045-6535. DOI: https://doi.org/10.1016/j.chemosphere.2024.143978. URL: https://www.sciencedirect.com/science/article/pii/S0045653524028868.

[59] W. Zhang, L. Killian, and A. Thevenon. "Electrochemical recycling of polymeric materials". In: *Chemical Science* 15.23 (2024), pp. 8606–8624. ISSN: 2041-6520. DOI: https://doi.org/10.1039/d4sc01754d. URL: https://www.sciencedirect.com/science/article/pii/S2041652024007557.

[60] M. Solis and S. Silveira. "Technologies for chemical recycling of household plastics – A technical review and TRL assessment". In: *Waste Management* 105 (2020), pp. 128–138. ISSN: 0956-053X. DOI: https://doi.org/10.1016/j.wasman.2020.01.038. URL: https://www.sciencedirect.com/science/article/pii/S0956053X20300465.

[61] R. Miandad et al. "Catalytic pyrolysis of plastic waste: A review". In: *Process Safety and Environmental Protection* 102 (2016), pp. 822–838. ISSN: 0957-5820. DOI: https://doi.org/10.1016/j.psep.2016.06.022. URL: https://www.sciencedirect.com/science/article/pii/S0957582016301082.

[62] G.C. Laredo, J. Reza, and E.M. Ruiz. "Hydrothermal liquefaction processes for plastics recycling: A review". In: *Cleaner Chemical Engineering* 5 (2023), p. 100094. ISSN: 2772-7823. DOI: https://doi.org/10.1016/j.clce.2023.100094. URL: https://www.sciencedirect.com/science/article/pii/S2772782323000025.

[63] G. Popelier et al. "A critical review of the influence of supercritical water on the pyrolysis of plastic waste: Modelling approaches and process effects". In: *Journal of Analytical and Applied Pyrolysis* 183 (2024), p. 106805. ISSN: 0165-2370. DOI: https://doi.org/10.1016/j.jaap.2024.106805. URL: https://www.sciencedirect.com/science/article/pii/S0165237024004601.

[64] Kintek Solution (Kindle-Tech). *What Is the Difference Between Gasification, Pyrolysis, and Combustion? Key Insights Explained*. 2024. URL: https://kindle-tech.com/faqs/what-is-the-difference-between-combustion-pyrolysis-and-gasification (visited on 08/21/2025).

[65] A. Jayanarasimhan et al. "Tar Formation in Gasification Systems: A Holistic Review of Remediation Approaches and Removal Methods". In: *ACS Omega* 9.2 (2024), pp. 2060–2079. DOI: 10.1021/acsomega.3c04425. URL: https://doi.org/10.1021/acsomega.3c04425.

[66] S. Tosti et al. "Process analysis of refuse derived fuel hydrogasification for producing SNG". In: *International Journal of Hydrogen Energy* 44.39 (2019), pp. 21470–21480. ISSN: 0360-3199. DOI: https://doi.org/10.1016/j.ijhydene.2019.06.117. URL: https://www.sciencedirect.com/science/article/pii/S0360319919323900.

[67] M.A.S. Khan et al. "Chapter 6 - Hydrogenolysis and hydrocracking of biomass and plastic wastes to produce high-value products". In: *Thermochemical Conversion of Biomass Feedstock and Solid Waste into Biofuels*. Ed. by Yanjun Hu et al. Woodhead Series in Bioenergy. Woodhead Publishing, 2025, pp. 101–116. ISBN: 978-0-443-29291-0. DOI: https://doi.org/10.1016/B978-0-443-29291-0.00006-5. URL: https://www.sciencedirect.com/science/article/pii/B9780443292910000065.

[68] M.G. Davidson, R.A. Furlong, and M.C. McManus. "Developments in the life cycle assessment of chemical recycling of plastic waste – A review". In: *Journal of Cleaner Production* 293 (2021), p. 126163. ISSN: 0959-6526. DOI: https://doi.org/10.1016/j.jclepro.2021.126163. URL: https://www.sciencedirect.com/science/article/pii/S0959652621003838.

[69] H. Jeswani et al. "Life cycle environmental impacts of chemical recycling via pyrolysis of mixed plastic waste in comparison with mechanical recycling and energy recovery". In: *Science of The Total Environment* 769 (2021), p. 144483. ISSN: 0048-9697. DOI: https://doi.org/10.1016/j.scitotenv.2020.144483. URL: https://www.sciencedirect.com/science/article/pii/S0048969720380141.

[70] S. Das, C. Liang, and J.B. Dunn. "Plastics to fuel or plastics: Life cycle assessment-based evaluation of different options for pyrolysis at end-of-life". In: *Waste Management* 153 (2022), pp. 81–88. ISSN: 0956-053X. DOI: https://doi.org/10.1016/j.wasman.2022.08.015. URL: https://www.sciencedirect.com/science/article/pii/S0956053X22004238.

[71] A. Somoza-Tornos et al. "Realizing the Potential High Benefits of Circular Economy in the Chemical Industry: Ethylene Monomer Recovery via Polyethylene Pyrolysis". In: *ACS Sustainable Chemistry & Engineering* 8.9 (2020), pp. 3561–3572. DOI: 10.1021/acssuschemeng.9b04835. URL: https://pubs.acs.org/doi/10.1021/acssuschemeng.9b04835.

[72] H.H. Khoo. "LCA of plastic waste recovery into recycled materials, energy and fuels in Singapore". In: *Resources, Conservation and Recycling* 145 (2019), pp. 67–77. ISSN: 0921-3449. DOI: https://doi.org/10.1016/j.resconrec.2019.02.010. URL: https://www.sciencedirect.com/science/article/pii/S0921344919300679.

[73] S. Afzal et al. "Techno-economic analysis and life cycle assessment of mixed plastic waste gasification for production of methanol and hydrogen". In: *Green Chem.* 25 (13 2023), pp. 5068–5085. DOI: 10.1039/D3GC00679D. URL: http://dx.doi.org/10.1039/D3GC00679D.

[74] S.M. Al-Salem, S. Evangelisti, and P. Lettieri. "Life cycle assessment of alternative technologies for municipal solid waste and plastic solid waste management in the Greater London area". In: *Chemical Engineering Journal* 244 (2014), pp. 391–402. ISSN: 1385-8947. DOI: https://doi.org/10.1016/j.cej.2014.01.

066. URL: https://www.sciencedirect.com/science/article/pii/S1385894714000916.

[75] Kintek Solution Tech Team. *What are the different types of reactors in pyrolysis?* 2025. URL: https://kindle-tech.com/faqs/ (visited on 11/17/2025).

[76] N. Fueyo and C. Dopazo. "Fluidization fundamentals". In: *Pressurized Fluidized Bed Combustion*. Ed. by M. Alvarez Cuenca and E. J. Anthony. Dordrecht: Springer Netherlands, 1995, pp. 38–79. ISBN: 978-94-011-0617-7. DOI: 10.1007/978-94-011-0617-7_2. URL: https://doi.org/10.1007/978-94-011-0617-7_2.

[77] Y. Zhang et al. "Liquid oils produced from pyrolysis of plastic wastes with heat carrier in rotary kiln". In: *Fuel Processing Technology* 206 (2020), p. 106455. ISSN: 0378-3820. DOI: https://doi.org/10.1016/j.fuproc.2020.106455. URL: https://www.sciencedirect.com/science/article/pii/S0378382020301508.

[78] M. Zhang et al. "Numerical investigation on the heat transfer of plastic waste pyrolysis in a rotary furnace". In: *Chemical Engineering Journal* 445 (2022), p. 136686. ISSN: 1385-8947. DOI: https://doi.org/10.1016/j.cej.2022.136686. URL: https://www.sciencedirect.com/science/article/pii/S1385894722021817.

[79] Siemens Digital Industries Software. *Simcenter STAR-CCM+ User Guide*. Version 2510. 2025.

[80] Y.A. Cengel and A.J. Ghajar. *Heat and Mass Transfer: Fundamentals and Applications (Fifth Edition in SI Units)*. McGraw-Hill Education, 2015. ISBN: 9789814595278.

[81] Altair Engineering Inc. *What is DEM: Theoretical Background behind the Discrete Element Method*. 2023. (Visited on 11/17/2025).

[82] Fire Safety Research Institute. *Polypropylene (PP) — Materials and Products Database*. 2025. URL: https://materials.fsri.org/materialdetail/polypropylene-pp (visited on 11/21/2025).

[83] INEOS Olefins & Polymers USA. *Engineering Properties of Polypropylene*. 2014. URL: https://www.ineos.com/globalassets/ineos-group/businesses/ineos-olefins-and-polymers-usa/products/technical-information--patents/ineos-engineering-properties-of-pp.pdf (visited on 11/21/2025).

[84] Thermtest Inc. *Materials Database*. n.d. URL: https://thermtest.com/thermal-resources/materials-database (visited on 05/06/2026).

[85] Seralgaz. *Nitrogen*. n.d. URL: https://www.seralgaz.com/en/nitrogen.php (visited on 05/14/2026).

[86] Europlas. *Melting Point of All Types of Polyethylene You Should Know*. n.d. URL: https://europlas.com.vn/en-US/blog-1/melting-point-of-all-types-of-polyethylene-you-should-know (visited on 05/14/2026).

[87] M. S. Qureshi et al. "Pyrolysis of plastic waste: Opportunities and challenges". In: *Journal of Analytical and Applied Pyrolysis* 152 (2020), p. 104804. ISSN: 0165-2370. DOI: https://doi.org/10.1016/j.jaap.2020.104804. URL: https://www.sciencedirect.com/science/article/pii/S0165237019308241.

[88] Alfa Laval. *Pyrolysis of plastics: Challenges and solutions*. Nov. 2025. URL: https://www.alfalaval.us/media/stories/sustainability/pyrolysis-of-plastics-challenges-and-solutions/ (visited on 04/22/2026).

[89] M.M Hasan et al. "Pyrolysis of plastic waste for sustainable energy Recovery: Technological advancements and environmental impacts". In: *Energy Conversion and Management* 326 (2025), p. 119511. ISSN: 0196-8904. DOI: https://doi.org/10.1016/j.enconman.2025.119511. URL: https://www.sciencedirect.com/science/article/pii/S0196890425000342.

[90] A. Fivga and I. Dimitriou. "Pyrolysis of plastic waste for production of heavy fuel substitute: A techno-economic assessment". In: *Energy* 149 (2018), pp. 865–874. ISSN: 0360-5442. DOI: https://doi.org/10.1016/j.energy.2018.02.094. URL: https://www.sciencedirect.com/science/article/pii/S0360544218303220.

[91] M. Larrain et al. "Economic performance of pyrolysis of mixed plastic waste: Open-loop versus closed-loop recycling". In: *Journal of Cleaner Production* 270 (2020), p. 122442. ISSN: 0959-6526. DOI: https://doi.org/10.1016/j.jclepro.2020.122442. URL: https://www.sciencedirect.com/science/article/pii/S0959652620324896.

[92] A. Pacheco-López et al. "Economic and environmental assessment of plastic waste pyrolysis products and biofuels as substitutes for fossil-based fuels". In: *Frontiers in Energy Research* 9 (2021), p. 676233.

[93] Zero Waste Europe. *Leaky Loop Recycling: A Technical Correction on the Quality of Pyrolysis Oil Made from Plastic Waste*. Technical report. Zero Waste Europe, 2022. URL: https://zerowasteeurope.eu/library/leaky-loop-recycling-a-technical-correction-on-the-quality-of-pyrolysis-oil-made-from-plastic-waste/ (visited on 04/24/2026).

[94] Enval Ltd. *Enval*. n.d. URL: https://www.enval.com/ (visited on 04/24/2026).

[95] Klean Industries. *SPR Japan: Plastic Pyrolysis Project*. n.d. URL: https://kleanindustries.com/projects/plastic-pyrolysis/spr-japan/ (visited on 04/29/2026).

[96] Å. Stenmarck et al. *Hazardous substances in plastics:–ways to increase recycling*. Nordic Council of Ministers, 2017.

[97] C. Ludlow-Palafox and H.A. Chase. "Microwave-Induced Pyrolysis of Plastic Wastes". In: *Industrial & Engineering Chemistry Research* 40.22 (2001), pp. 4749–4756. ISSN: 0888-5885. DOI: 10.1021/ie010202j. URL: https://doi.org/10.1021/ie010202j.

Appendices

Steady state flow field

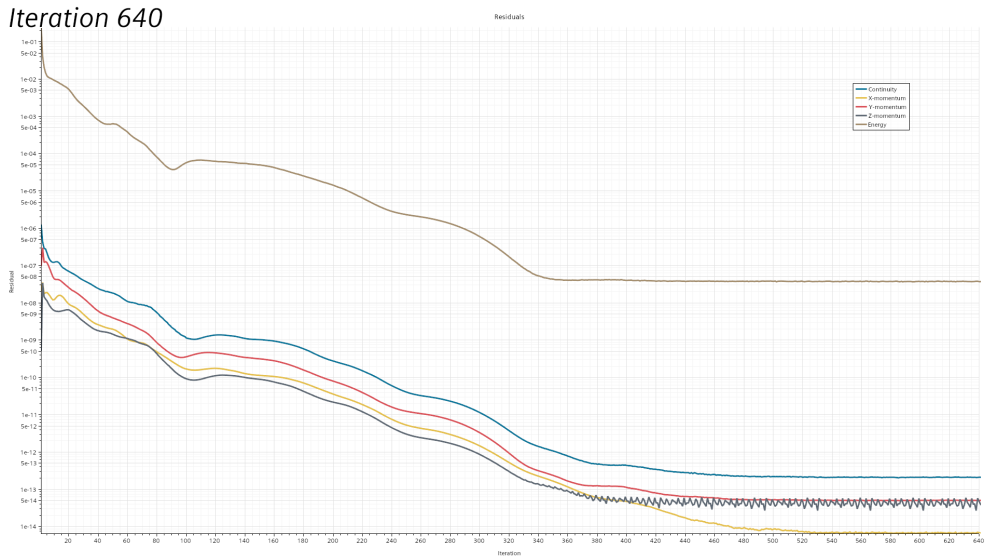

Figure 1: Residuals for steady state simulation.

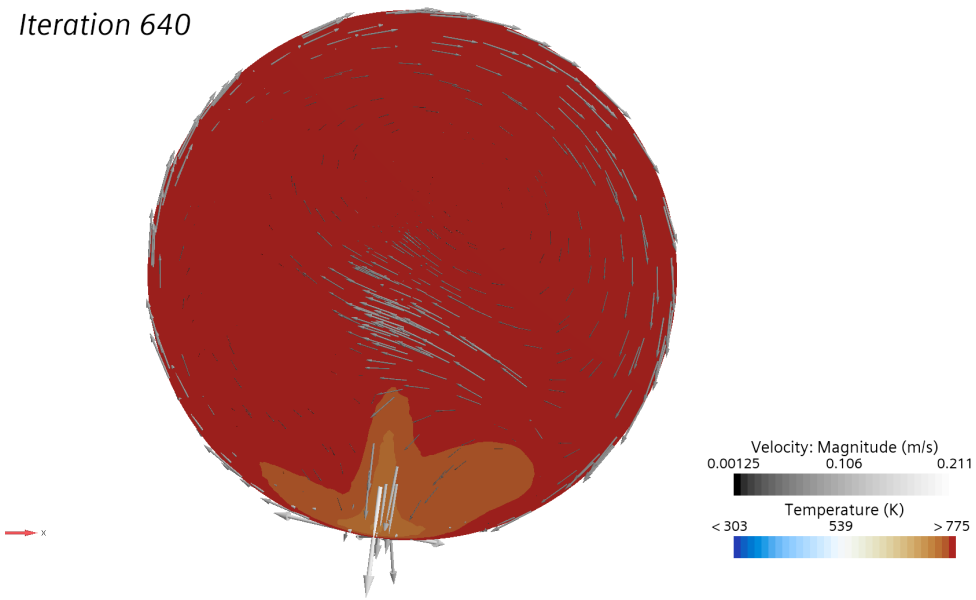

Figure 2: Temperature field and velocity vectors for steady state simulation on cross section through the rotary kiln.

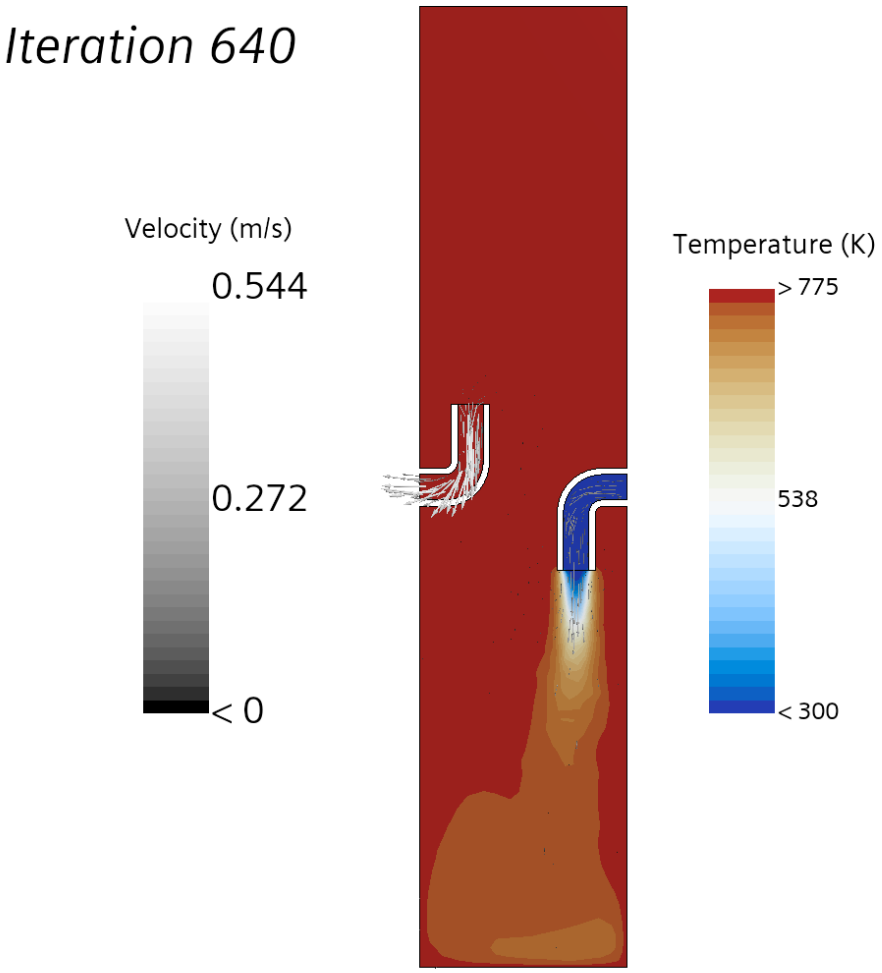

Figure 3: Temperature field and velocity vectors for steady state simulation on different cross section through kiln.

Mesh sensitivity and validation

Meshes

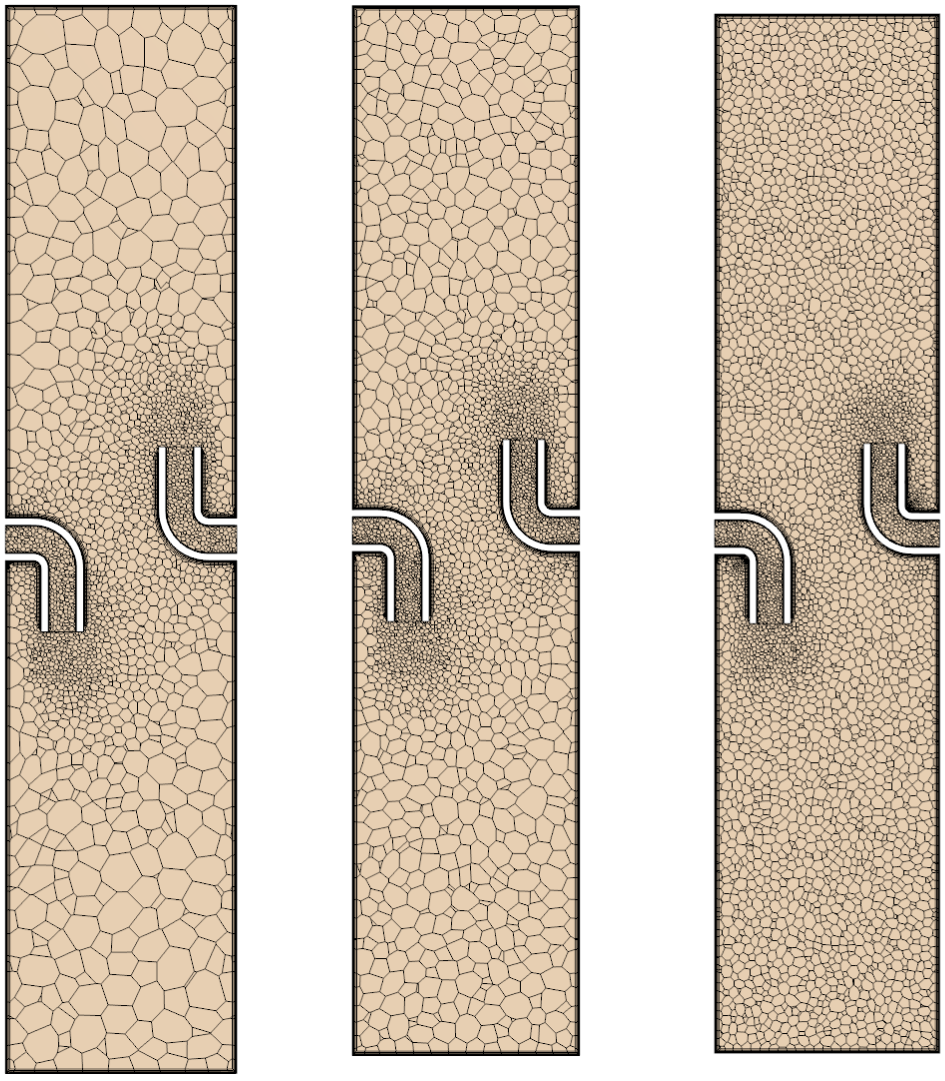

(a) 7.5 mm (b) 5 mm (c) 2.5 mm

Figure 4: Cross section of the rotary kiln for the three meshes. From left to right; coarse, medium and fine mesh.

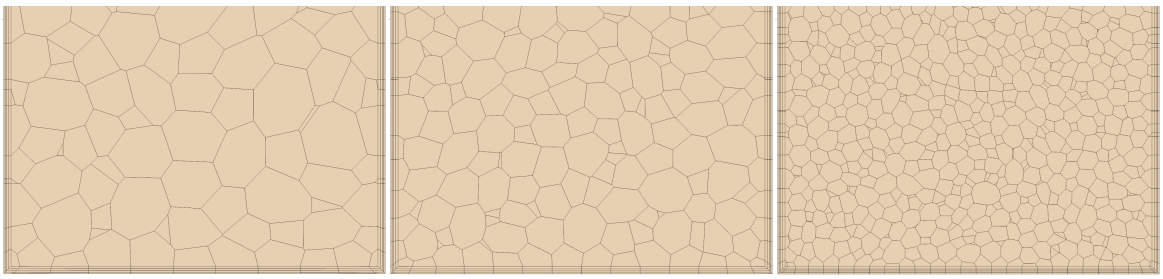

(a) 7.5 mm (b) 5 mm (c) 2.5 mm

Figure 5: Zoomed in cross section of the rotary kiln for the three meshes. From left to right; coarse, medium and fine mesh.

Sensitivity and validation

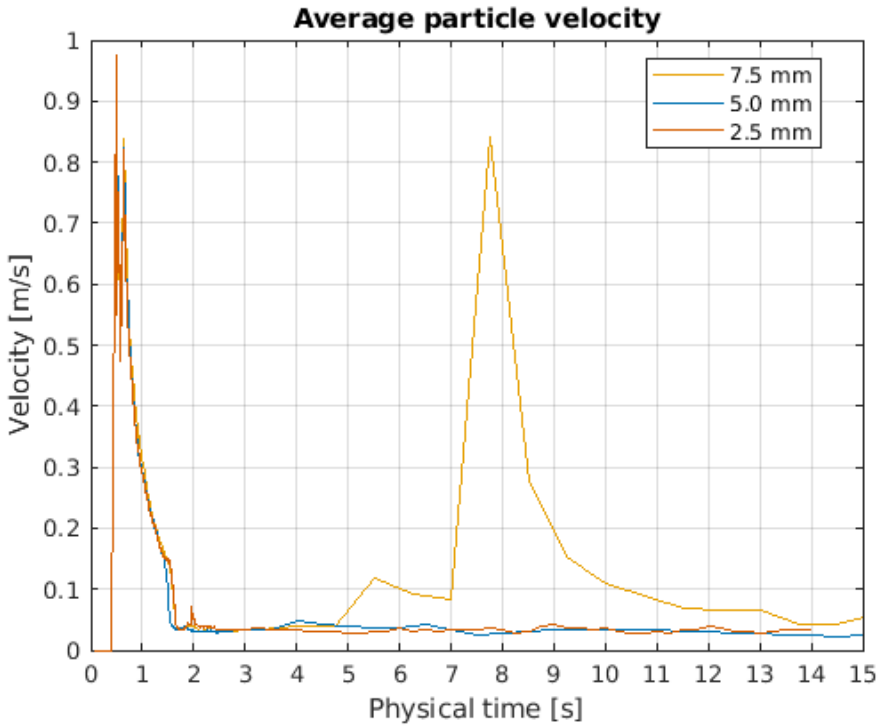

Figure 6: Average particle velocity for the three meshes.

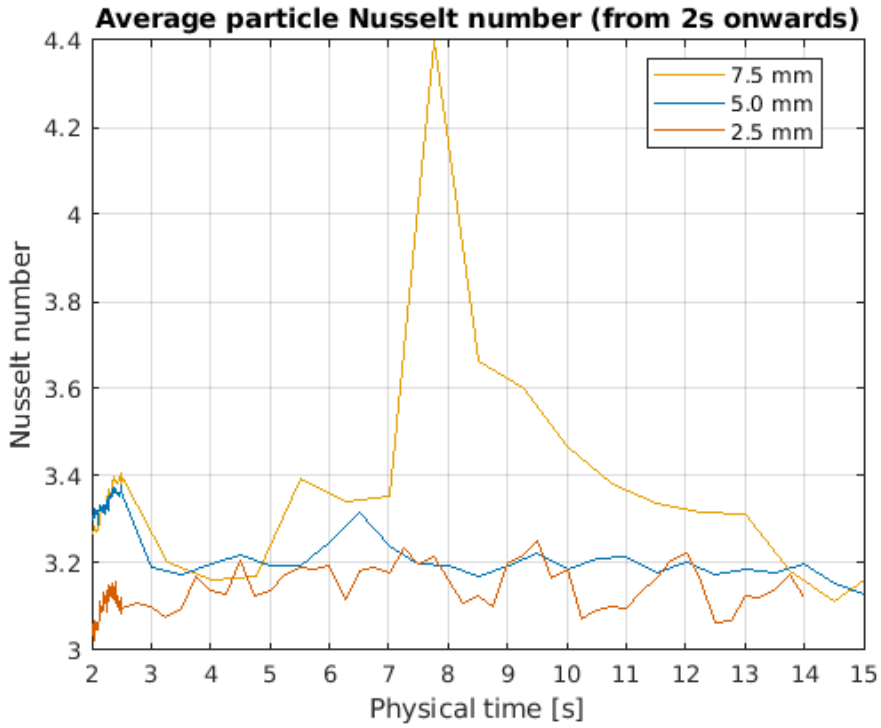

Figure 7: Average particle Nusselt number from 2s onwards for the meshes.

Mesh metrics medium mesh

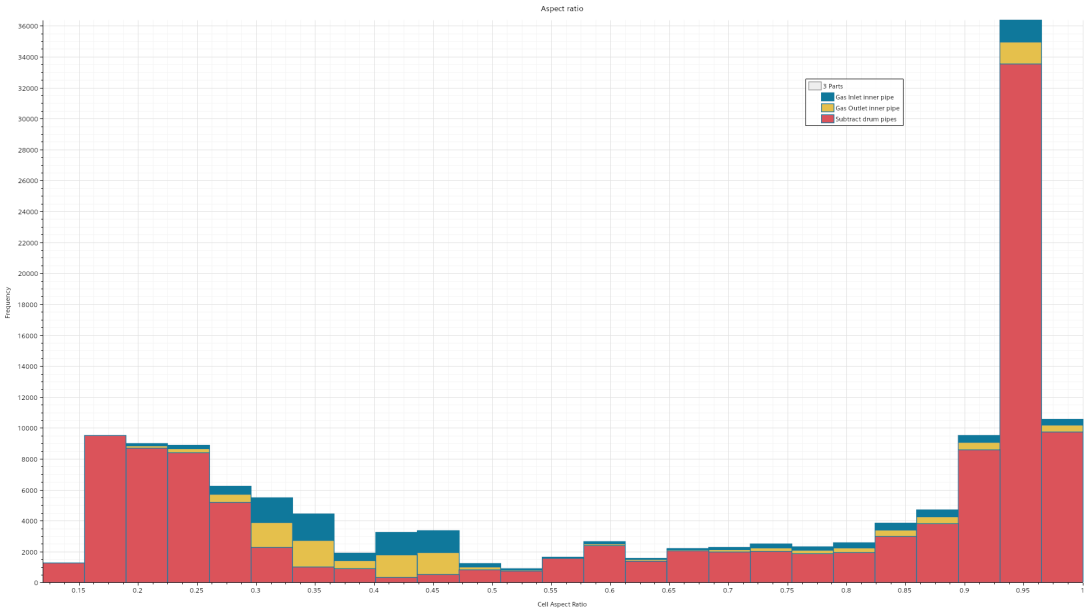

Figure 8: Aspect ratio for medium mesh.

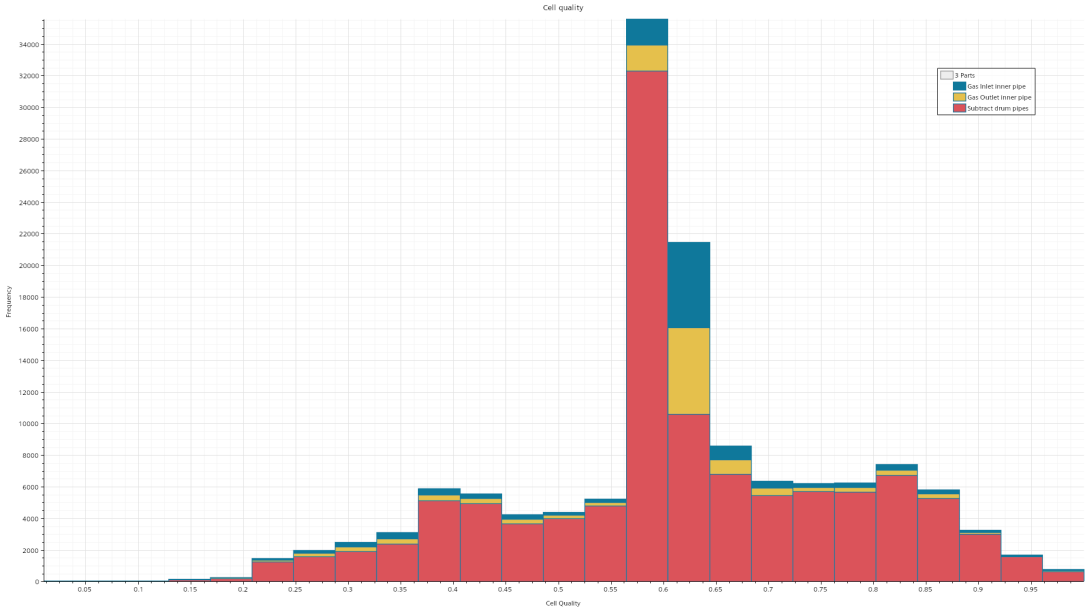

Figure 9: Cell quality for medium mesh.

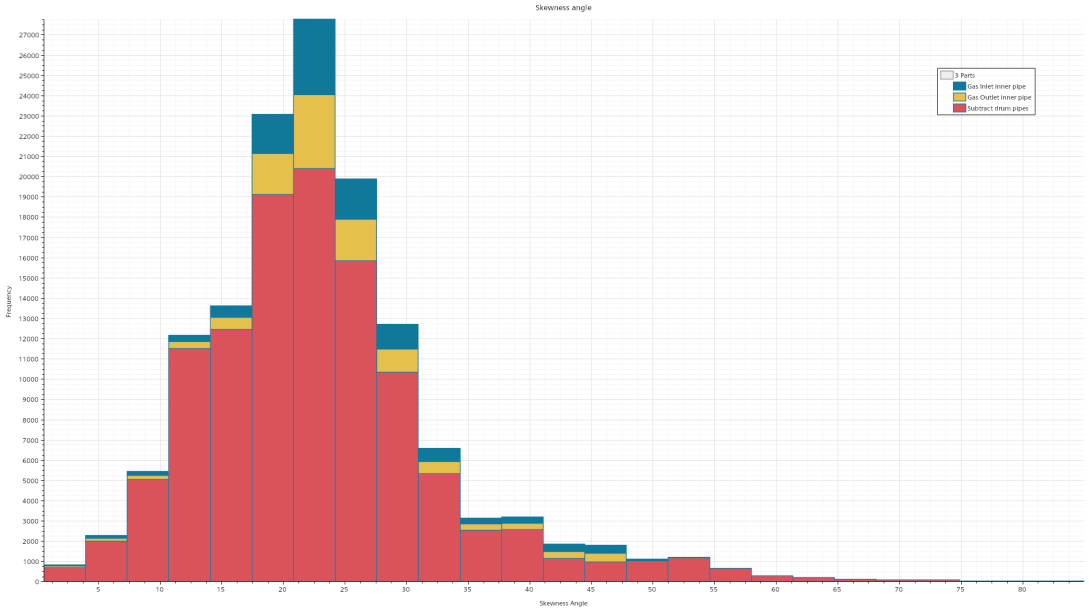

Figure 10: Skewness angle for medium mesh.

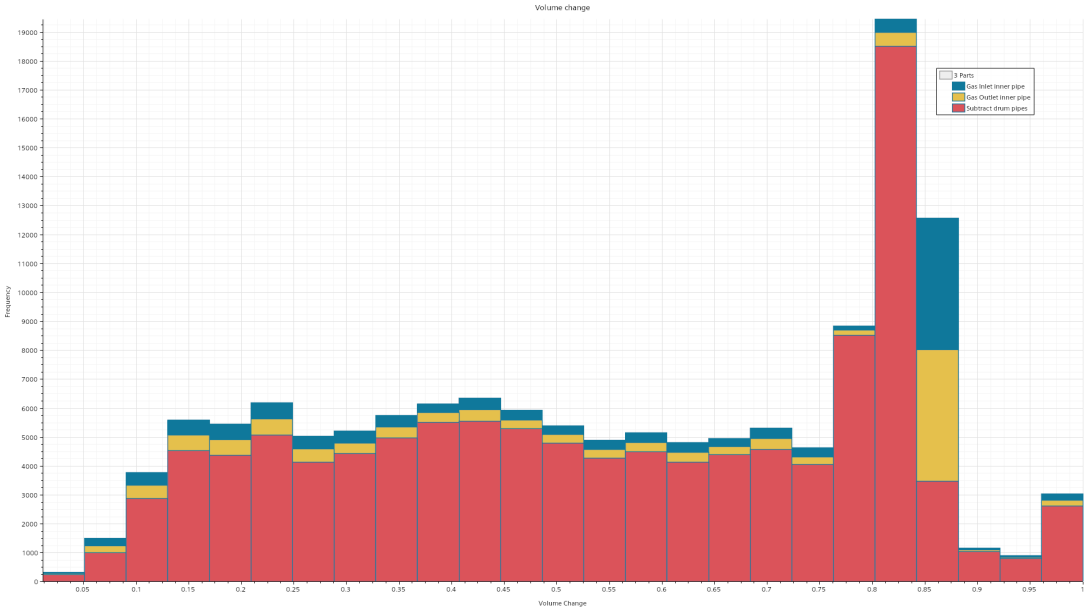

Figure 11: Volume change for medium mesh.

CFD-DEM simulations of MPW pyrolysis

Table 1: Total elapsed solver time for cases 1.0-5

Case	**Time**
Case 1.0 (PE)*	142.9 hours ≈ 6 days
Case 1.1 (PE)	16.24 hours
Case 2.0 (PE+PP)	276.2 hours ≈ 11.5 days
Case 2.1 (PE+PP)	16.42 hours
Case 3.0 (PE+PP+polyAl)	398.2 hours ≈ 16.6 days
Case 3.1 (PE+PP+polyAl)	21.47 hours
Case 4 (PP)	227.9 hours ≈ 9.5 days
Case 5 (polyAl)	197.7 hours ≈ 8.2 days

* Case 1.0 was run full simulation time on 64 cores.

Case 1

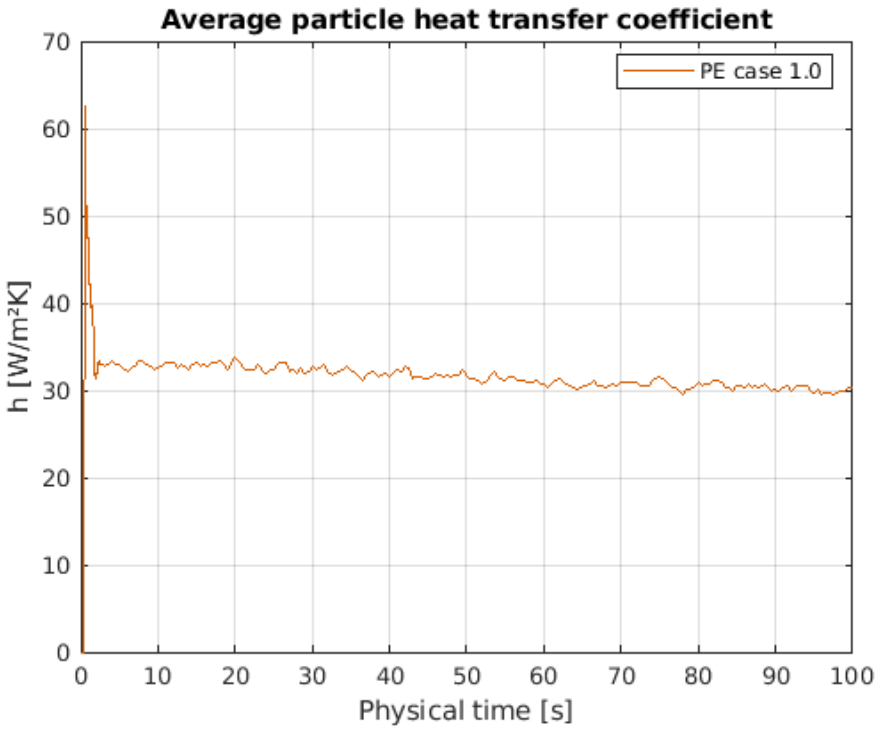

Figure 12: Calculated particle heat transfer coefficient for PE particles case 1.0.

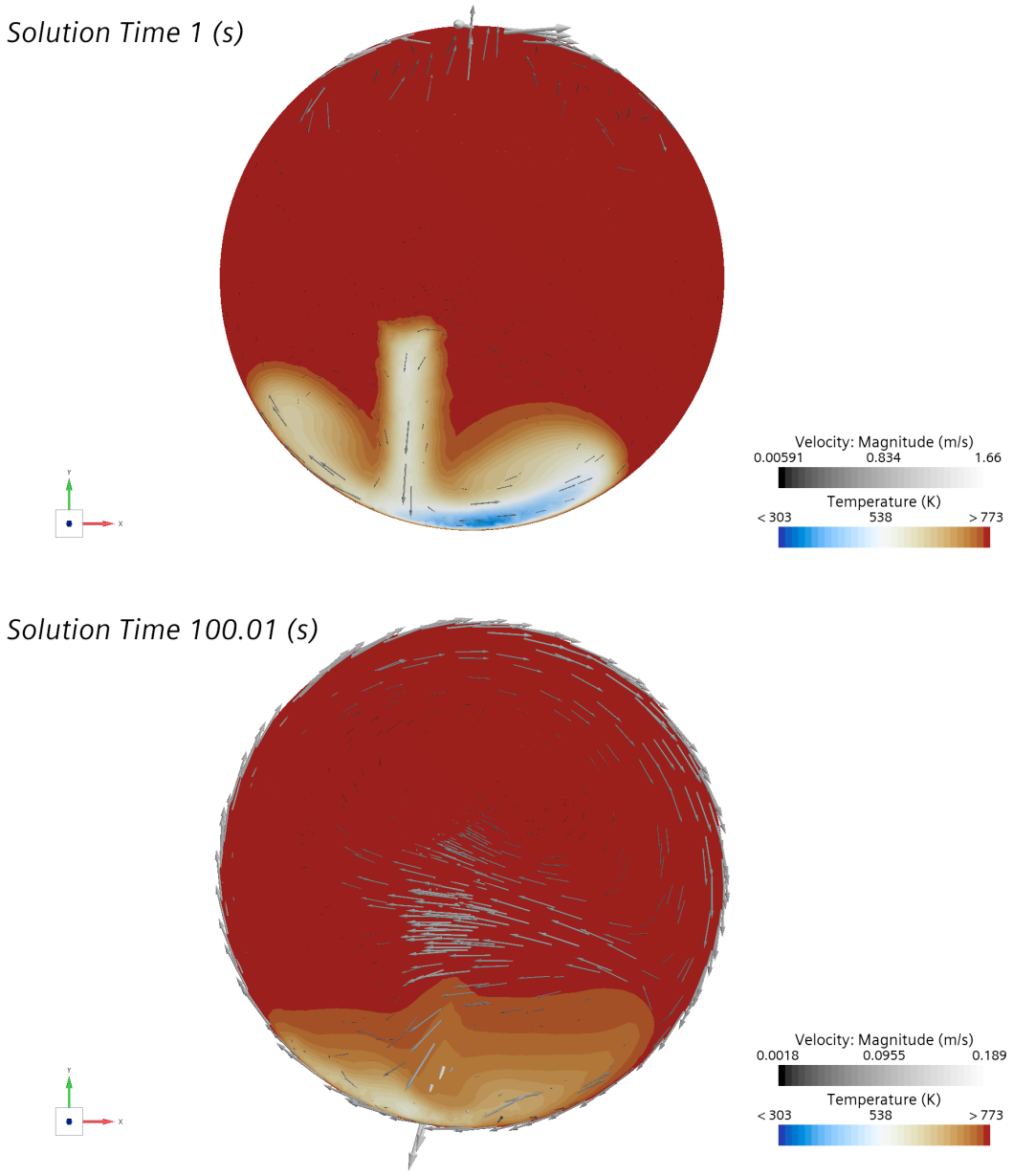

Figure 13: Gas temperature field and velocity vectors for case 1.0.

Case 2 & 4

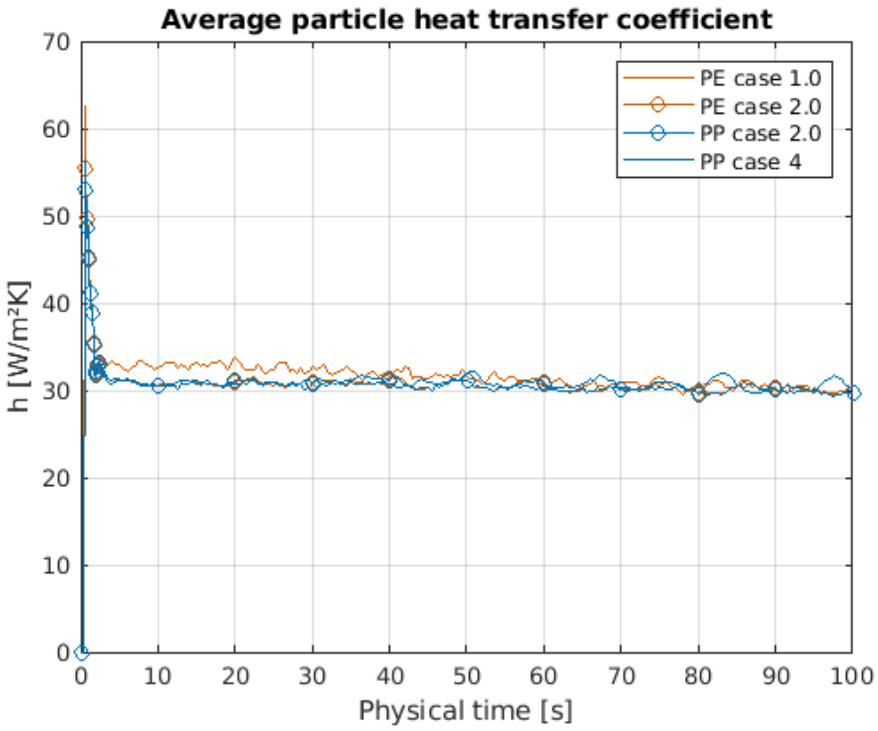

Figure 14: Calculated particle heat transfer coefficient for case 1.0, 2.0 and 4.

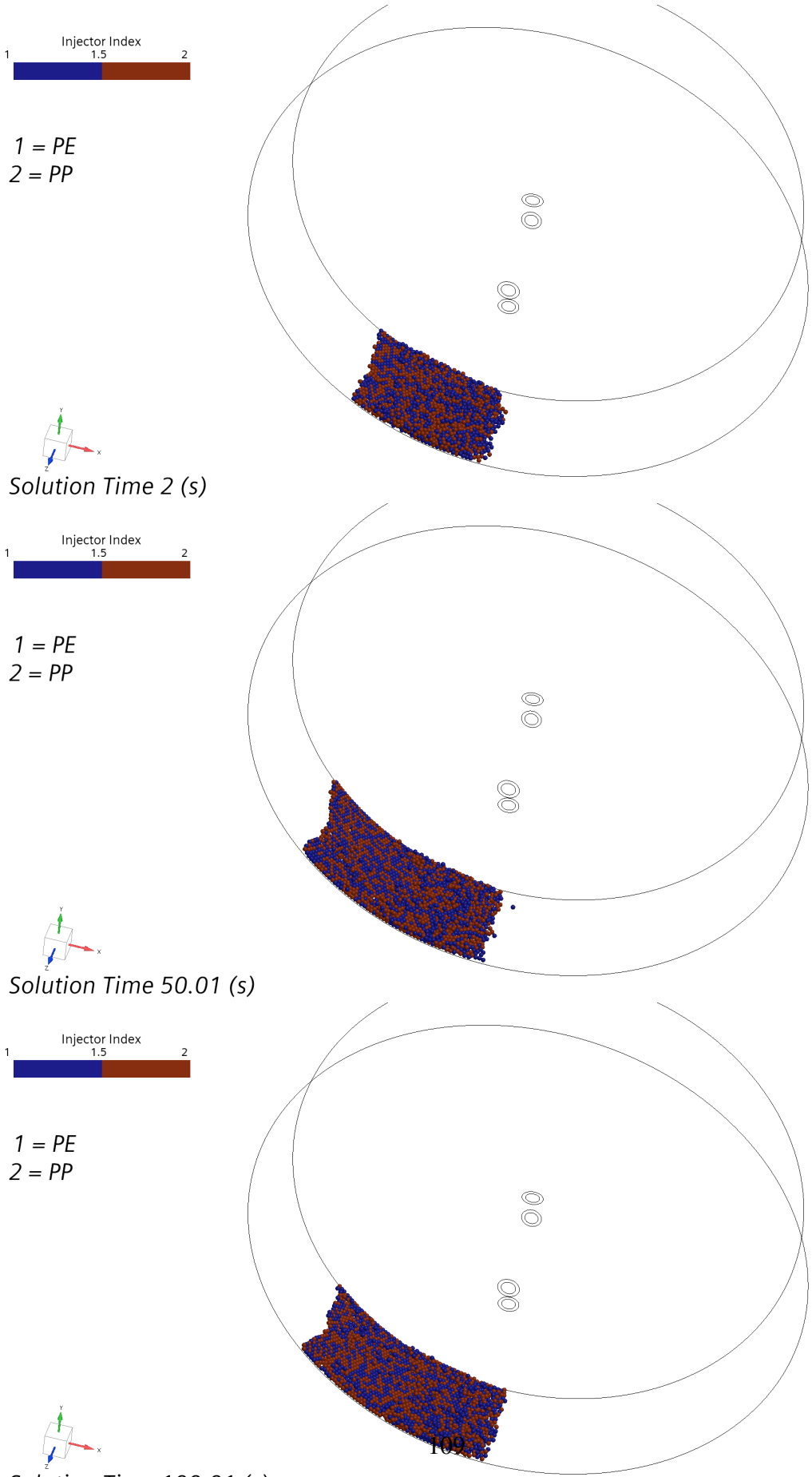

Figure 15: Particle mixing case 2.0.

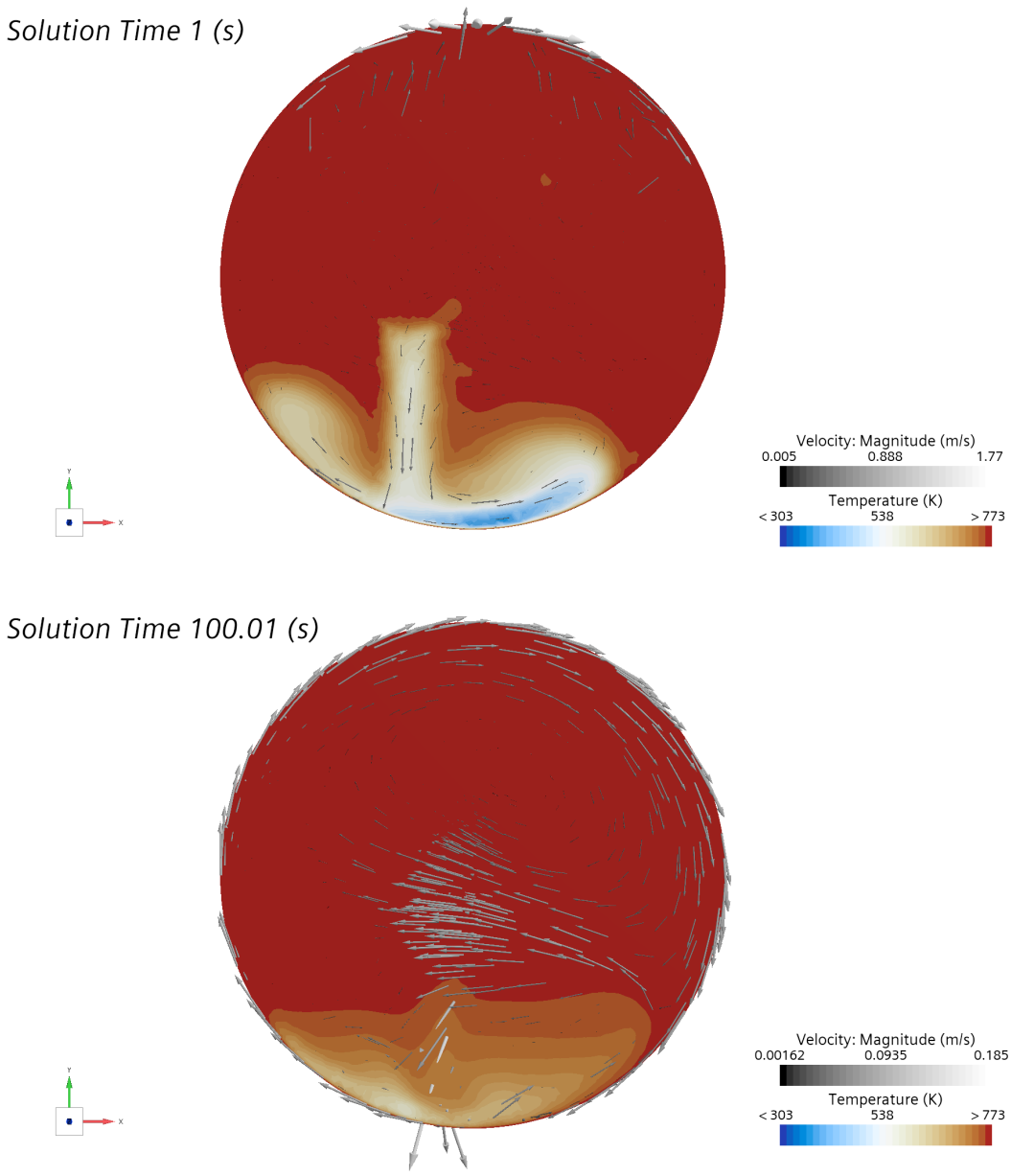

Figure 16: Gas temperature field and velocity vectors for case 2.0.

Case 3 & 5

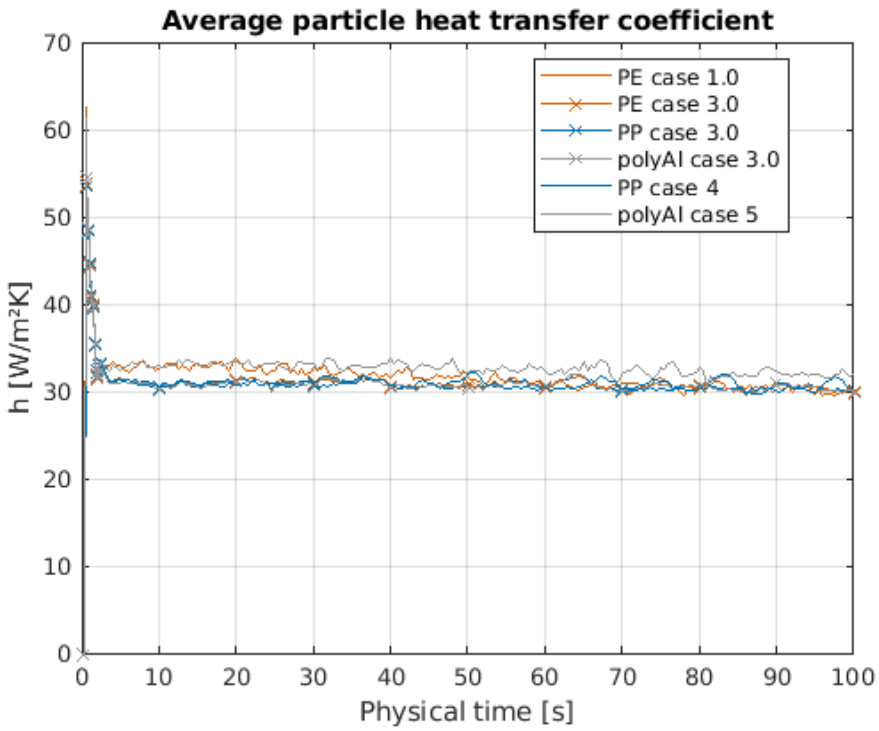

Figure 17: Calculated particle heat transfer coefficient for case 1.0, 3.0, 4 and 5.

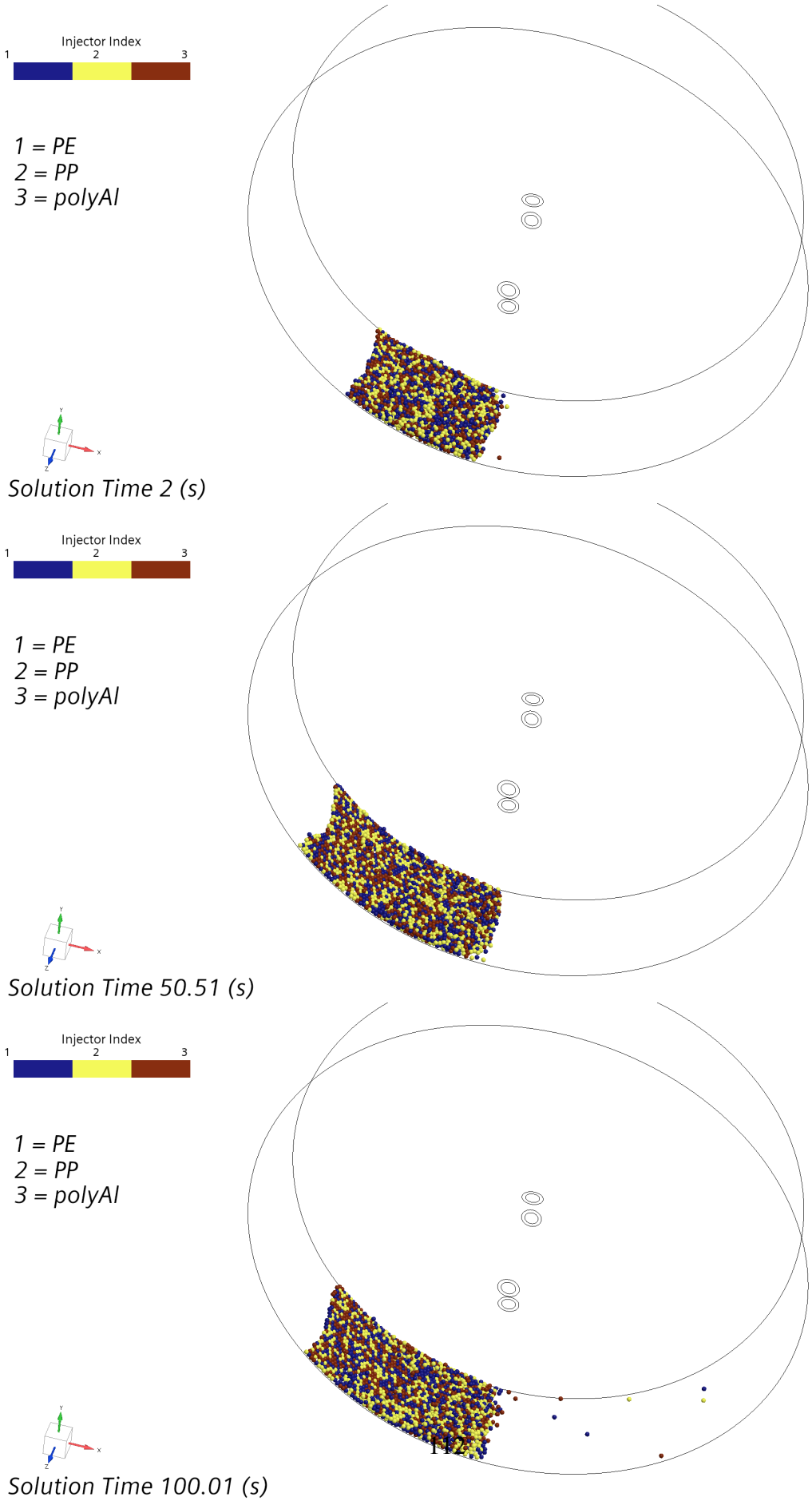

Figure 18: Particle mixing case 3.0.

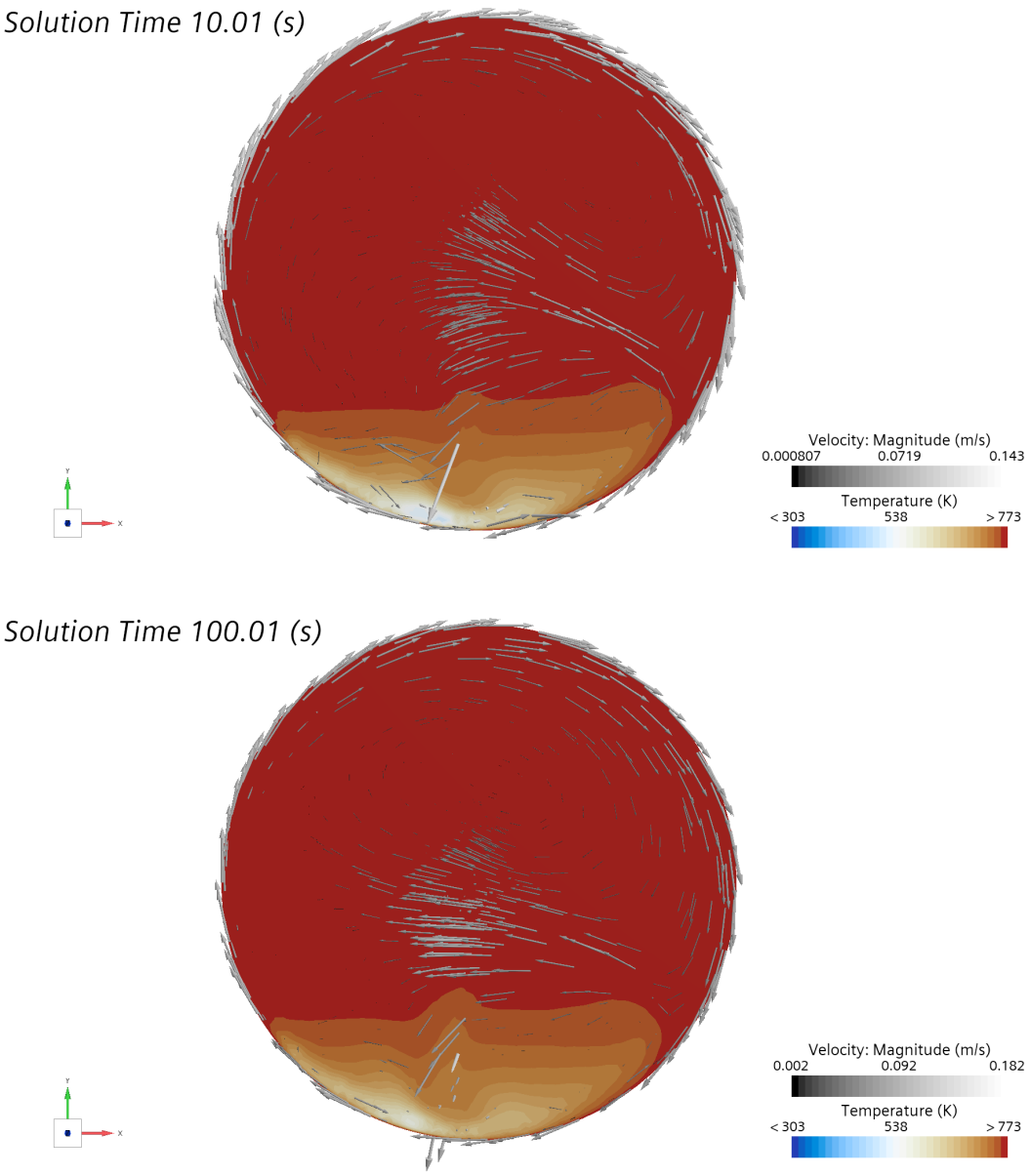

Figure 19: Gas temperature field and velocity vectors for case 3.0.

Plots per particle type

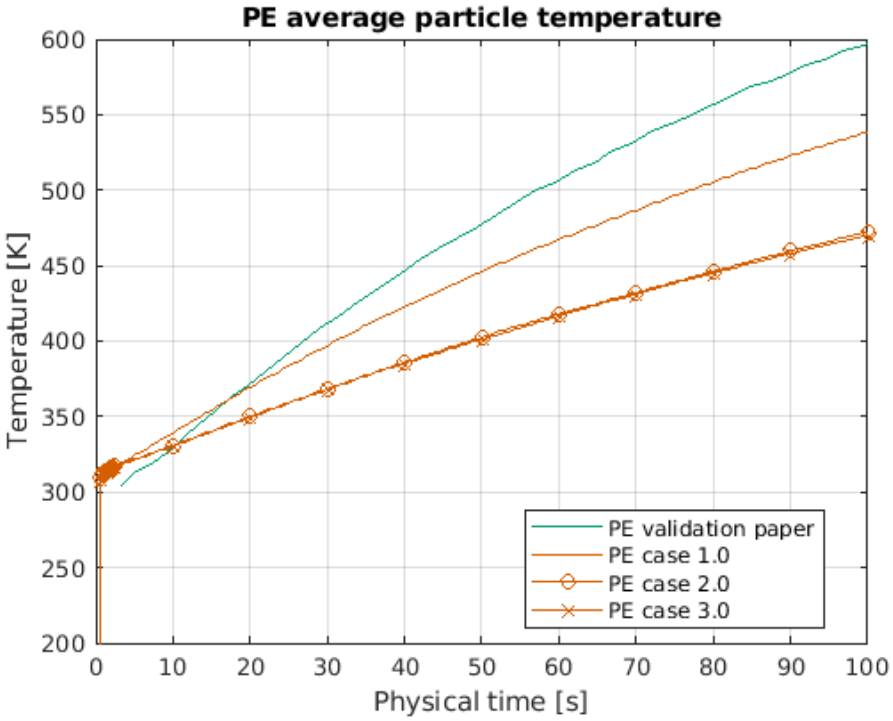

Figure 20: Average particle temperature for PE particles in case 1.0, 2.0 and 3.0, including data from the validation paper [78].

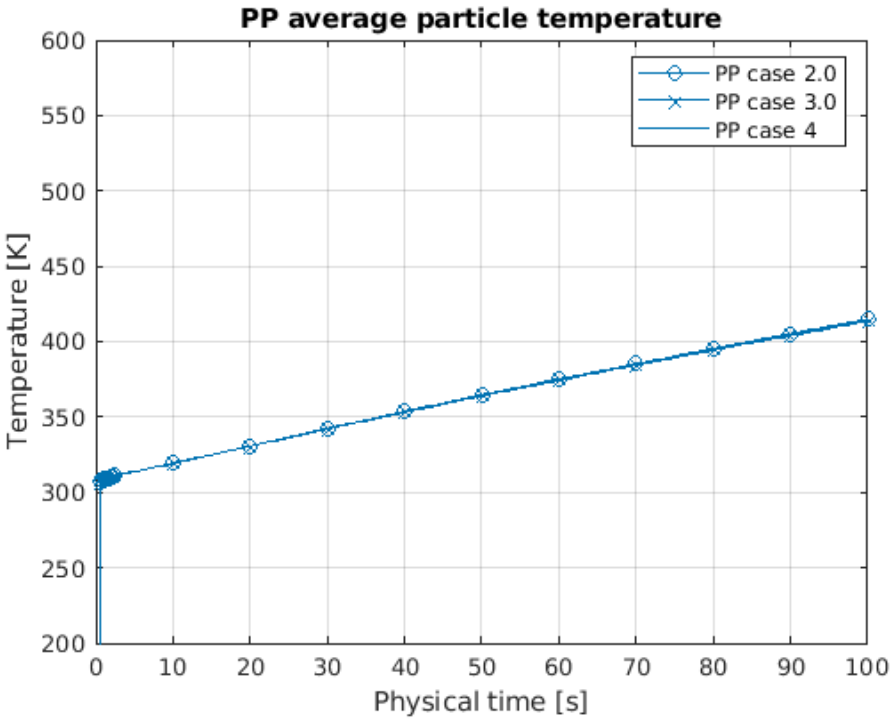

Figure 21: Average particle temperature for PP particles in case 2.0, 3.0 and 4.

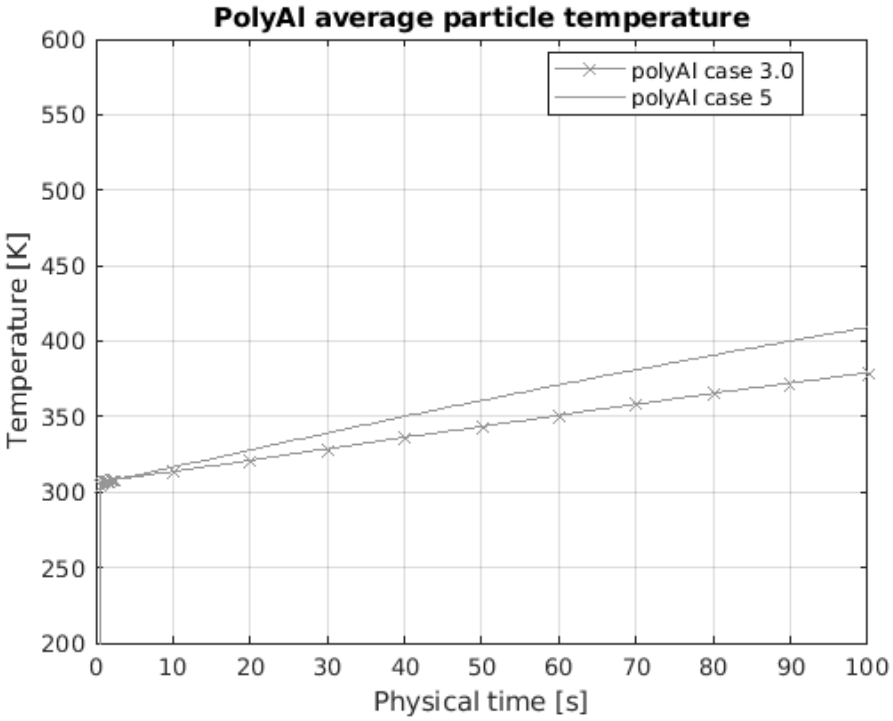

Figure 22: Average particle temperature for polyAl particles in case 3.0 and 5.

Findings from iterative process

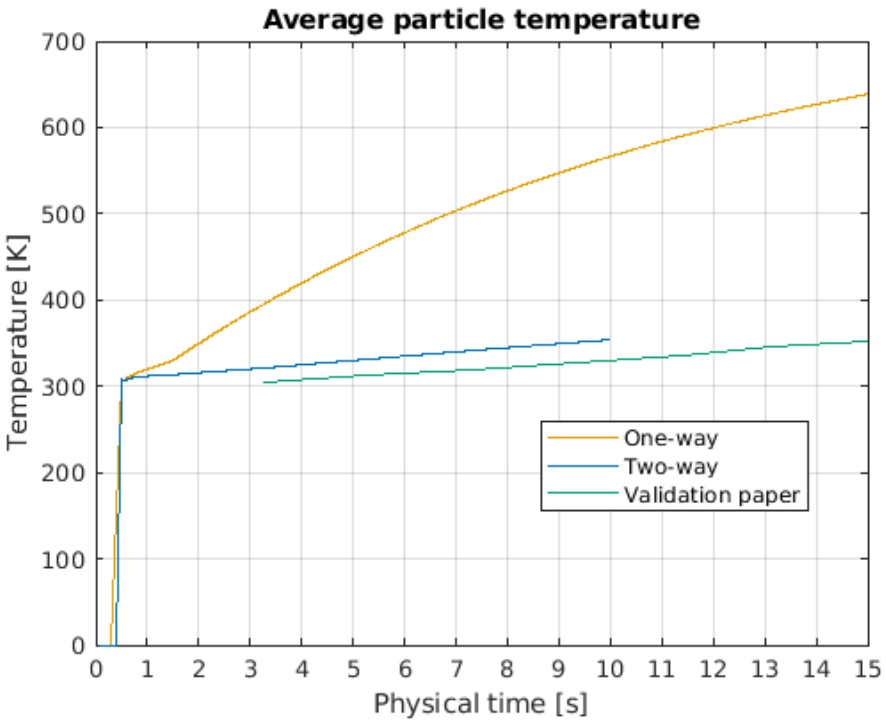

Figure 23: Average PE particle temperature using one-way vs two-way coupling with validation paper as reference.